ISBN:978-90-393-6682-0

Printed by: Uitgeverij BOXPress | Proefschriftmaken.nl

Cover design by Inge Veldhoen (www.ingeveldhoen.com): artistic impression of breast cancer progression stages from healthy mammary ducts to malignant growth and metastasis.

The research described in this thesis and the printing of this thesis was financially supported by the Dutch Cancer Society (KWF), the Department of Pathology at the UMC Utrecht, and ChipSoft BV.

Breast cancer progression cues driven by adherens junction inactivation

Borstkanker progressie-signalen gedreven door adherens junctie inactivatie

(met een samenvatting in het Nederlands)

Proefschrift

ter verkrijging van de graad van doctor aan de Universiteit Utrecht op gezag van de rector magnificus, prof.dr. G.J. van der Zwaan, ingevolge het besluit van het college voor promoties in het openbaar te verdedigen op dinsdag 13 december 2016 des middags te 4.15 uur

door

Milou Tenhagen

geboren op 26 augustus 1988

te Deventer

Promotor: Prof. dr. P.J. van Diest

Copromotor: Dr. P.W.B. Derksen

Table of contents

Chapter 1

General introduction

1. The adherens junction as glue to control epithelial homeostasis

Adherens junctions are cell-cell contacts that are essential for epithelial tissues to establish a barrier and maintain a polarized structure. A central constituent of the AJ is the transmembrane protein E-cadherin (*CDH1*) that provides basolateral cell-cell contacts through Ca^{2+} dependent homotypic interactions [1,2]. Together with N-cadherin (*CDH2*), P-cadherin (*CHD3*), R-cadherin (*CDH4*) and M-cadherin (*CDH15*), E-cadherin forms the type I classical cadherin family which are phylogenetically distinct from type II classical cadherins (reviewed in [3]). All classical cadherins contain an extra-cellular domain that consists of 5 ectodomains forming the interaction surface for homo- and heterotypic in cis and/or in trans interactions between neighboring classical cadherins (reviewed in [2]). The intracellular domain of classical cadherins comprises two conserved binding sites. First, β-catenin (*CTNNB1*) is able to directly bind to the most C-terminal domain of E-cadherin via its 12 armadillo (ARM) domains [4–6]. Second, the cytoplasmic cadherin tail juxtaposed to the cell membrane provides a binding site for for another ARM-domain containing protein called p120-catenin (p120, *CTNND1*) Figure 1) ([7-9] and reviewed in [10])

p120 controls classical cadherin stability

Direct binding of p120 to classical cadherins controls junctional stability and turnover [11–13]. Cadherin stability is controlled by p120 through multiple mechanisms. First, p120 prevents clathrin-mediated endocytosis through masking an endocytic motif in classical cadherins [9,14]. Second, p120 prevents proteosomal targeting of E-cadherin by preventing binding of the E3 ubiquitin ligase called Hakai to E-cadherin [15]. Interestingly, family members of p120, which include δ-catenin, p0071 and Armadillo Repeat gene deleted in Velo-Cardio-Facial syndrome (ARVCF) can also bind and stabilize classical cadherins, which suggests functional redundancy in the regulation of cadherin turnover at the membrane (reviewed in [16]).

Nuclear functions of p120

Nuclear localization of p120 enables p120 to regulate transcription. Shuttling of p120 between the cytosol and nucleus is facilitated by the presence of two nuclear localization seqeunces (NLS) [17,18] and one nuclear export sequence (NES) [19]. Additionally, p120, like many other ARM-domain containing proteins, has the intrinsic capacity to mediate its own nuclear import via its ARM domains [20]. Nuclear p120 was shown to interact with several transcription factors including Glis2 and REST-CoREST, which are both transcriptional repressors involved in neuronal differentiation [21,22]. Loss of E-cadherin induced a p120-dependent increase in REST-CoREST target gene expression, thereby linking the AJ to transcription [22].

Most research on the nuclear function of p120 has been focused on the direct interaction of p120 with a transcriptional repressor called Kaiso [23]. Binding to Kaiso is mutually exclusive with the ability of p120 to bind to E-cadherin, as the interaction with Kaiso was mapped to the first 7 ARM domains [23]; the same domains as those involved in binding to E-cadherin[9]. The C-terminus of Kaiso is essential for the interaction with p120 [23]. This region contains

three C2H2-type zinc fingers (ZF), which are also required for binding of Kaiso to the DNA [24,25]. Subsequently, binding of p120 to Kaiso prevents the interaction of Kaiso with its target DNA, resulting in relief of transcriptional repression [26–28]. Finally, p120 facilitates shuttling of Kaiso from the nucleus to the cytosol, thereby providing another mechanism to block Kaiso-DNA binding by way of nuclear export [28,29]. In section 4, the function of Kaiso will be discussed in detail.

Linkage of the AJ to the cytoskeleton

Intracellular binding partners of E-cadherin enable a dynamic interplay of the AJ with the underlying actin and microtubule cytoskeleton to both stabilize the AJ and facilitate directed cell movements (reviewed in [30], Figure 1). While linkage to the actin cytoskeleton depends on direct interaction of β-catenin with α-catenin, the precise mechanism of coupling the AJ to the actin cytoskeleton remains elusive. Although α-catenin is capable of directly binding F-actin [31], this interaction is mutually exclusive with its ability to bind to β-catenin suggesting that there is no static bridge between the AJ and the actin cytoskeleton [32,33]. Alternatively, α-catenin can interact with other actin-binding proteins, thereby providing an indirect linkage of the AJ with the actin cytoskeleton (reviewed in [34]).

The involvement of the AJ in migratory processes depends on the ability of p120 family members to regulate rearrangements of the actin cytoskeleton via Rho family GTPases RhoA, Cdc42 and Rac1 [35–38]. First, inhibition of RhoA by p120 [39–41] reduces actin contractility and decreases cell-matrix interaction by loss of focal adhesions [39,42]. Second, p120 stimulates actin polymerization at the cell periphery by activating Cdc42 and Rac1 which leads to increased cellular protrusions [35,40,43].

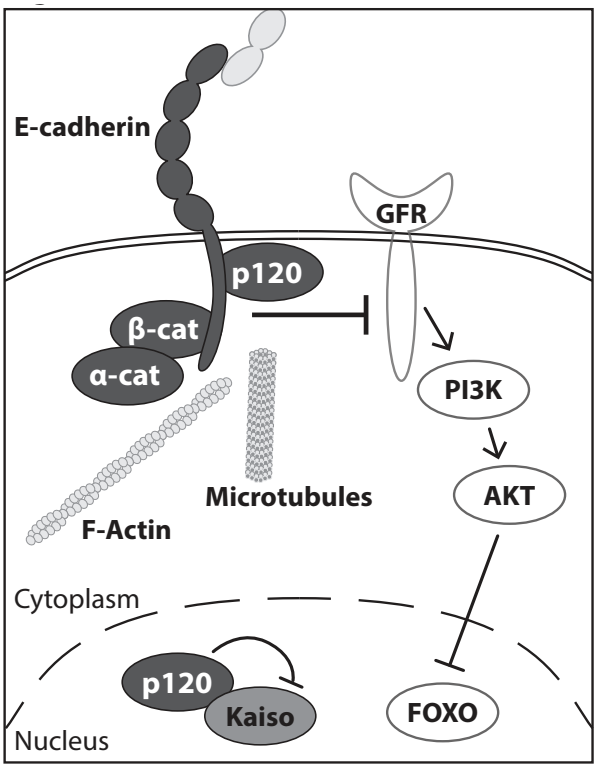

Figure 1 Epithelial adherens junction and its interaction partners
p120, β-catenin and α-catenin form the core interactors of E-cadherin. Via these catenins, the epithelial AJ is linked to the actin and microtubule cytoskeleton. Direct interaction of p120 with Kaiso relieves transcriptional regulation by Kaiso. Additionally, intact AJs are able to inhibit growth factor receptor (GFR) signaling such as PI3K/AKT signaling. Phosphorylation of FOXO by AKT results in nuclear exclusion of FOXO, thereby inhibiting FOXO-mediated transcription.

In addition to the actin cytoskeleton, the adherens junction is linked to the microtubule cytoskeleton via both plus and minus ends of microtubules. These microtubules are recruited during AJ formation and disturbance of their dynamics impairs the clustering of E-cadherin mediated junctions [44,45]. The link between the AJ and microtubule cytoskeleton is established both via p120 which stabilizes plus ends of microtubules [46], and via β-catenin which ensures tethering of microtubules to the junction [47].

E-cadherin controls growth factor signaling

Interplay of E-cadherin with receptor tyrosine kinases (RTKs) modulates mitogenic signaling (Figure 1). This was first observed when restoration of E-cadherin-dependent cell-cell contacts reduced cell proliferation [48]. Additionally, epidermal growth factor receptor (EGFR) activity was reduced upon accumulation of E-cadherin mediated cell contacts as a result of increased cell density [49,50]. In fact, E-cadherin was shown to negatively regulate the activity of several receptors including c-MET and insulin growth factor receptor (IGFR) [51]. Most studies however have focused on the EGFR that could interact with the extracellular domain of E-cadherin [51,52] both directly as well as via β-catenin [50,53]. As a result, formation of E-cadherin dependent junctions induced a transient increase in mitogenic signaling downstream of the EGFR [52,54,55]. Stable AJs however negatively regulated both ligand-dependent and -independent EGFR activation [49–51,56] by reducing receptor-ligand binding affinity and receptor mobility [51]. Moreover, E-cadherin inhibited interaction of EGFR with downstream components like Sos, Grb2, PLCγ and Cbl thereby preventing signaling and internalization of EGFR [57]. As a consequence, inhibition of homotypic interactions by an E-cadherin neutralizing antibody induced an increase in DNA synthesis [49,51]. Moreover, E-cadherin mutations found in diffuse gastric cancer enhanced activation of EGFR and downstream components like Grb2, Shc and p38 MAPK resulting in the acquisition of a motile phenotype [58–60].

2. Architecture of the mammary gland

Mammary gland development and structure

In the mammary gland, E-cadherin is expressed by luminal epithelial cells while myoepithelial cells express P-cadherin (reviewed in [61,62]). These two cell types form the epithelial bilayer that lines the ducts of the mammary gland. At birth, the mammary gland only consists of a primitive ductal system that becomes fully branched during puberty through a process called branching morphogenesis (reviewed in [63]). During this period, the tip of each duct, also known as terminal end bud (TEB), starts to proliferate and migrate into the mammary fat pad. The outer monolayer of these buds is formed by cap cells which penetrate the basal lamina and ultimately give rise to the myoepithelial cell layer [64,65] that can be distinguished by cytokeratin (CK) 14, CK5 and smooth muscle actin (SMA) expression [66]. Body cells form the inner cell layers of the terminal end buds and collectively migrate alongside the cap cells and give rise to the luminal epithelial layer [64,65] (Figure 2A). These luminal cells express several markers including CK8, CK18 and CK19 [66]. Contractile properties of myoepithelial cells enable excretion of milk produced by alveolar cells, which have differentiated from

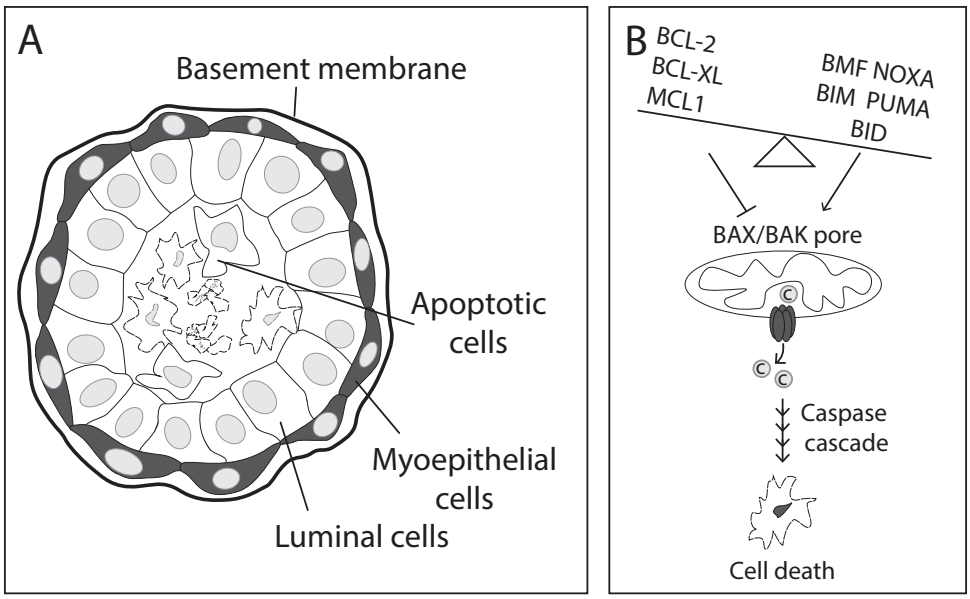

Figure 2 Lumen formation in mammary ducts
A. Schematic representation of the mammary duct. Myoepithelial and luminal cells form a bilayer that lines mammary ducts while being surrounded by a basement membrane. Release of cell-cell and cell-matrix interaction of inner luminal cells induces apoptosis.
B. Intrinsic apoptosis is induced by BAX/BAK oligomerization as a result of the balance between anti-apoptotic (left) and pro-apoptotic proteins (right). Upon BAX/BAK pore formation, cytochrome C (C) is released from the mitochondriainto the cytoplasm where it induces activation of the proteosomal caspase cascade leading to cell death.

luminal progenitors and form the secretory lobular structures of the mammary ductal system (reviewed in [67]). These milk-producing compartments however are only expanded during pregnancy. Upon termination of lactation the mammary gland undergoes a process called involution, which involves clearing of the alveoli through extensive apoptosis, resulting in a resting state similar to the adult virgin mammary gland (reviewed in [68]).

Controlled cell death during mammary gland morphogenesis

During formation of the mammary gland, the ducts are initially completely filled with luminal body cells forming a solid tubular structure. To form a hollow lumen, controlled cell death of these inner cells has to take place [69] (Figure 2). This apoptotic process is a result of the inner cells losing their interaction with surrounding cells and the extracellular matrix (ECM), a process known as anoikis [70,71]. This involves activation of the intrinsic apoptosis pathway leading to cleavage and activation of caspase-3 which induces a proteolytic cascade to control cell death. Activation of caspase-3 in the intrinsic pathway is triggered by cytochrome C release from mitochondria upon membrane pore formation by BAX and BAD oligomerization. These two pro-apoptotic proteins are part of the BCL2 family of pro- and anti-apoptotic proteins. Anti-apoptotic proteins include BCL-2, BCL-XL and MCL1 which interact with the aforementioned BAX and BAD to prevent their oligomerization. Next to BAX and BAD, there

is another group of pro-apoptotic proteins that are known as BH3-only proteins. In contrast to BAX and BAD these proteins do not perforate mitochondria but instead favor BAX and BAD oligomerization (reviewed in [72]) (Figure 2B).

During formation of the ductal lumen in MCF10A cells in 3D culture, controlled cell death occurs via upregulation of BMF and BIM [73–75]. Conversely, resistance to anoikis could be induced by increased growth factor signaling; hyperactive PI3K/AKT inhibited BMF upregulation induced by matrix detachment, and prevented anoikis [75]. In addition, constitutively activated MEK could inhibit both *BIM* and *BMF* mRNA upregulation in suspension [73,75]. Interestingly, overexpression of anti-apoptotic proteins BCL-XL or BCL2, or proteins that induce hyper-proliferation such as Cyclin D1, was not sufficient to prevent lumen formation in 3D culture of MCF10A cells. In contrast, overexpression of Her2 or oncogenic vSrc, proteins capable of inducing proliferation and at the same time inhibiting apoptosis, quickly resulted in a high degree of luminal filling, pointing towards the importance of both proliferation and resistance to apoptosis in evading ductal clearance [73,75].

During involution in the mouse mammary gland, both *Bmf* and *Bim* were transcriptionally upregulated via Stat5 and required for epithelial clearance [75,76]. Moreover, apoptosis in TEBs was inhibited by a mammary gland specific *Bim* knockout. However, later during development cells filling the luminal space were cleared nonetheless, likely due to redundancy by other pro-apoptotic factors or caspase-independent apoptosis [77]. So far, no in vivo role for BMF in anoikis of luminal cells in TEB morphogenesis has been described [75].

E-cadherin in the mammary gland

The function of E-cadherin in the mammary gland has been studied using a variety of temporal and cell-type specific Cre recombinases. This identified a function for E-cadherin in the survival and differentiation of alveolar epithelial cells as reduced milk production and increased apoptosis at parturition was observed in *MMTVCre;Cdh1$^{flox/ko}$* mice [78]. During terminal endbud differentiation however, study of E-cadherin function has remained difficult as loss of E-cadherin in the mammary gland is not tolerated [78–80]. This is likely due to mosaic Cre expression causing E-cadherin wildtype cells to compensate for the effects of E-cadherin loss, resulting in normal gland development [81,82]. However, orthotopic transplantation and organoid cultures have revealed that E-cadherin is required during formation, branching and maintenance of the epithelial ductal network [83,84]. E-cadherin knockout mammary epithelial cells were unable to form 3D polarized ductal structures *in vitro*. Instead, multilayered structures without a lumen were formed, suggesting the involvement of E-cadherin in the apoptotic process during lumen formation [84]. Giving the stabilizing function of p120 at the AJ, it was not surprising that inactivation of p120 in the mammary gland resulted in a similar phenotype. This phenotype was characterized by an exclusion of p120 negative cells in TEB morphogenesis ultimately leading to a healthy mammary gland consisting of p120 wildtype cells [85].

3. Invasive lobular breast cancer

Loss of E-cadherin in breast cancer

In order for tumor growth and metastatic dissemination to occur, epithelial cells have to acquire several characteristics including sustained proliferation, resistance to programmed cell death, local invasion, intra- and extravasation, and colonization (reviewed in [86]). Given the aforementioned functions of the AJ it is not surprising that loss of E-cadherin is frequently observed in advanced cancers (reviewed in [87]). In the majority of tumor types E-cadherin loss is transcriptionally regulated via promotor hyper-methylation or increased expression of transcriptional repressors of E-cadherin (reviewed in [88]). In invasive lobular breast carcinoma (ILC) and diffuse gastric carcinoma however, genetic lesions in the *CDH1* gene encoding E-cadherin are frequently observed [89–91]. Invasive lobular carcinoma accounts for 10-15% of all invasive breast cancer cases. As such, it is the second most common subtype of breast cancer after invasive ductal carcinoma (IDC). IDC comprises 75-80% of all invasive breast cancers but consists of a heterogeneous group of tumors encompassing a large variety of histological entities [92,93].

In ILC, genetic lesions in *CDH1* are mostly somatic frame-shift mutations that are often accompanied by loss of heterozygosity [94–96]. Alternatively, transcriptional silencing of E-cadherin due to promotor methylation has also been observed in ILC [95,96], although this has been questioned recently [97]. In total, approximately 90% of all ILC cases show uniform loss of E-cadherin protein expression [94,98]. Interestingly, E-cadherin is already inactivated in lobular carcinoma *in situ* (LCIS) [99], suggesting that this a driver event in ILC development. Indeed, causality was established using conditional mouse models in which E-cadherin and p53 were inactivated in the mouse mammary gland. In these mice metastatic tumors developed that resembled human ILC morphology and dissemination patterns [79,80].

ILC morphology and treatment

The majority of ILC is of the classic subtype and consists of small cells that are characterized by monomorphous, rounded nuclei and a low mitotic index. Invasive ILC cells grow in a non-coherent pattern forming rows of single cells known as indian files [100,101]. Because of this growth pattern no distinct mass is formed, which hampers the detection by palpation or standard mammography [102]. In addition to classical ILC, several subtypes can be distinguished based on morphology, including pleomorphic, solid and alveolar ILC (reviewed in [103]).

The estrogen receptor (ER) and progesterone receptor (PR) are expressed in the majority of ILC, a feature that renders this subtype susceptible to endocrine therapy [104]. Surprisingly, in spite of the expression of these favorable hormone receptors, the prognosis of ILC patients not better than other breast cancer subtypes [101,105]. This has been attributed to low chemo-responsiveness and resistance to endocrine therapy [104–106]. Over the last five years, much effort has been put into developing additional targeted therapies based on the signaling pathways that drive the breast cancer progression and those conferring resistance to therapy (reviewed

in [107–109]). Unfortunately, clinical success has remained low due to insufficient knowledge about pathway crosstalk, mechanisms of resistance and unanticipated side effects, providing a rationale for a continuous effort to unravel the signaling mechanisms.

Catenin expression in ILC

Loss of E-cadherin in cancer leads to loss of cell-cell adhesion and dismantling of the AJ complex. In breast cancer, loss of E-cadherin coincides with loss of β-catenin. This means that Wnt signaling, at least mediated via β-catenin, does not contribute to ILC development or progression [96,110–113]. In contrast, expression of α-catenin is preserved in ILC and is essential for survival of ILC cells in vitro (our unpublished data). In contrast, upon loss of the scaffolding function of E-cadherin at the membrane, p120 is not degraded but instead becomes diffusely localized throughout the cytoplasm and nucleus [11,110–112,114]. This staining pattern is a distinct feature of lobular breast lesions and can be used to distinguish them from ductal tumors, even at the in situ stage [115–117]. Additionally, even in E-cadherin-expressing ILC, the integrity of the adherens junction complex is impaired and associates with cytoplasmic p120, advocating for the use of this protein in diagnostics [118].

Activated pathways in ILC

Five distinct intrinsic breast cancer subtypes have been identified based on mRNA expression profiling: luminal A, luminal B, normal-like, Her2-amplified and basal-like, of which the latter two have the shortest overall survival and relapse-free survival [119–122]. When comparing these molecular subtypes to histopathological subtypes there is not a clear overlap although the majority of ILC can be categorized as luminal A [97,123]. Analysis of signaling pathways in ILC and IDC based on mRNA and (phospho) protein expression data revealed differential activation of several pathways including fatty acid metabolism, cell migration, DNA repair, proliferation and cell adhesion [123–126]. Recently, two research groups reported on the molecular profile of ILC based on genomic and expression data from 126 ILC and 490 IDC cases present in the cancer genome atlas (TCGA) database [97], and a cohort of 144 ILCs selected from the rational therapy for breast cancer (RATHER) consortium [127]. Since the gene encoding E-cadherin (*CDH1*) is located on *16q*, it was no surprise that loss of that chromosome arm was frequently observed in ILC [97,125,127,128]. Additionally, while *CDH1* is the most frequently mutated gene, mutations in *PIK3CA* (encoding p110α, the catalytic subunit of PI3K) were another dominant feature of ILC as it was observed in 33-48% of ILC patients [97,127,129,130], while in (ductal) breast cancer the frequency lay between 22% and 33% [97,129,131,132]. Interestingly, several other mutations activating the PI3K pathway were frequently observed in ILC [127]. These included activating mutations in other PI3K subunits, *AKT1*, and inactivating mutations and/or focal loss of *PTEN*, a negative regulator of PI3K signaling [97,127]. To study activation of the PI3K pathway, assessment of AKT phosphorylation at serine 473 or threonine 308 marking activation by the mTorc2 complex [133] or PDK1 [134] respectively, is common practice. Phosphorylation status of downstream targets such as p70S6K, 4EBP1 or mTor [135], or mRNA and protein expression profiling, are also in use as markers of pathway activation. Assessment of the expression of these markers confirmed hyperactivation of PI3K signaling in ILC [97]. Interestingly, in contrast to

loss of *PTEN*, the mutation status of *PIK3CA* was not a good predictor for pathway activation, suggesting that a mutation in p110α is not sufficient to hyperactivate the PI3K pathway [97,130,131,136,137].

Oncogenic and tumor-suppressor functions of p120 in the breast

Decreased p120 levels were linked to increased aggressiveness, poor prognostic markers and/or reduced survival in several tumor types including breast cancer, suggesting a tumor suppressive function of p120 [10,138–140]. Accordingly, dual inactivation of p120 and p53 in the mammary gland resulted in the development of metastatic tumors [56]. However, in spite of the function of p120 in stabilizing the AJ complex, the tumors formed in these *Wcre;Ctnnd1$^{F/F}$;Trp53$^{F/F}$* mice did not phenocopy the ILC model, but instead led to the development of high-grade, EMT-like IDC tumors. In this *Wcre;Ctnnd1$^{F/F}$;Trp53$^{F/F}$* model, loss of p120 contributed to tumor progression by inducing anoikis resistance. Additionally, loss of p120 increased sensitivity to growth factors, possibly through relieving the inhibitory function of E-cadherin on RTKs as described above [56]. A tumor suppressive function for p120 was confirmed in the gut, salivary gland, upper gastrointestinal (GI) tract and skin. Ablation of p120 in these organs destabilized the AJ and coincided with increased proliferation, leading to hyperplasia in the salivary gland and skin, and tumors in the gut and upper GI tract [141–145].

As described above, stabilization of the junction is not the sole function of p120. Relocalization of p120 upon E-cadherin loss facilitates the interaction of p120 with its cytosolic and nuclear interaction partners. These additional functions of p120 could explain the different tumor types arising in *Wcre;Cdh1$^{F/F}$;Trp53$^{F/F}$* and *Wcre;Ctnnd1$^{F/F}$;Trp53$^{F/F}$* mice [56,80]. In ILC, cytosolic p120 was shown to mediate Rock-dependent anchorage-independent survival through binding and inhibition of MRIP, an antagonist of Rho/Rock. As a consequence, loss of p120 in mouse LC cells resulted in reduced anoikis resistance which was accompanied by a reduced capability to form tumors and to metastasize *in vivo*, putting p120 forward as an oncogene in ILC [112]. In other E-cadherin negative breast cancer cells (MDA-MB-231 and SKBR-3) p120 also mediated anchorage independent growth and additionally increased migration and invasion [114]. However, these oncogenic effects were attributed to p120 mediated activation of Rac1 [114,146] through a mechanism that required stabilization of p120 by mesenchymal cadherins [146,147]. These results indicate that, depending on the cell type and oncogenic drivers, the effect of p120 on Rho GTPase signaling can be different.

4. Transcriptional regulation by Kaiso

Structure and expression of Kaiso

Kaiso is encoded by the *ZBTB33* gene on the X chromosome and is ubiquitously expressed in many cell types [23,148]. The protein consists of the aforementioned C2H2-type ZFs, and a C-terminal BTB/POZ (Broad complex, Tramtrac, Bric-a-brac/POx virus and Zinc finger) domain. This highly conserved BTB/POZ domain can be found in more than 60 ZF transcription factors and ensures protein-protein interactions, thereby regulating localization, expression and

positioning within transcription regulation complexes (reviewed in [149,150]). The BTB/POZ domain is essential for Kaiso homodimerization [23,151] and stabilization of the interaction of the ZF domain with the DNA [24,25]. Also, the BTB/POZ domain mediates interaction with other proteins such as CTCF [152], p53 [153], NCoR1 [154], p300 [153] and znf131 [155], which will be discussed later (Figure 3). In cultured cells Kaiso is mostly expressed in the nucleus [23,156,157], which is dependent on the NLS present in Kaiso [158]. In contrast, Kaiso expression *in vivo* is mostly cytoplasmic [148,159]. Interestingly however is the observation that upon transplantation of human colorectal cancer cells into mice, Kaiso relocalized to the cytosol, while transfer back to an *in vitro* setting reversed this phenotype [148]. These data suggest that a microenvironmental cue regulates localization of Kaiso.

Two faces of Kaiso: bimodal DNA binding capacity

The first direct interaction of Kaiso with genomic DNA was mapped to methylated CpG dinucleotides in an intron of the *S100A4* gene [160]. *In vitro*, also binding to hemimethylated or a single methylated CG dinucleotide has been observed [25]. Binding of Kaiso to methylated CpGs enabled Kaiso to repress transcription in a methylation-dependent manner as shown by a reporter assay containing repeats of the S100A4 motif [160]. After this initial observation, several other genes have been identified that are repressed by Kaiso binding to methylated CpGs. These include *MTA2* (Metastasis associated family member 2, [154,161]) and *CDKN2A* (Cyclin-dependent kinase inhibitor 2A, [162]) (Figure 4A). Interestingly, Kaiso is also able to interact with

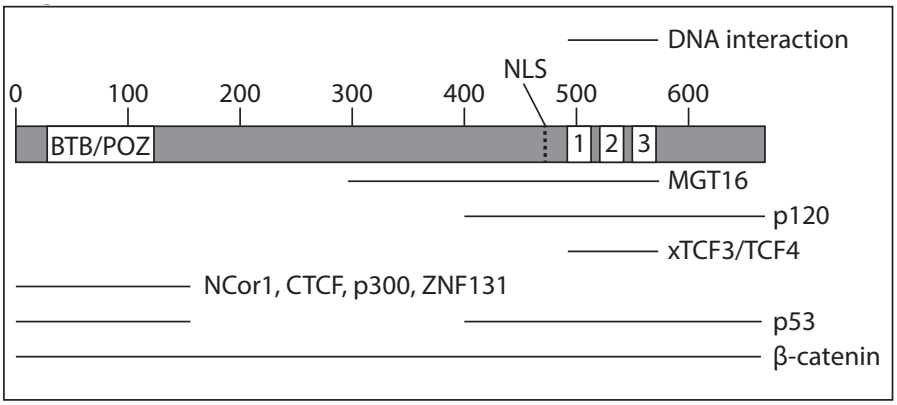

Figure 3 Schematic representation of Kaiso structure
Kaiso consists of a C-terminal BTB/POZ and three N-terminal ZF domains (1-3). Shown are the interaction domains of Kaiso with the DNA and various proteins. NLS: nuclear localization sequence.

a methylation-independent classic Kaiso Binding Sequence (cKBS; TCCTGCNA) [26] via the same three ZFs as those involved in binding to methylated CpGs [24,25]. Like the binding of Kaiso to methylated CpGs, binding to this cKBS repressed the expression of oncogenes that include *MMP7* (metalloproteinase 7, [23]) and *Wnt11* [27](Figure 4A). Additionally, like its family members Miz-1 and ZF-5 [163,164], Kaiso did not only function as a repressor but was also observed to directly activate transcription; in myotubes, Kaiso induced transcription of *Rapsyn* by binding

to the cKBS in the promotor of this gene [165]. Subsequent genome-wide analysis only identified the cKBS in a small subset of Kaiso binding sites, whereas binding to regions containing CpGs was clearly enriched [166,167]. However, bisulfite sequencing revealed that methylation levels at these CpG-containing binding sites were below 20%, thereby questioning the requirement of DNA methylation for Kaiso-binding to CpGs *in vivo* [166].

Transcriptional regulation by Kaiso via chromatin modification

Similar to its family members PLZF and BCL-6 [168,169], Kaiso forms a complex with nuclear receptor corepressor 1 (NCoR1) and silencing mediator of retinoic acid and thyroid hormone receptor (SMRT, also known as NCoR2) in a cell-type and/or species-specific manner [154,167]. SMRT and NCoR1 proteins often form a complex with G protein pathway suppressor 2 (GPS2), transducin β-like protein 1 (TBL1), TBL1-related protein 1 (TBLR1) and histone deacytelase 3 (HDAC3), which ensures histone deacetylation [170]. Indeed, at the methylated *MTA2* promotor, Kaiso mediated recruitment of NCoR1, HDAC3 and TBL1 [154]. While the interaction of Kaiso with NCoR1 and SMRT was identified at Kaiso binding sites containing CpGs, myeloid translocation gene 16 (MTG16) was identified as a Kaiso binding partner and cofactor specifically at the cKBS in the MMP7 promotor [171]. Since MTG16 has been shown to interact with NCoR [172], this suggests that a similar set of cofactors is recruited to methylated CpGs and to the cKBS. Given the presence of chromatin modifiers in the corepressor complexes recruited by Kaiso, Kaiso is likely to act as a transcriptional repressor by altering the chromatin landscape, thereby influencing the recruitment of general transcription factors (reviewed in [173,174]). Indeed, depletion of Kaiso resulted in increased levels of markers of active transcription at the *Siamois* and methylated *MTA2* promotor [154,175]. Genome-wide assessment of the influence of Kaiso on the chromatin status however has not been performed yet.

Interaction of Kaiso with other transcription factors

Besides Kaiso binding to corepressors, Kaiso interacts with several DNA-binding transcription factors (Figure 4B). In a yeast two-hybrid screen for interaction partners of Kaiso the transcriptional activator ZNF131 was identified as a direct binding partner. Although Kaiso did not directly bind to the ZNF131 DNA-binding-element, interaction of Kaiso with ZNF131 inhibited the activating function of ZNF131. This suggests that Kaiso functions as a cofactor, possibly by preventing interaction of ZNF131 with the DNA or by controlling the recruitment of co-activator and/or co-repressor complexes [155]. Another yeast two-hybrid screen identified Kaiso as a direct binding partner of CTCF. CTCF is known to be present at insulator regions which are responsible for the partitioning of genomic DNA into transcriptionally active and inactive regions (reviewed in [176]). At the 5' β-*globin* insulator, CTCF acted as an enhancer blocker by establishing chromatin loops, thereby physically separating the enhancer from the promotor, resulting in inhibition of β-*globin* transcription [177]. Examination of the 5' β-globin insulator region revealed binding of Kaiso to the cKBS 30 basepairs upstream from the CTCF binding site. Binding of Kaiso to this cKBS inhibited the enhancer blocking function of CTCF, resulting in increased β-*globin* gene expression thereby putting Kaiso forward as an indirect transcriptional activator [152].

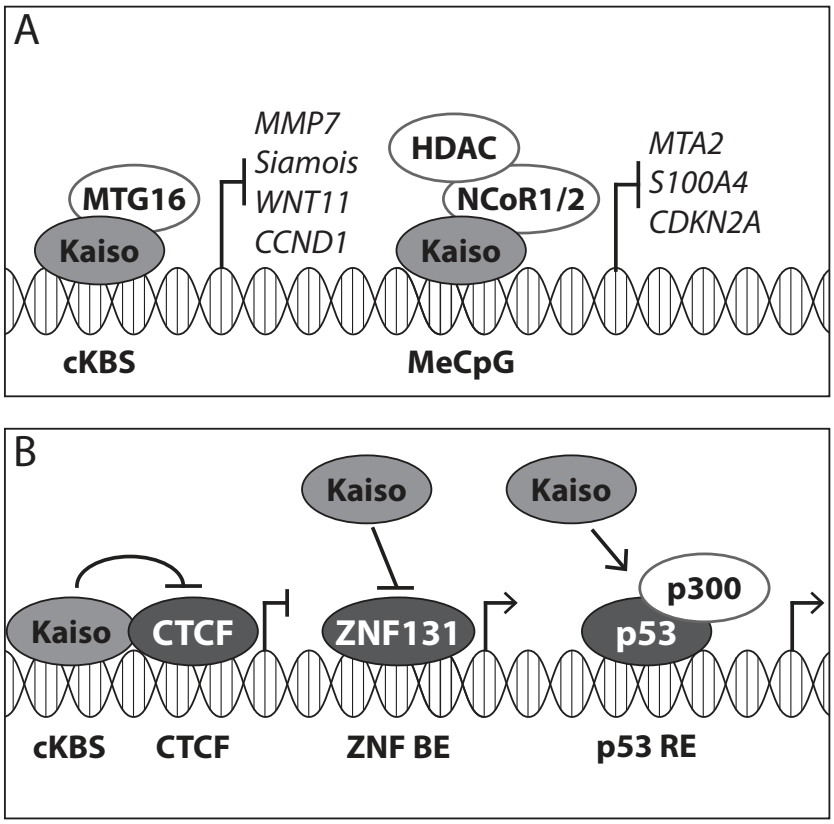

Figure 4 Regulation of transcription by Kaiso
A. Direct transcriptional repression by Kaiso at the cKBS and methylated CpGs. At the cKBS Kaiso interacts with the corepressor MTG16 and enables repression of *MMP7, Siamois, WNT11* and *CCND1.* Transcriptional repression of *MTA2, S100A4* and *CDKN2A* by Kaiso occurs through binding to methylated CpGs (MeCpG). At these sites, Kaiso interacts with NCoR1 or SMRT (NCor2) in complex with HDAC. B. Indirect transcriptional regulation of Kaiso by influencing transcriptional activity of Kaiso binding partners. Left: interaction of Kaiso with CTCF blocks the enhancer blocking function of CTCF, resulting in β-globin expression. Middle: interaction of Kaiso with ZNF131 inhibits the transcriptional activity of ZNF131. Right: Interaction of Kaiso with p53 and p300 increases binding of this complex to the DNA, thereby increasing p53 target gene expression. ZNF BE: ZNF131 DNA binding element. p53 RE: p53 responsive element.

Moreover, Kaiso can indirectly control p53-mediated transcriptional activation upon DNA-damage. Kaiso interacted with p53 and p300 at a p53-responsive element, resulting in acetylation of p53. This modification stabilized the binding of p53 and p300 to the p53-responsive element, which enhanced the expression of pro-apoptotic genes [153]. The ability of Kaiso to influence gene expression in collaboration with CTCF and p53 only occurred when CTCF and p53 were bound to the DNA, which points to a cofactor role for Kaiso to drive gene transcription [152,153].

Kaiso and Wnt crosstalk in development

Since the discovery of xWnt11 and Siamois as direct and p120-dependent Kaiso targets [27,175], much research has focused on the interplay between Kaiso and Wnt signaling. Canonical Wnt signaling is characterized by retention of β-catenin in the cytosol and nuclear translocation of β-catenin where it binds to TCF/LEF transcription factors and mediates transcription of Wnt target genes [178]. Interaction between Kaiso and Wnt signaling occurs at several levels. First, a direct interaction between Kaiso and TCF4/xTCF3 and β-catenin results in an inhibition of Kaiso and TCF binding to their target DNA [162,175,179,180]. Second, several Wnt target genes contain a cKBS in close proximity to a TCF binding site [175,179,181]. Third, Kaiso-mediated transcriptional regulation could be influenced by upstream canonical Wnt signaling through CK1-dependent phosphorylation of p120 at serine 268. This event resulted in a reduced binding affinity of p120 to E-cadherin while p120 binding to Kaiso was increased. Functionally, increased binding of p120 to Kaiso prevented Kaiso-mediated repression of the β-catenin/TCF4 transcriptional complex [162]. Finally, Wnt-induced binding of Frodo to p120 protected p120 from GSK3-β-mediated proteosomal degradation, also resulting in increased p120-Kaiso interaction and decreased Kaiso-DNA binding [182,183].

As regulation of Wnt signaling is key to proper vertebrate development (reviewed in [184]), it is not surprising that loss of Kaiso in Xenopus and zebrafish embryos caused major developmental defects at the gastrulation stage [27,175,185]. Surprisingly, Kaiso knockout mice were viable, fertile and did not display overt developmental phenotypes or differential expression of the Kaiso target genes *Wnt11, Mta2, Rapsyn* or *S100a4* [186]. Redundancy of Kaiso family members ZBTB4 and/or ZBTB38 could be an explanation for this lack of phenotype, since these two family members contained highly similar ZF and BTB/POZ domains [150]. Like Kaiso, both ZBTB4 and ZBTB38 were capable of binding to methylated DNA and MTG16 [171].

Linking Kaiso to cancer

BTB/POZ family members that have been previously implicated in cancer development include BCL6 and PLZF which are involved in non-Hodgkin's lymphoma and acute promyelocytic leukemia respectively (reviewed in [150]). Kaiso is potentially another BTB/POZ family member involved in tumor formation and/or progression since it represses several known oncogenes and because it is involved in Wnt signaling, a well-known oncogenic pathway [178]. *In vivo* studies on the contribution of Kaiso to cancer have been performed in the $APC^{min/+}$ mouse model for Wnt-driven intestinal cancer. Conditional loss of Kaiso in this tumor model delayed tumor onset [186]. Conversely, the introduction of a Kaiso transgene in this model reduced survival and increased polyp burden [187].

Loss of Kaiso in lung cancer cells increased the expression of the Kaiso target *MMP7*, which enhanced the invasive capacity of lung cancer cells *in vitro* [188]. In contrast, invasive breast and prostate cancer cell lines displayed a less migratory and invasive phenotype upon loss of Kaiso [189–191]. Relief of transcriptional repression by Kaiso was observed to increase metastatic capacity in mouse ILC cells; upon transfer to anchorage independence, an increase in nuclear

p120 and a subsequent relief of Kaiso-mediated repression of Wnt11 expression led to an increase in RhoA activation driving anoikis resistance [111]. Another tumor suppressive role for Kaiso was attributed to its ability to inhibit cell cycle progression in lung cancer cells [157,188,192], which is likely mediated via repression of the Kaiso target gene *CCND1* (encoding Cyclin D1 [28,192]). Also, as described above, Kaiso was involved in p53-mediated cell cycle arrest and apoptosis upon DNA damage. In fact, administration of the DNA damaging agent etoposide induced upregulation of Kaiso, enabling increased p53-mediated expression of target genes like *CDKN1A* and *PUMA*, while loss of Kaiso rendered these cells more resistant to etoposide [153].

Relocalization and altered expression levels of Kaiso also suggested a role for Kaiso in cancer. Increased cytoplasmic expression levels of Kaiso have been observed during the progression of thymic carcinomas, non-small cell lung cancer and colorectal cancer[29,187,188,193]. In lung cancer, increased cytoplasmic levels associated with a higher stage and decreased overall survival [29,161,188] while nuclear Kaiso in prostate tumors and IDC associated with high-grade tumors [159,189,190]. Moreover, in ILC and lung carcinomas cytoplasmic Kaiso associated with cytoplasmic p120 [29,159], supporting the idea that p120 facilitates nuclear/cytosolic Kaiso shuttling. In cultured cells however, Kaiso expression was restricted to the nucleus, suggesting that microenvironmental cues might control Kaiso localization [111]. Given the high frequency of E-cadherin loss and subsequent relocalization of p120 in cancer, Kaiso can function as a potential regulator of tumorigenesis in a wide variety of tumors, including ILC.

Outline of this thesis

This thesis focuses on the effect of E-cadherin loss on the progression of breast cancer. Chapter 2 studies the contribution of p120, an E-cadherin stabilizing factor that is translocated to the cytosol in invasive lobular breast cancer (ILC), to the development of this disease. Complex genetic mouse models are used to enable somatic inactivation of p120 in a mammary-specific conditional E-cadherin and p53 mouse model of human ILC. The findings in this chapter reveal a critical role for p120 in the formation of ILC. In Chapter 3 we identify repression of the pro-apoptotic BH3-only protein BMF as a critical step that controls anchorage independence in E-cadherin negative metastatic breast cancer cells. We show that E-cadherin loss leads to growth factor signaling-dependent inhibition of FOXO3; a cue that prevents transcriptional activation of BMF. In Chapter 4 we determined pathway activation in ILC using reverse protein arrays and demonstrate that increased autocrine-induced PI3K/AKT activation is a direct result of E-cadherin loss. In addition, we show that endogenous PI3K/AKT signals are essential for ILC cell growth and survival, which opens options for clinical intervention. Next, Chapter 5 explores the genome-wide binding sites of Kaiso to map its target genes in breast cancer. This shows that Kaiso functions as a modulator of actively transcribed genes involved in cell cycle and DNA damage processes. Finally, the findings in this thesis and their implications for clinical intervention of E-cadherin mutant breast cancer are summarized and discussed in chapter 6.

Chapter 2

p120-Catenin is critical for the development of invasive lobular carcinoma in mice

Milou Tenhagen[1], Sjoerd Klarenbeek[2], Tanya M. Braumuller[2], Ilse Hofmann[3,4], Petra van der Groep[5],Natalie ter Hoeve[1], Elsken van der Wall[5], Jos Jonkers[2] and Patrick W. B. Derksen[1]

[1] Department of Pathology, University Medical Center Utrecht, Utrecht, The Netherlands
[2] Division of Molecular Pathology, The Netherlands Cancer Institute, Amsterdam, The Netherlands
[3] Vascular Oncology and Metastasis, German Cancer Research Center (DKFZ), Heidelberg, Germany
[4] Vascular Biology and Tumor Angiogenesis, Medical Faculty Mannheim, Heidelberg University, Heidelberg, Germany
[5] Department of Medical Oncology, Cancer Center, UMC Utrecht, Utrecht, The Netherlands

Accepted in Journal of Mammary Gland Biology and Neoplasia (Advance online publication July 2016)

Abstract

Loss of E-cadherin expression is causal to the development of invasive lobular breast carcinoma (ILC). E-cadherin loss leads to dismantling of the adherens junction and subsequent translocation of p120-catenin (p120) to the cytosol and nucleus. Although p120 is critical for the metastatic potential of ILC through the regulation of Rock-dependent anoikis resistance, it remains unknown whether p120 also contributes to ILC development. Using genetically engineered mouse models with mammary gland-specific inactivation of E-cadherin, p120 and p53, we demonstrate that ILC formation induced by E-cadherin and p53 loss is severely impaired upon concomitant inactivation of p120. Tumors that developed in the triple-knockout mice were mostly basal sarcomatoid carcinomas that displayed overt nuclear atypia and multinucleation. In line with the strong reduction in ILC incidence in triple-knockout mice compared to E-cadherin and p53 double-knockout mice, no functional redundancy of p120 family members was observed in mouse ILC development, as expression and localization of ARVCF, p0071 or δ-catenin was unaltered in ILCs from triple-knockout mice. In conclusion, we show that loss of p120 in the context of the p53-deficient mouse models is dominant over E-cadherin inactivation and its inactivation promotes the development of basal, epithelial-to-mesenchymal-transition (EMT)-type invasive mammary tumors.

Introduction

Loss of E-cadherin is a driver event in cancer that has been linked to tumor development and progression [87]. In breast cancer, mode and timing of E-cadherin inactivation appears to determine tumor type and etiology [194]. In diffuse gastric cancer and invasive lobular breast cancer (ILC), E-cadherin loss is an early and causative lesion [89,94,99,116,195], while most other tumors show loss of E-cadherin during later stages of disease progression (reviewed in: [196]). Cre-lox based conditional mouse models have demonstrated that mutational inactivation of E-cadherin in the mammary gland is not tolerated, leading to clearance of E-cadherin negative cells [78,79]. However, in the context of p53 deficiency, E-cadherin loss induces the formation and progression of mouse ILC (mILC), which mimics its human counterpart in phenotype and metastatic dissemination [79,80].

As an integral part of the adherens junction (AJ), E-cadherin is responsible for homotypic cell-cell connections [197]. E-cadherin stability and turnover is regulated by p120- catenin (p120), an armadillo-repeat containing molecule that binds directly to the E-cadherin juxtamembrane domain at the cell cortex [12,13]. In ILC cells, loss of E-cadherin results in a translocation of p120 to the cytosol [114–116], where it controls constitutive activation of autocrine induced RhoA-Rock signaling, which underpins actomyosin-dependent anoikis resistance and subsequent tumor dissemination [111,112]. In contrast, p120 expression patterns in ductal breast cancers are not related to E-cadherin expression [97]. Localization of p120 can therefore be used to aid differential diagnosis between ductal and lobular breast cancer [115,198].

Three closely related p120 family members can be found in vertebrates: ARVCF, δ-catenin (*CTNND2*) and p0071 (*PKP4*) [199]. Although these family members can also bind and stabilize E-cadherin [16], their redundancy in relation to each other has only been partially addressed. Of note, p120 appears to have evolved together with the non-neural classical cadherins, separately from ARVCF, δ-catenin and p0071, suggesting different functional roles [199].

Although loss of p120 leads to a dissociation of the AJ, conditional loss of p120 in the mouse mammary gland in combination with p53 does not lead to ILC formation but instead induces the formation of high-grade metaplastic-type ductal tumors that metastasize to lungs and lymph nodes [56]. These observations showed that, although the effect of AJ inactivation is the acquisition of tumor invasion and metastasis, the phenotypical outcome of the resulting tumor is determined by the AJ member that is inactivated. To study the contribution of p120 to the development of ILC we introduced a p120 conditional allele [141] into the mILC mouse model [80], and observed that concomitant loss of p120 at the early stages of tumor development largely prevents the formation of mouse ILC (mILC). Our studies indicate that p120 is a crucial factor in ILC etiology.

Results

Early loss of p120 constrains formation of ILC in *Wcre;Cdh1$^{F/F}$;Trp53$^{F/F}$* female mice

Using two independent tissue-specific Cre drivers (*K14cre* and *Wcre*) it was previously shown that combined loss of E-cadherin (encoded by *Cdh1*) and p53 (encoded by *Trp53*) in mouse mammary epithelium results in the formation of tumors that resemble human invasive lobular carcinoma (ILC) [79,80]. To study the contribution of p120 to the development of ILC we introduced a previously generated conditional p120 (Ctnnd1F) allele [141] into the *Wcre;Cdh1$^{F/F}$;Trp53$^{F/F}$* ILC model [80] to produce *Wcre;Ctnnd1$^{F/+}$;Cdh1$^{F/F}$;Trp53$^{F/F}$* and *Wcre;Ctnnd1$^{F/F}$;Cdh1$^{F/F}$;Trp53$^{F/F}$* (Triple Knock Out: TKO) female mice that were followed for tumor

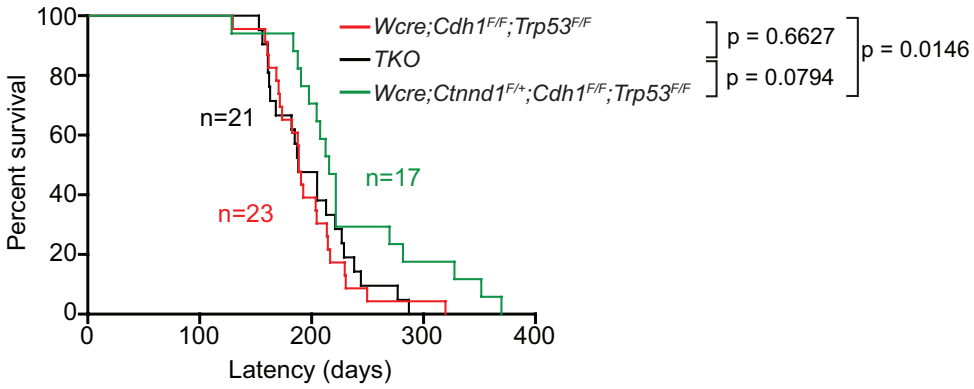

Figure 1 Tumor incidence in Wcre females carrying conditional *Ctnnd1, Cdh1* and *Trp53* alleles
Kaplan-Meier tumor-free survival curves are shown for mammary tumors from *Wcre;Cdh1$^{F/F}$;Trp53$^{F/F}$* (red curve) TKO (black curve) and *Wcre;Ctnnd1$^{F/+}$;Cdh1$^{F/F}$;Trp53$^{F/F}$* (green curve). Mice were sacrificed when tumors reached an average diameter of 10 mm.

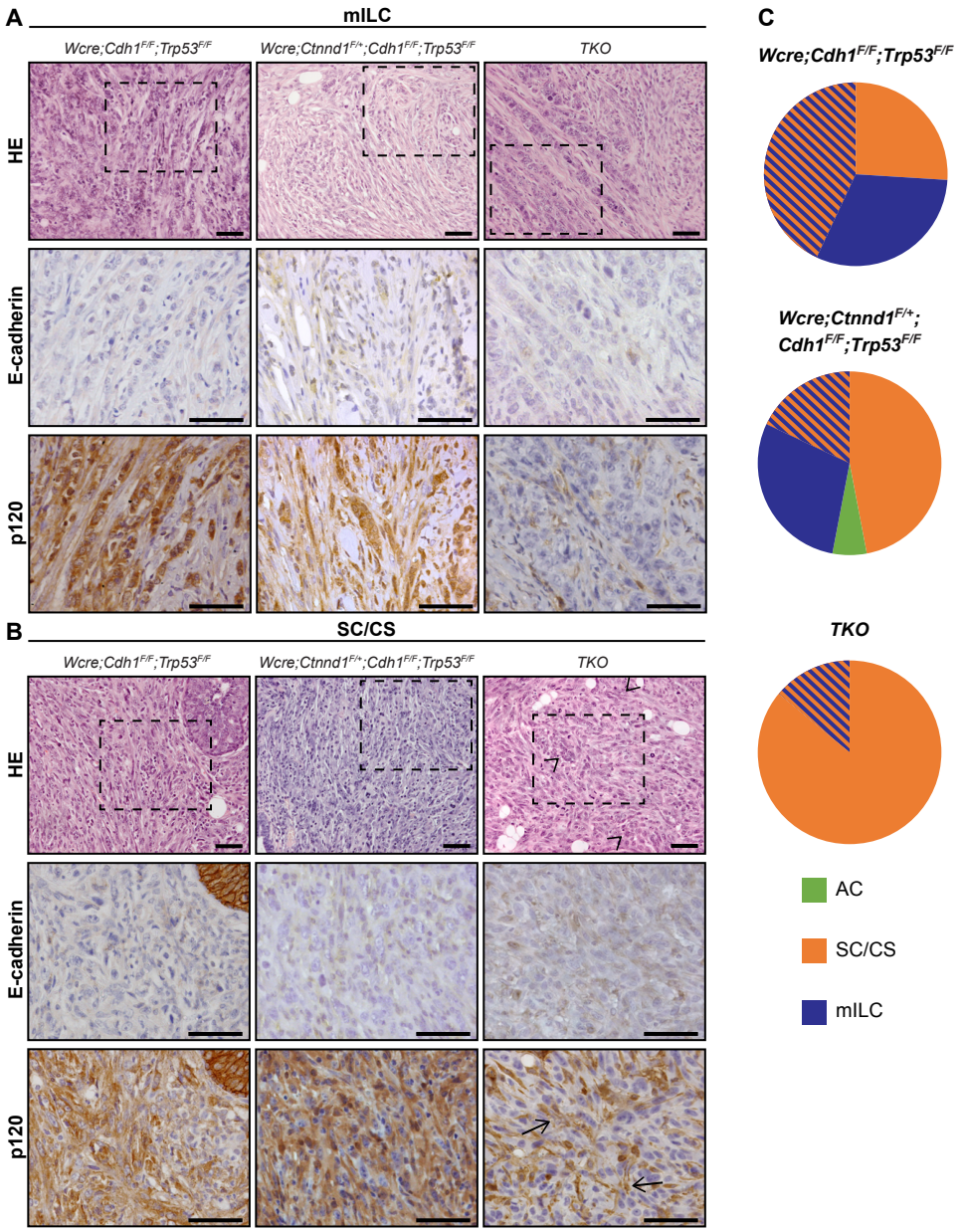

Figure 2 E-cadherin and p120 expression in the mammary tumor spectrum
A-B Sections showing representative examples for mouse ILC (mILC) (A) and solid carcinoma/carcinosarcoma (SC/CS) (B) for the different genotypes studied. Sections were stained for E-cadherin (middle panels) and p120 (bottom panels). In TKO tumors p120 is only expressed by stromal cells (arrows). Nuclear atypia is present in p120 negative tumors (arrow heads). The middle and bottom panels are magnifications that correspond to the area indicated in the upper panels. Size bar = 25 µm. C. Distribution of AC (green), mILC (blue) and SC/CS tumors (orange) in mammary glands of *Wcre;Cdh1$^{F/F}$;Trp53$^{F/F}$*, *Wcre;Ctnnd1$^{F/+}$;Cdh1$^{F/F}$;Trp53$^{F/F}$* and TKO female mice.

Table 1: Comparative tumor spectrum and invasiveness

	Wcre;Cdh1$^{F/F}$; Trp53$^{F/F}$ (n=23)	*Wcre;Ctnnd1$^{F/+}$; Cdh1$^{F/F}$;Trp53$^{F/F}$* (n= 17)	p value (vs. *Wcre;Cdh1$^{F/F}$; Trp53$^{F/F}$*)	*TKO* (n= 21)	p value (vs. *Wcre;Cdh1$^{F/F}$; Trp53$^{F/F}$*)
Invasive	20 (86%)	15 (88%)	p= 1.0000	19 (90%)	p= 1.0000
Metastasis	17 (74%)	7 (41%)	p = 0.0531	10 (48%)	p = 0.1210
AC	0 (0%)	1 (6%)	p = 0.4250	0 (0%)	-
SC/CS	16 (70%)	11 (65%)	p = 1.0000	21 (100%)	**p = 0.0094**
mILC	17 (74%)	8 (47%)	p = 0.1074	3 (14%)	**p<0.0001**

formation. Although heterozygous inactivation of p120 in the mILC model influenced the median tumor-free survival (T50; 214 versus 187 days, p = 0,0146), TKO female mice showed similar T50 values when compared to *Wcre;Cdh1$^{F/F}$;Trp53$^{F/F}$* mice (188 versus 187 days; p = 0.6627) (Fig. 1). We also observed no significant T50 differences when comparing *Wcre;Ctnnd1$^{F/+}$;Cdh1$^{F/F}$;Trp53$^{F/F}$* versus TKO female mice (Fig. 1).

To explore if p120 controls ILC development we examined tumor histopathology based on H&E staining and diagnosed all primary tumors (Table 1, and Supplementary Table 1). Interestingly, heterozygous deletion of p120 in *Wcre;Ctnnd1$^{F/+}$;Cdh1$^{F/F}$;Trp53$^{F/F}$* female mice resulted in a marked increase in the incidence of solid ILC compared to *Wcre;Cdh1$^{F/F}$;Trp53$^{F/F}$* control mice (47.1 % versus 4.3 %; p = 0.02, Supplementary Table 1 and [80]). Solid-type mILC is a rare ILC subtype characterized by large solid sheets of uniform cells with round nuclei and little stroma, and was only rarely diagnosed in the *Wcre;Cdh1$^{F/F}$;Trp53$^{F/F}$* control cohort

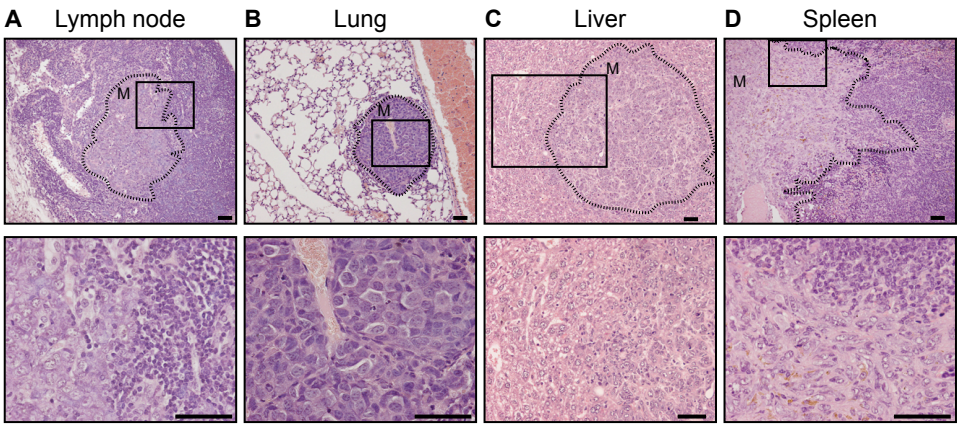

Figure 3 Metastases of mouse tumors from the TKO mouse model.
Tumor dissemination showing metastasis into the axillary lymph node (A), lungs (B), liver (C) and spleen (D). Primary tumors were diagnosed as carcinosarcoma. Dotted lines outline the metastatic area (M). The bottom panels are magnifications that correspond to the area indicated in the top panels. Size bar = 25 µm.

[80]. We did not observe statistically significant changes regarding formation of ILC, solid adenocarcinoma (AC) or solid carcinoma/carcinosarcoma (SC/CS) which were characterized by a metaplastic and biphasic histology which comprised mesenchymal elements (Fig. 2) [80,200]. Furthermore, the percentage of invasive tumors or tumor dissemination (lungs or

lymph nodes) did not change upon heterozygous deletion of p120 (Table 1). As with the *Wcre;Cdh1$^{F/F}$;Trp53$^{F/F}$* model we detected occasional tumor dissemination to the abdominal organs, including spleen and liver, in *Wcre;Ctnnd1$^{F/+}$;Cdh1$^{F/F}$;Trp53$^{F/F}$* and TKO female mice (1 and 2 cases respectively, Supplementary Table 1 and Fig. 3).

Homozygous deletion of p120 in TKO female mice resulted in a tumor spectrum of mainly SC/CS lesions (p =0.0094 compared to *Wcre;Cdh1$^{F/F}$;Trp53$^{F/F}$* mice; Table 1 and Fig. 2) that showed a metaplastic and biphasic histology with overt nuclear atypia and multinucleation. Interestingly, formation of mouse ILC was nearly absent upon homozygous p120 loss (p < 0.0001 compared to *Wcre;Cdh1$^{F/F}$;Trp53$^{F/F}$* mice; Table 1). All tumors that developed in the female TKO cohort lacked p120 and E-cadherin expression (Fig. 2 and Supplementary Table 1). In contrast, all tumors from the heterozygous *Wcre;Ctnnd1$^{F/+}$;Cdh1$^{F/F}$;Trp53$^{F/F}$* mice expressed cytoplasmic and nuclear p120, identical to the expression pattern of p120 in *Wcre;Cdh1$^{F/F}$;Trp53$^{F/F}$* mice (Fig. 2 and Supplementary Table 1). We did not detect overt differences in

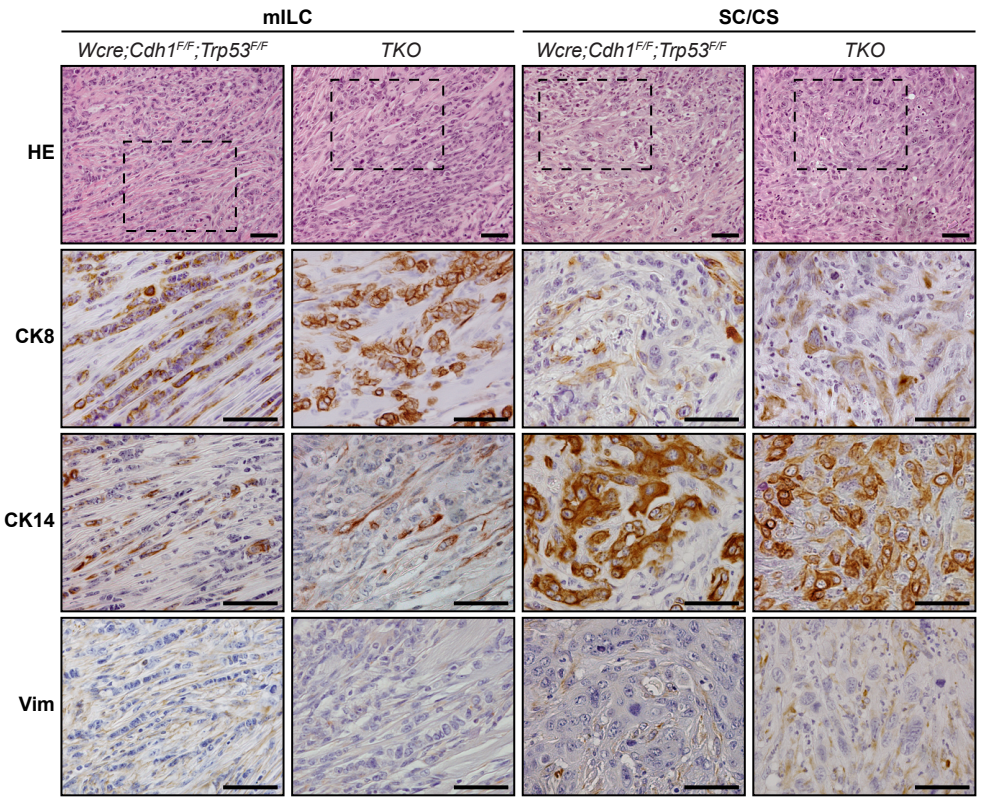

Figure 4 Comparative immunohistochemistry of mammary tumors.
Analysis of marker expression in tumor types of Wcre;Cdh1$^{F/F}$;Trp53$^{F/F}$ and TKO mice. Luminal cells were identified by CK8 expression, while CK14 staining was performed to detect basal cells. Vimentin (Vim) was used as a mesenchymal marker. The bottom panels are magnifications that correspond to the area indicated in the top panels. Size bar = 50 μm.

cytokeratin (CK) and vimentin expression in tumors from the *Wcre;Ctnnd1$^{F/+}$;Cdh1$^{F/F}$;Trp53$^{F/F}$* and TKO cohort compared to tumors that had developed in *Wcre;Cdh1$^{F/F}$;Trp53$^{F/F}$* mice (Supplementary Table 1).Overall, tumors showed a mutually exclusive expression pattern of CK8 and CK14, while vimentin was expressed at low levels, mostly in the sarcomatoid/ mesenchymal-type tumors (SC/CS) (Fig. 4). None of the tumor types expressed the estrogen or progesterone receptor (ER, PR), in line with previous observations that ER and PR are not expressed in tumors that developed in *Wcre;Trp53$^{F/F}$* and *Wcre;Cdh1$^{F/F}$;Trp53$^{F/F}$* female mice [79,80]. The metastases that formed in *Wcre;Ctnnd1$^{F/+}$;Cdh1$^{F/F}$;Trp53$^{F/F}$* and TKO displayed marker expression patterns similar to the primary tumors (Supplementary Fig. 1 and Supplementary Table 2). Taken together, our data show that early inactivation of p120 in the context of combined E-cadherin and p53 loss largely prevents formation of mouse ILC, and leads to the formation of high-grade basal mammary tumors that are characterized by a more prominent expression of the basal markers CK14 and vimentin, metaplastic and sarcomatoid histology, and strong nuclear atypia.

p120 family members lack functional redundancy during mammary carcinoma development

Because we diagnosed three p120-negative tumors as mILC in female TKO mice, we wondered whether compensation by one or more p120 family members could have accounted for the formation of these sporadic ILC tumors. Given that ARVCF, δ-catenin and p0071 are structurally related to p120 and share several functions at the membrane and in the cytosol, we investigated the effects of p120 loss on the expression and localization of these family members in mILC. We started by testing specificity of the antibodies by assessing expression in normal mammary epithelial ductal structures using immunofluorescence. Expression of ARVCF, δ-catenin and p0071 in normal ducts showed partial overlap with p120 at the plasma membrane (Fig. 5a). However, we also observed ARVCF, δ-catenin and p0071 expression in the cytoplasm and nucleus (Fig. 5a, left panels).

Next we determined the expression of ARVCF, δ-catenin and p0071 in the different tumor subtypes from TKO mice, which were compared to tumors from *Wcre;Cdh1$^{F/F}$;Trp53$^{F/F}$* mice. In accordance with previous findings we observed cytosolic and nuclear p120 expression in mILC and SC/CS tumors from *Wcre;Cdh1$^{F/F}$;Trp53$^{F/F}$* mice (Fig. 5b-d, top lanes and Supplementary Fig. 2), while in TKO mice p120 expression

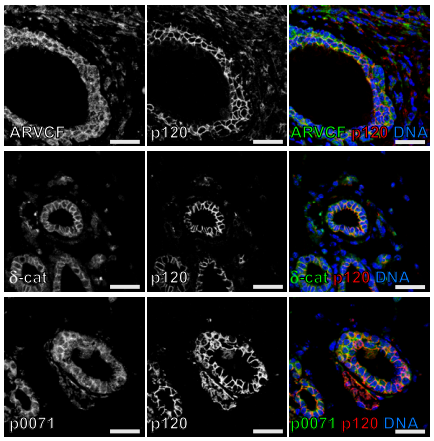

Figure 5 Expression of p120 family members in mILC
A. p120 family member expression (left panels, green) in the mouse mammary gland. Expression of p120 is depicted in the middle panels (red). B-D. Immunofluorescence showing expression of p120 (red) and its family members (green) ARVCF (B), δ-catenin (C) and p0071 (D) in mILCs from Wcre;Cdh1$^{F/F}$;Trp53$^{F/F}$ (top panels) and TKO mice (bottom panels). DAPI (blue) was used to visualize nuclei. The merged images are shown in the right panels. Size bar = 25 µm.
(Figure continues on next page).

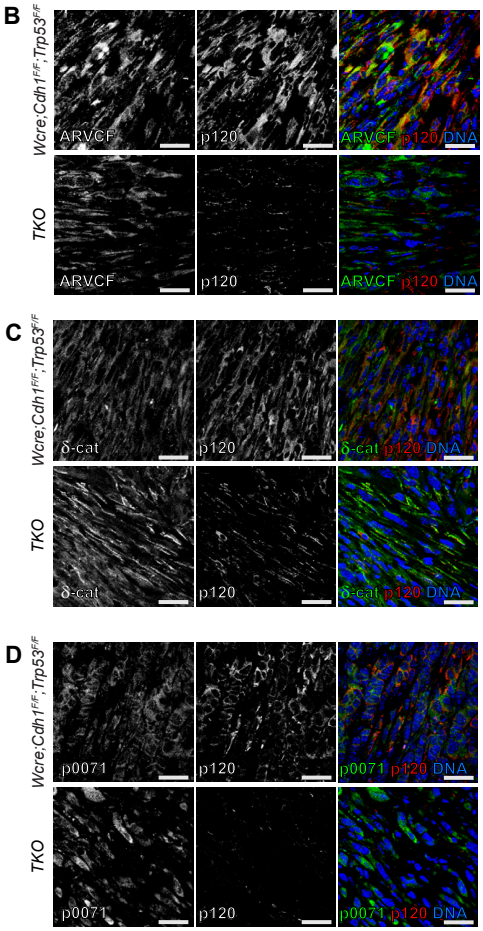

was only observed in stromal cells (Fig. 5 and Supplementary Fig. 2, bottom lanes). ARVCF, δ-catenin and p0071 showed diffuse localization patterns regardless of tumor type or p120 status (Fig. 5 and Supplementary Fig. 2). Based on these results and the fact that mILC incidence is drastically reduced in TKO tumors, we conclude that ARVCF, p0071 or δ-catenin do not play redundant roles in mammary tumor formation in TKO mice.

Discussion

Cytoplasmic p120 is a hallmark of lobular breast cancer [112,114–116]. Here we examined the contribution of p120 to ILC development in mice, and demonstrate that p120 is critical for the development of invasive lobular carcinoma in mice.

Previous data demonstrated that dual inactivation of p120 and p53 in the mouse mammary gland leads to sarcomatoid, epithelial-to-mesenchymal-transition (EMT)-like mammary carcinomas. These p120 negative mammary tumors presented with anaplastic histological features and expression of basal markers such as CK14 and/or vimentin [56]. In this study we have introduced conditional p120 alleles into the WAP-cre driven mouse ILC model [80]. Mouse ILC (like most conditional mouse models of human breast cancer) is an ER negative tumor type [79,80], and as such models a minority of human ILC that is either ER negative or non-responsive to ER antagonists treatment. Moreover, because mouse ILC appears refractory to cisplatin, docetaxel or doxorubicine (our unpublished results), we use mouse ILC as a model for advanced- stage, metastatic and chemo-refractory human ILC. In contrast, poorly differentiated basal tumors, which we also observe in tumors lacking p120, are usually devoid of ER expression [201]. Although Cre expression in our WAPcre mouse models is mostly restricted to luminal cells, basal ductal cells ($CK14^{POS}/CK8^{NEG}$) occasionally also express Cre [80]. Because Cre expression is already evident in virgin *Wcre;Cdh1$^{F/F}$;Trp53$^{F/F}$* female mice, and tumor incidence occurs independent of parity [80], tumorigenesis in these models is most likely instigated in a mammary progenitor cell type. Because of these data and the fact that most mILC in *Wcre;Cdh1$^{F/F}$;Trp53$^{F/F}$* female mice predominantly expressed CK8, we assume that p120 could play a role in the progression of a luminal-type cancer-initiating cell. Indeed, we show that early dual loss of

E-cadherin and p120 almost completely prevents development of mILC. Furthermore, the mILCs that arose in a minority of TKO female mice, displayed biphasic features and consisted mostly of mesenchymal SC/CS tumor cells. Finally, all other tumors that developed in p120 knockout mice were diagnosed as basal-type invasive carcinosarcomas, indicating that loss of p120 predisposes mammary progenitors to a basal lineage commitment and prevents the formation of luminal type ILC.

In spite of this shift towards a basal tumor spectrum we still observed occasional formation of classical mILC lesions in TKO female mice. TKO mILC expressed the luminal CK8 marker, which might be a result of p120 deletion in a luminal-type committed progenitor. We studied expression of ARVCF, p0071 and δ-catenin in TKO mILC lesions, which yielded no indication that p120 loss induced a change in expression levels or localization of these proteins. While this does not formally exclude the possibility of functional redundancy, we conclude that this is not a likely scenario underpinning the occasional formation of ILC in TKO female mice. Also the fact that inactivation of p120 in the context of p53 loss leads to basal-type invasive and metastatic mammary tumors, renders a redundant role for these p120 family members highly unlikely.

Forced dual inactivation of p120 and p53 at the early stages of tumor development might induce two scenarios. First, p120 loss induces an EMT leading to high-grade, basal-type tumors that show a large degree of nuclear atypia and metastasize to lungs and lymph nodes. This process is dominant over E-cadherin loss and its downstream biochemical consequences, preventing ILC formation in triple-knockout mice (Figure 6). We envisage a second scenario, in which E-cadherin loss triggers cytosolic p120 to provide cues essential for ILC development and progression. Concomitant inactivation would then remove p120 from the ILC-initiating cells and enforce a p120-negative basal breast cancer phenotype. We hypothesize that either scenario can contribute equally to the observed tumor phenotypes.

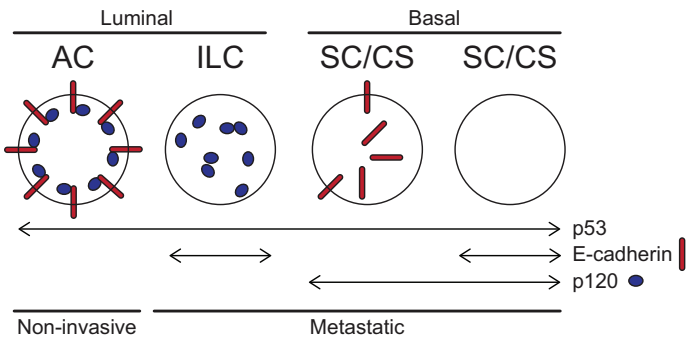

Figure 6 Inactivation of E-cadherin or p120 has divergent consequences on mammary tumor etiology
WAP-cre dependent stochastic loss of p53 predisposes tumor-initiating cells to the development of non-metastatic luminal adenocarcinoma (AC) and basal solid carcinoma/carcinosarcoma (SC/CS) [11]. Inactivation of E-cadherin in this context drives the luminal tumor spectrum towards metastatic invasive lobular cancer (ILC). In contrast, p120 ablation tilts the balance towards formation of basal EMT-type SC/CS. In general, conditional loss of either E-cadherin or p120 results in invasive and metastatic tumors. Inactivation of the adherens junction through p120 loss is dominant over E-cadherin loss in TKO mice, largely preventing ILC development, and driving the formation of EMT-type basal mammary tumors. Arrows indicate mammary-specific Cre-LoxP mediated gene inactivation.

In human breast cancer, loss of p120 is observed in approximately 15–20% of invasive ductal carcinomas,

with a marked complete loss of p120 expression in metaplastic breast cancer [56,112,138,139,202]. Despite the fact that conditional p120 inactivation in the mouse mammary gland induces invasive mammary carcinomas, human p120-negative breast cancers are mostly devoid of inactivating *CTNND1* mutations and do not show silencing through promotor methylation. Moreover, p120 is mostly lost focally in human IDC, indicating that p120 inactivation is a late event in breast cancer. This notion is supported by the fact that (i) p120 loss in the absence of additional oncogenic mutations will negatively impact both luminal and myoepithelial cells of the mammary gland through destabilization of all classical cadherins, and (ii) p120 controls key biological processes such as activation of Rho-dependent actomyosin contractility and distinct transcriptional programs through Kaiso [23,203,204]. Thus, although p120 loss can propel tumor progression in both cell lineages, this probably only occurs during later stages of human breast cancer progression.

In sum, we show that loss of p120 promotes the development of EMT-type basal invasive mammary tumors. In a p53-deficient context, p120 loss is dominant over E-cadherin inactivation in driving mammary tumorigenesis, thus largely preventing the formation of ILC. Conversely, in the context of early mutational E-cadherin activation, p120 will take center stage to unveil its oncogenic role to drive anchorage-independence and metastatic ILC.

Materials and methods

Generation and genotyping of *Wcre;Ctnnd1$^{F/+}$;Cdh1$^{F/F}$;Trp53$^{F/F}$* and TKO mice

Mammary-specific p120 knockout mice were generated by crossing the conditional Ctnnd1F-allele [141] onto the *Wcre;Cdh1$^{F/F}$;Trp53$^{F/F}$* mice [80]. Genotyping was done as described previously [79,80,141]. Mice were euthanized when tumors reached a diameter of 10 mm. Date of sacrifice was used for the tumor-free survival analyses. Histology of the primary tumor was used as diagnosis while full autopsies were performed to detect additional tumors and metastases. All animal experiments were approved by the Animal Ethics Committee (DEC) of the Netherlands Cancer Institute (DEC-A: 09014, DEC-B: 2/6, work protocol 3620.1939). *Wcre;Cdh1$^{F/F}$;Trp53$^{F/F}$* mouse data were described previously [80].

Antibodies

Primary antibodies used include mouse anti-p120-catenin (1:500, BD Biosciences 610134), mouse anti-E-cadherin (1:200, BD Biosciences 610182) rat anti-CK8 (1:125, Developmental Studies Hybridoma Bank, Troma-1), rabbit anti-CK14 (1:10.000, Covance, PRB-155P), guinea pig anti-vimentin (1:400, Fitzgerald, 20R-VP004), rabbit anti-δ-catenin (EMD-millipore, 07-259), guinea pig anti-ARVCF (1:100, previously used in [85]), guinea pig anti-p0071 (1:100, previously used in [85]). Secondary antibodies used were rabbit anti-guinea pig (DAKO, p0141), HRP conjugated rabbit anti-rat (DAKO p0450), poly HRP anti-rabbit (Immunologic, DPVR500HRP), poly HRP anti-mouse/rabbit/rat (Immunologic, DPVO500HRP), Alexa568 conjugated anti-mouse (1:500, Invitrogen, A11031) and Alexa488 conjugated anti-rabbit (1:500, Invitrogen, A11034).

Immunohistochemistry and immunofluorescence

Tissues were fixed in 4% formaldehyde for 24hr. After dehydration, tissues were embedded in paraffin and cut into 4 mm sections. Slides were rehydrated and endogenous peroxidase was blocked in 1.5% H2O2 containing buffer. Depending on the primary antibody used, antigen retrieval was performed either by proteinase K (DAKO) treatment for 5 minutes (for vimentin and CK8) or by boiling of the slides in 10 mM citrate buffer (pH 6.0) for 20 minutes (for E-cadherin and p120). For CK14 no additional procedures for antigen retrieval was performed. Primary antibody incubation took place overnight at 4°C, followed by staining with HRP-conjugated secondary antibodies for 30 minutes. The substrate was developed using diaminobenzidine (DAB) followed by hematoxylin staining. Finally, sections were dehydrated and mounted with pertex for microscopic examination. For immunofluorescence, sections were incubated with Alexa conjugated secondary antibodies for 2 hours followed by DAPI incubation to stain for DNA. The slides were mounted using Vectashield fluorescence (Vector Labs) and images were

Supplementary table 1: Comparative histopathology

	Mouse	Age (days)	Primary tumor(s)	p120	Ecad	CK8	CK14	Vim	metastasis
WCre;Ctnnd1F/+;Cdh1F/F;Trp53F/F	09DER004	127	mILC (solid)	+	-	±	±	+	no
	10DER011	182	mILC (solid)	+	-	-	+	±	lungs
	10SJK252	186	AC	+	-	ND	+	-	no
	09DER011	189	SC/CS	+	-	±	±	±	no
	10SJK254	196	CS CS	ND +	ND -	ND ND	ND ++	ND -	axillary lymph node
	09DER005	203	CS	+	-	-	±	+	no
	10SJK262	206	mILC (solid)	+	-	+	+	±	no
	09SJK136	211	mILC (solid)	+	-	+	+	+	axillary lymph node
	10SJK214	214	CS and mILC (solid)	+	-	-	+	-	no
	09DER007	220	SC/CS	-	-	±	±	±	no
	10DER009	220	mILC (solid)	+	-	++	+	±	lungs
	10DER016	220	CS	+	-	±	+	-	no
	10DER021	268	CS	+	-	±	±	-	abdominal cavity
	10DER007	280	CS and mILC mILC (solid)	+ +	- -	+ ++	± ND	± -	renal, lumbar, caudal lymph nodes
	11SJK032	326	CS and mILC mILC (classic and solid)	ND +	ND -	ND -	ND +	ND -	lung
	10SJK236	350	CS	+	-	±	±	±	no
	10SJK196	368	SC/CS	ND	ND	ND	ND	ND	no
TKO	10DER008	153	CS	-	-	++	+	±	axillary lymph node, lung
	09DER018	156	SC	-	-	-	+++	±	no
	09DER006	161	CS + mILC	-	-	+	+	+*	axillary lymph node, lung
	10DER004	161	SC/CS	-	-	±	±	±	abdominal cavity
	09DER001	162	SC	-	-	±	±	+	no
	09DER019	163	SC	-	-	±	++	+	no
	10DER006	168	CS	-	-	+	++	-	no
	09DER012	182	SC	-	-	+	±	+	axillary lymph node, lung
	09DER008	185	SC	-	-	-	±	+	no
	10DER002	187	SC	-	-	-	+	+	no
	10SJK041	188	CS	-	-	-	±	±	no
	10DER010	205	CS	-	-	+	+	-	no
	10DER015	205	CS	-	-	±	±	-	no
	09DER013	213	CS	-	-	±	++	-	axillary lymph node
	09DER003	221	CS	-	-	±	+	+	lumbal lymph node
	09DER010	227	SC SC + mILC	- -	- -	+ +++	+++ +	- -	axillary lymph node
	10DER013	229	CS	-	-	+	+	±	axillary lymph node, spleen, liver
	09DER016	238	SC + mILC CS	- -	- -	++ +	+ ±	- ±	axillary lymph node
	09DER017	244	SC	-	-	-	±	±	axillary lymph node
	10DER014	277	CS	-	-	±	-	-	no
	10SJK132	287	SC/CS	-	-	±	-	+	no

- = no staining, ±= focal expression in less than 10% of the tumor cells, + = expression ranging between 10% and 40% positive tumor cells, ++ = 40% - 80% positive tumor cells, +++ = > 80% positive tumor cells, * mILC Vim -

collected by confocal laser microscopy using a Zeiss LSM510 Meta.

Statistical analysis

Statistics were calculated using Graphpad Prism 5. For survival analysis, the Log-Rank test was used. For analysis of growth patterns, metastasis and histological types, Fisher's exact test was used. P values < 0.05 were considered statistically significant.

Supplementary table 2: Comparative histopathology of metastasis

	Mouse	metastasis	CK8	CK14	Vim
WCre;Ctnnd1F/+; Cdh1F/F;Trp53F/F	10DER011	lungs	+	-	-
	10SJK254	axillary lymph node	+	±	-
	09SJK136	axillary lymph node	+	-	+
	10DER009	lungs	+	-	-
	10DER021	abdominal cavity	-	-	-
	10DER007	distant lymph nodes	+	-	-
	11SJK032	lungs	+	-	±
TKO	10DER008	axillary lymph node	+	-	-
		lung	±	+	-
	09DER006	axillary lymph node	+	+	-
		lung	+	+	-
	10DER004	abdominal cavity	+	±	-
	09DER012	lungs	+	+	-
	09DER013	axillary lymph node	+	+	-
	09DER003	lumbal lymph node	+	+	±
	09DER010	axillary lymph node	+	-	-
	10DER013	axillary lymph node	+	-	-
		spleen	+	-	-
		liver	+	+	±
	09DER016	axillary lymph node	+	-	-
	09DER017	axillary lymph node	+	-	+

- = no staining, ±= focal expression in less than 10% of the tumor cells, + = expression in at least 10% of all tumor cells

Acknowledgements

We would like to thank members of the Derksen and Jonkers labs for help and discussion. We express our gratitude to Al Reynolds for providing the *Ctnnd1*^{F} mice. We thank Corlinda ten Brink and The UMC Utrecht Cell Microscopy Center for imaging support.

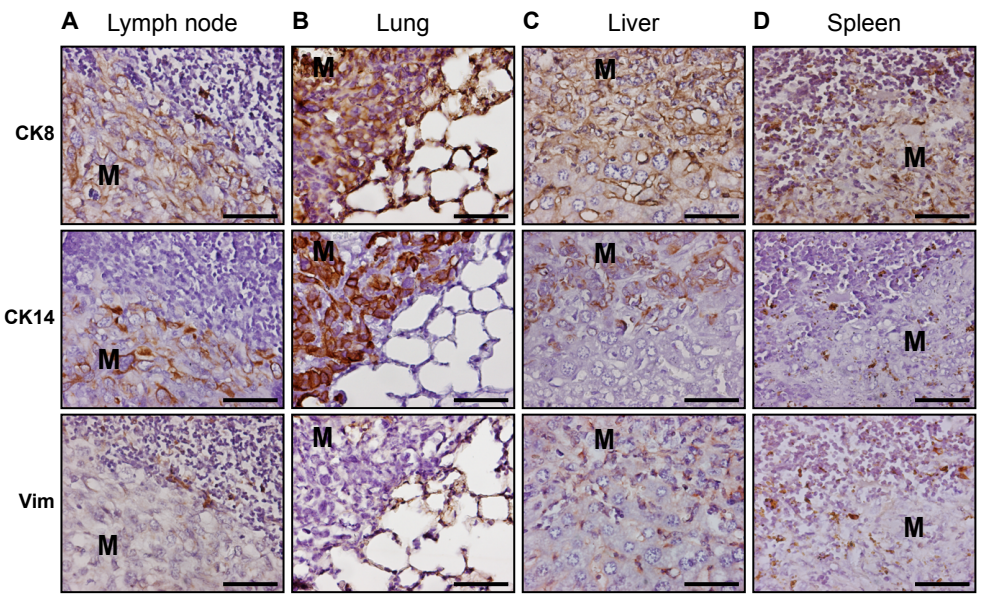

Figure S1 Comparative immunohistochemistry of metastasis in TKO mice

Analysis of marker expression in metastasis of TKO mice in an axillary lymph node (A), lung (B), liver (C) and spleen (D). Primary tumors were diagnosed as carcinosarcoma. M marks the metastatic tissue. Size bar = 50 µm.

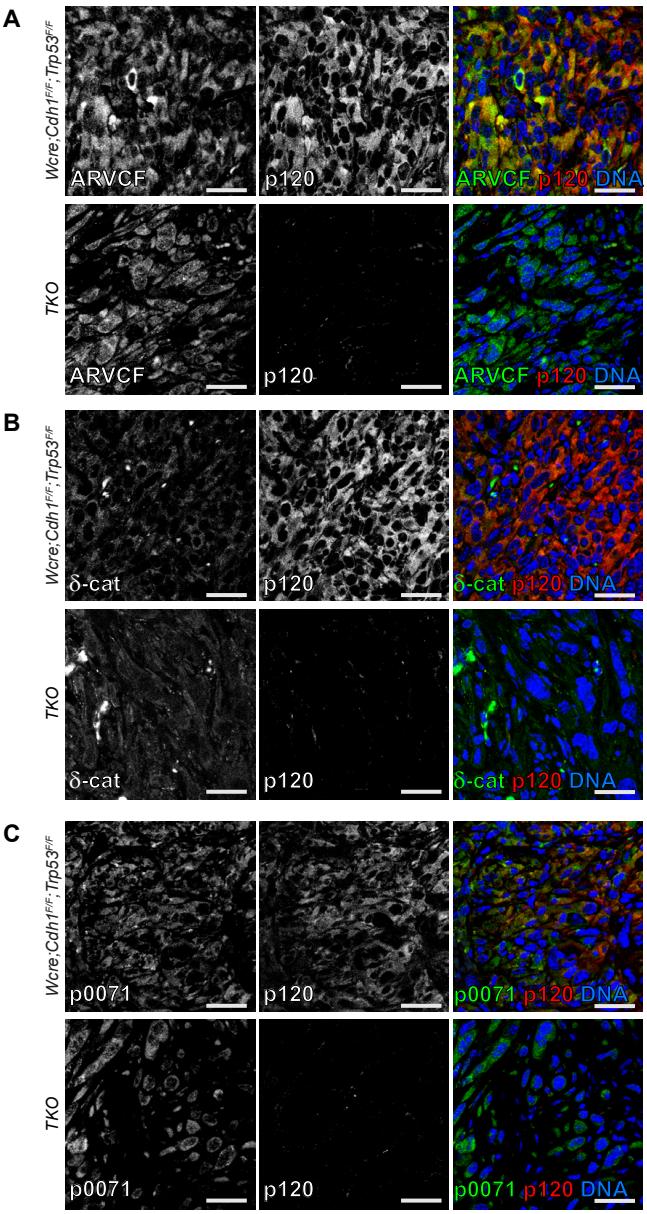

Figure S2 Expression of p120 family members in SC/CS tumors from Wcre;Cdh1$^{F/F}$;Trp53$^{F/F}$ and TKO mice
A-C. Expression of ARVCF (A, green), δ-catenin (B, green) p0071 (C, green) and p120 (A-C, red) in SC/CS tumors from Wcre;Cdh1$^{F/F}$;Trp53$^{F/F}$ (top panels) and TKO mice (bottom panels). DAPI (blue) was used to visualize nuclei. The merged images are shown in the right panels. Size bar = 25 µm

Chapter 3

Restraining FOXO3-dependent transcriptional BMF activation underpins tumour growth and metastasis of E-cadherin-negative breast cancer

M Hornsveld[1,*], M Tenhagen[2,*], RA van de Ven[2], AMM Smits[1], MH van Triest[1], M van Amersfoort[2], DEA Kloet[1], TB Dansen[1], BM Burgering[1] and PWB Derksen[2]

[1] Department of Molecular Cancer Research, University Medical Center Utrecht, Utrecht, The Netherlands

[2] Department of Pathology, University Medical Center Utrecht, Utrecht, The Netherlands

[*] These authors contributed equally to this work.

Cell death and differentiation. 2016; 23(9): 1483-1492
http://www.nature.com/cdd/journal/v23/n9/abs/cdd201633a.html

Abstract

Loss of cellular adhesion leads to the progression of breast cancer through acquisition of anchorage independence, also known as resistance to anoikis. Although inactivation of E-cadherin is essential for acquisition of anoikis resistance, it has remained unclear how metastatic breast cancer cells counterbalance the induction of apoptosis without E-cadherin-dependent cellular adhesion. We report here that E-cadherin inactivation in breast cancer cells induces PI3K/AKT-dependent FOXO3 inhibition and identify FOXO3 as a novel and direct transcriptional activator of the pro-apoptotic protein BMF. As a result, E-cadherin-negative breast cancer cells fail to upregulate BMF upon transfer to anchorage independence, leading to anoikis resistance. Conversely, expression of BMF in E-cadherin-negative metastatic breast cancer cells is sufficient to inhibit tumour growth and dissemination in mice. In conclusion, we have identified repression of BMF as a major cue that underpins anoikis resistance and tumour dissemination in E-cadherin-deficient metastatic breast cancer.

Introduction

Development and homeostasis of glandular structures such as the mammary gland depend on spatiotemporal induction of apoptosis upon loss of cell–cell and cell–matrix attachment, a process known as anoikis [70,205]. Proper anoikis regulation ensures the formation of hollow lumen within a glandular epithelium structure by induction of apoptosis in selective non-polarised luminal epithelial cells that line the ductal structures [69,206]. In the mammary gland, the pro-apoptotic proteins BIM and BMF induce apoptosis upon cell detachment and as such contribute to the formation of mammary ductal lumen [75,77].

Anoikis is regulated by an intricate regulation of the balance between pro-apoptotic and anti-apoptotic proteins [207]. Anti-apoptotic BCL-2 family proteins (BCL-2, BCL-xL and MCL1) compete with the pro-apoptotic molecules (BIM, PUMA, NOXA, BID, BAD or BMF) for binding to BAK and BAX to prevent mitochondrial membrane permeabilisation and subsequent apoptosis. Expression of pro-apoptotic proteins can be induced by a variety of stresses, including DNA damage, nutrient deprivation, heat and hypoxia [208]. BMF appears to specifically function to induce anoikis in epithelial cells [75,209]. It is, however, still controversial whether activation of factors such as BMF is induced through transcriptional activation or by posttranslational events in the cytosol [210].

Correct execution of apoptosis in luminal mammary cells is deregulated during the early stages of breast cancer, such as atypical hyperplasia and ductal carcinoma in situ, resulting in filling of the mammary duct with anoikis-resistant cells [211]. Several studies have shown that activation of oncogenic growth factor receptor (GFR) signalling can induce aberrant filling of the luminal space [69,75,212]. Similar effects have been observed upon inhibition of pro-apoptotic players such as BIM, BMF and p53 [75,77,213], indicating that either GFR activation and/or the inhibition of distal pro-apoptotic effectors underlie anchorage independence of breast cancer

cells. Indeed, mutations in the PI3K and p53 pathway are among the most observed mutations in epithelial cancers, including breast cancer [214]. Moreover, hyperactivation of PI3K and its downstream effector AKT/PKB can lead to repression of apoptosis through phosphorylation-dependent inactivation of pro-apoptotic proteins, such as BAD [75,215,216].

Enhanced growth factor signalling can also be induced through downregulation of the epithelial adherens junction (AJ) [51,56]. E-cadherin is the core component of the AJ and a master regulator of epithelial integrity, linking the cell membrane to the cytoskeleton [217]. Although loss of E-cadherin in the mammary gland is not tolerated [78,80,88], mammary-specific E-cadherin inactivation following loss of p53 in mice leads to the acquisition of anoikis resistance of tumour cells and subsequent dissemination, demonstrating E-cadherin loss as a prerequisite for metastatic disease progression [79].

Despite its repression by growth factor signals, the apoptotic machinery is functionally intact in cancer cells. Targeting the apoptotic machinery has become increasingly interesting in cancer therapy, as intervention strategies using novel BH-3-only protein mimetic compounds in combination with dual specificity inhibitors of PI3K and mTOR have shown promising results [218,219]. Here we have identified BMF as a direct transcriptional target of FOXO3 in breast cancer cells. Our data show that FOXO-dependent BMF expression is repressed in E-cadherin-negative and metastatic breast cancer cells and that expression of BMF is sufficient to inhibit tumour growth and dissemination in mice. We have thereby linked loss of E-cadherin to a cell intrinsic inhibition of BMF-dependent anoikis, a crucial step in malignant tumour progression.

Results

Anoikis-resistant breast cancer cells restrain the expression of BMF

To identify the proteins that control anchorage independence of metastatic breast cancer cells, we cultured E-cadherin-expressing anchorage-dependent and anoikis-resistant E-cadherin-negative breast cancer cells from mouse and human origin in suspension (Sus). Under these conditions, the non-metastatic mouse mammary carcinoma cell line $Trp53^{\Delta/\Delta}$-4 and human MCF7 underwent anoikis as previously demonstrated [80,112]. In contrast, mouse and human E-cadherin-negative mILC1 and MDA-MB-231 cells were anoikis resistant (Figures 1a and b).

To determine which of the key anti-apoptotic and pro-apoptotic molecules were induced during anoikis, we assayed the protein and mRNA expression levels of the anti-apoptotic family members *BCL2, BCL-XL* and *MCL1* and the pro-apoptotic *NOXA, PUMA, BIM, BID* and *BMF*. We observed that all cell lines upregulated BCL2 protein levels and showed increased BID cleavage under anchorage-independent conditions regardless of E-cadherin status. For NOXA and PUMA, no changes were detected in protein levels (Supplementary Figure S1A). In line with previous findings [73,75,77], we detected a clear induction of BIM and BMF in the anoikis-sensitive $Trp53^{\Delta/\Delta}$-4 and MCF7 (Figures 1c and d, Supplementary Figures S1B and C).

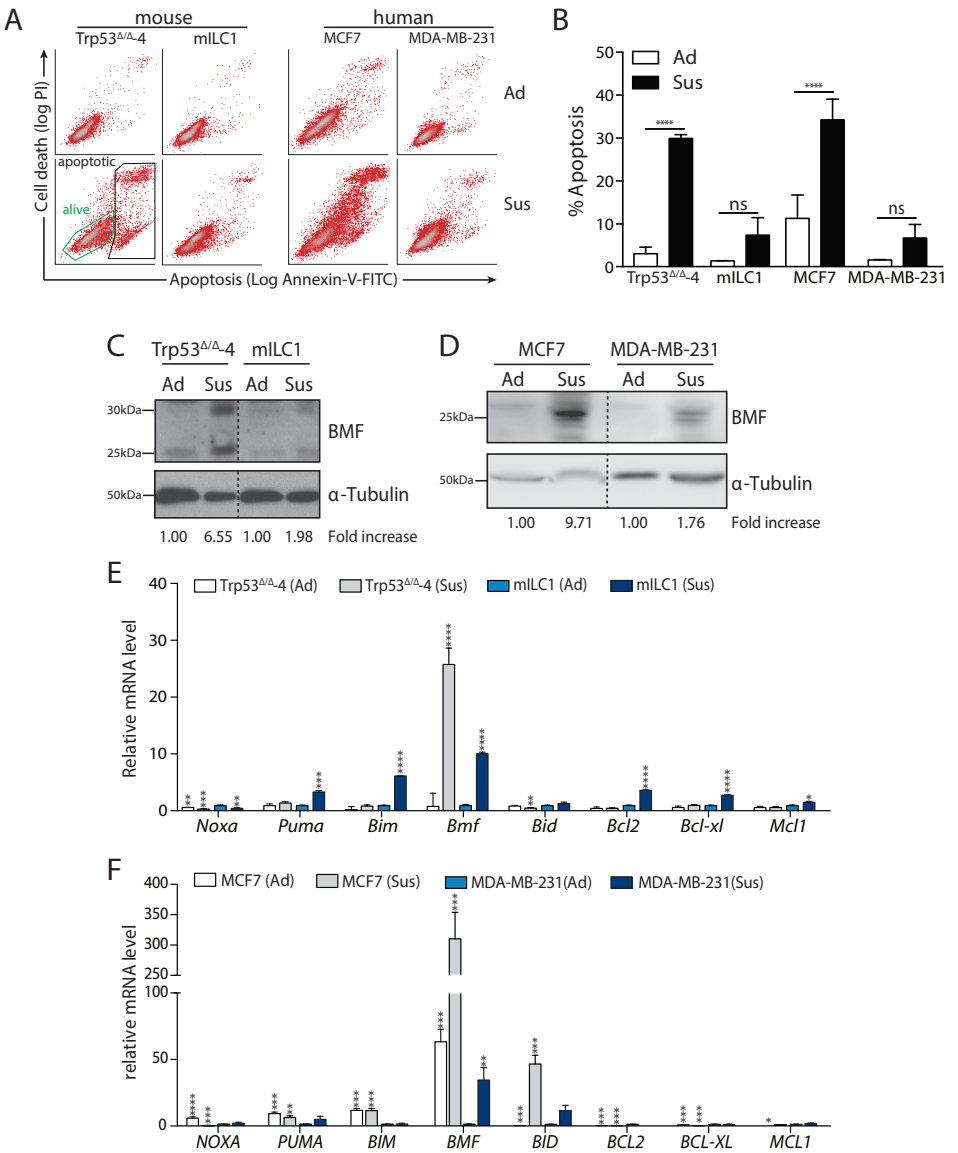

Figure 1 Anchorage independent E-cadherin negative breast cancer cells restrain BMF expression

A. Anoikis resistance in the E-cadherin negative breast cancer cell lines mILC1 and MDA-MB-231. Shown are flow cytometric analyses of apoptosis and cell death using Annexin-V-FITC and Propidiumiodide after 24 hours adherent (Ad) and suspension (Sus) conditions. Note the robust induction of anoikis in the E-cadherin expressing cells Trp53$^{\Delta/\Delta}$-4 and MCF7. B. Quantification of anoikis induction measured by flow cytometry in (A). Data represent mean ± SD, n=3, t-test p<0.05 = *, p<0.005 = **, p<0.0005=***. C-D. Western blot analysis of BMF and α-Tubulin protein levels in Trp53$^{\Delta/\Delta}$-4 and mILC1 (C) and MCF7 and MDA-MB-231 cells (D) grown under adherent (Ad) and suspension (Sus) conditions. Blots are cropped corresponding to the black box. E-F. qPCR analysis of Noxa, Puma, Bim, Bmf, Bid, Bcl2, Bcl-xl and Mcl1 mRNA expression in Trp53$^{\Delta/\Delta}$-4 and mILC1 and MCF7 and MDA-MB-231 cultured in adherent (Ad) and suspension (Sus) culture. Data are relative to mRNA levels in adherent mILC1 cells (E) or MDA-MB-231 cells (F). Data represent the mean ± SD, n=3, t-test p<0.05 = *, p<0.005 = **, p<0.0005=***.

In contrast, the metastatic cell lines mILC1 and MDA-MB-231 did not show a comparable upregulation of either BIM or BMF (Figures 1c and d, Supplementary Figures S1B and C). Subsequent quantitative PCR experiments demonstrated that the only pro-apoptotic gene that was transcriptionally upregulated in both mouse and human E-cadherin-expressing anchorage-independent cells was *BMF* (Figures 1e and f and Supplementary Figures S2A and B). We observed that, although E-cadherin-negative cells induced BMF under anchorage-independent conditions, the expression levels were 3–10-fold lower relative to Trp53$^{\Delta/\Delta}$-4 and MCF7. These data demonstrate that anchorage-independent E-cadherin-negative cells restrain transcriptional upregulation of *BMF*, a key inducer of anoikis.

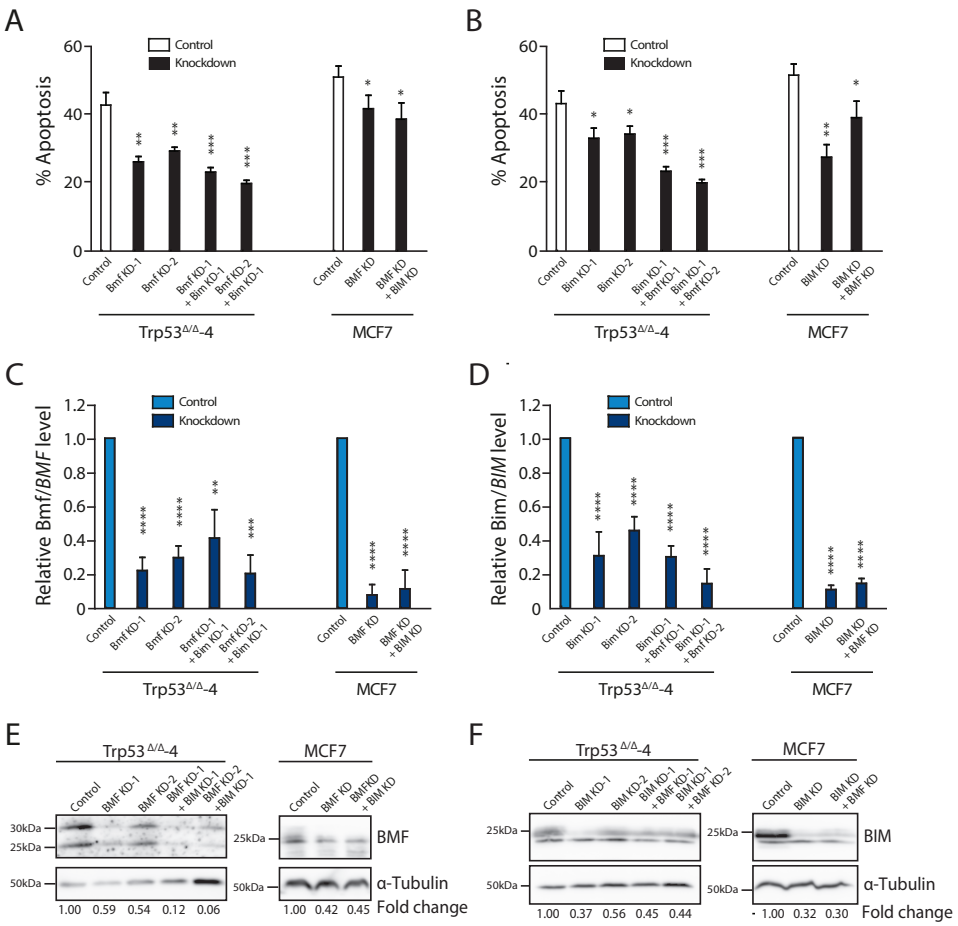

Figure 2 Loss of BMF or BIM increases anoikis resistance of E-cadherin expressing breast cancer cells
A-B. Knockdown of BMF and BIM reduces apoptosis of Trp53$^{\Delta/\Delta}$ and MCF7 cells cultured in suspension. Flow cytometric quantifications of apoptosis using Annexin-V-FITC and propidium iodide after 24 hours in suspension culture. C-D. qPCR analysis of BMF and BIM mRNA knockdown efficiency. Data represent the mean ± SD, n=3, t-test p<0.05 = *, p<0.005 = **, p<0.0005=***, p<0.0005=****. E-F. Western blot analysis of BMF and BIM protein levels shows succesful BMF and BIM knockdown in Trp53$^{\Delta/\Delta}$ and MCF7 cells cultured in suspension. Blots are cropped corresponding to the black box.

Despite the fact that BMF is the major pro-apoptotic factor that showed uniform transcriptional upregulation in suspension settings, at the protein level both BMF and BIM are increased (Figures 1c and d and Supplementary Figures S1B and C). To determine whether these two BH3-only factors are specifically required to induce anoikis, we performed loss-of-function studies and assessed the effect of BMF and/or BIM loss on anoikis resistance of mouse and human E-cadherin-positive cells. Using two independent targeting sequences, we induced knockdown and observed that loss of either BMF or BIM led to a significant increase in anoikis resistance of $Trp53^{\Delta/\Delta}$ and MCF7 cells (Figures 2a–f). Concomitant knockdown of BMF and BIM also resulted in a significant increase in anoikis resistance when compared with controls (Figures 2a–f). Overall, our data does not indicate that dual inhibition of BMF and BIM has an additive effect when compared with the single BMF knockdown experiments (Figures 2a and b). In short, our data demonstrate that BMF and BIM both contribute to the induction of anoikis in E-cadherin-positive breast cancer cells. Further, our data indicate that BMF and BIM are non-redundant and have overlapping functions in the regulation of anoikis of E-cadherin-expressing cells. Overall, we show that BIM and BMF expression is increased upon transfer to anchorage-independent conditions to induce anoikis. However, our data indicate that, in contrast to BIM, the upregulation of BMF under these conditions is transcriptionally regulated.

Loss of E-cadherin results in anoikis resistance and restricts BMF expression

To determine whether E-cadherin loss is causal to the repression of BMF expression in breast cancer, we generated E-cadherin knockout cell lines using the CRISPR/Cas9 system. Guide RNAs targeting the E-cadherin locus were expressed in $Trp53^{\Delta/\Delta}$ and MCF7 cells, which were subsequently fluorescent-activated cell sorted (FACS) based on E-cadherin expression, resulting in E-cadherin-negative cell lines. In contrast to control cells, the E-cadherin knockout cell lines failed to establish E-cadherin-based cell–cell junctions and consequently grew dispersed as solitary cells (Figure 3a). As expected, we observed that E-cadherin loss in mouse and human cells resulted in the acquisition of anoikis resistance (Figure 3b). Importantly, we noted a significant reduction of *BMF* expression in E-cadherin knockout cell lines relative to control cells upon transfer to anchorage independence (Figures 3c and d). These results confirm that loss of E-cadherin is causal to the acquisition of anoikis resistance and show that loss of E-cadherin leads to transcriptional repression of *BMF* expression upon loss of cell–matrix attachment.

BMF expression is inhibited by growth factor signalling-dependent repression of FOXO3

Because BMF was transcriptionally regulated upon transfer to anchorage independence, we hypothesised that either direct transcription repression or inhibition of a transcription factor could underlie the differential BMF expression in anoikis-resistant breast cancer cells. We therefore analysed the human genomic BMF promoter region and identified two FOXO consensus-binding sites (TTGTTTA). FOXOs are directly regulated and suppressed by canonical PI3K/AKT signalling and known transcription factors for the pro-apoptotic genes BIM, NOXA and PUMA [220].

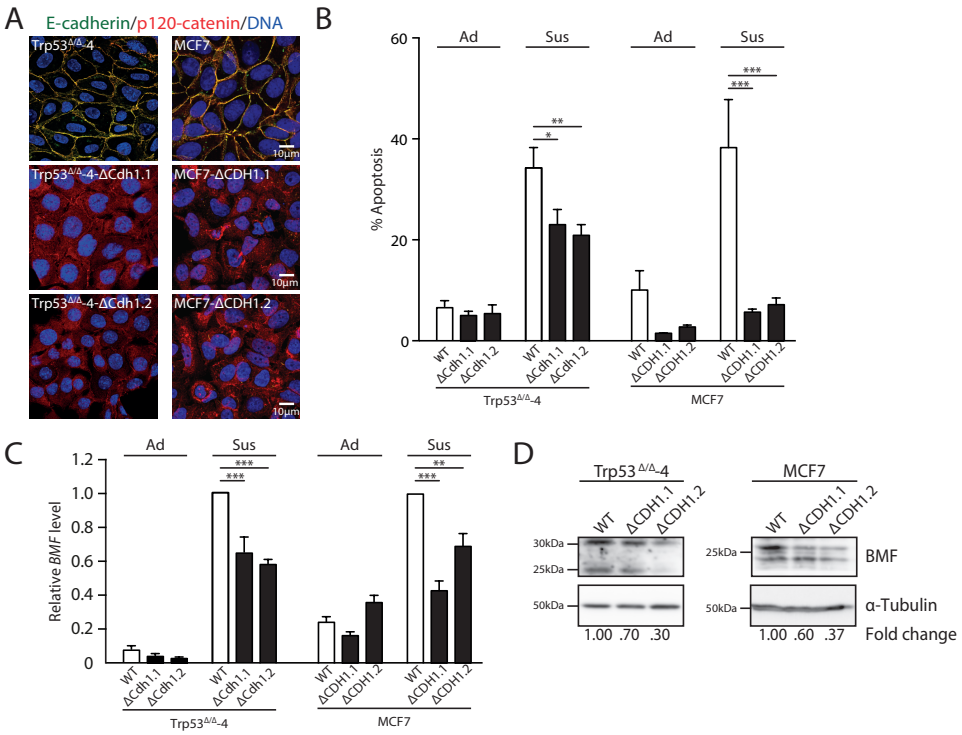

Figure 3 Loss of E-cadherin results in anoikis resistance and repression of BMF expression
A. Immunofluorescence analysis of Trp53$^{\Delta/\Delta}$ and MCF7 cells targeted with E-cadherin-specific gRNA. ΔCDH1.1 and ΔCDH1.2 cells grow dispersed; show loss of E-cadherin (Green), cytoplasmic translocation of p120-catenin (Red) and fail to establish cell-cell junctions. B. Acquisition of anoikis resistance upon loss of E-cadherin in Trp53$^{\Delta/\Delta}$ and MCF7 cells. Shown are quantifications of flow cytometry analyses of apoptosis and cell death using Annexin-V-FITC and propidium iodide after 24 hours in adherent (Ad) and suspension (Sus) culture. C. BMF is repressed in E-cadherin knockout Trp53$^{\Delta/\Delta}$ and MCF7 cells. qPCR analysis shows Bmf or BMF expression after 24 hours in adherent (Ad) and suspension (Sus) culture conditions. Data are relative to mRNA levels in suspension cells. Data represent the mean ± SD, n=3, t-test p<0.005 = **, p<0.0005=***. D. Western blot analysis shows increased BMF protein expression in Trp53$^{\Delta/\Delta}$ and MCF7 cells cultured in suspension. Blots are cropped corresponding to the black box.

To assess whether BMF is a direct FOXO target, we performed a chromatin immunoprecipitation (ChIP) with the most ubiquitously expressed FOXO transcription factor, FOXO3. To this end, we stably introduced a doxycycline (Dox)-inducible FOXO3 (iFOXO) construct in MCF7 cells and performed ChIP in the presence of the allosteric inhibitor VIII (AKTi) to prevent upstream inhibition of FOXO3 by AKT. In line with the predicted binding sites, we noticed binding of FOXO3 to both consensus sites in the BMF promoter (Figure 4a). We confirmed these results by analysing induction of BMF upon expression of a dominant active form of FOXO3 (FOXO3. A3) [221] and showing that administration of Dox indeed resulted in a robust induction of BMF mRNA and protein levels upon FOXO3 activation (Figures 4c and d, Supplementary Figures S3A–C and S4A and B).

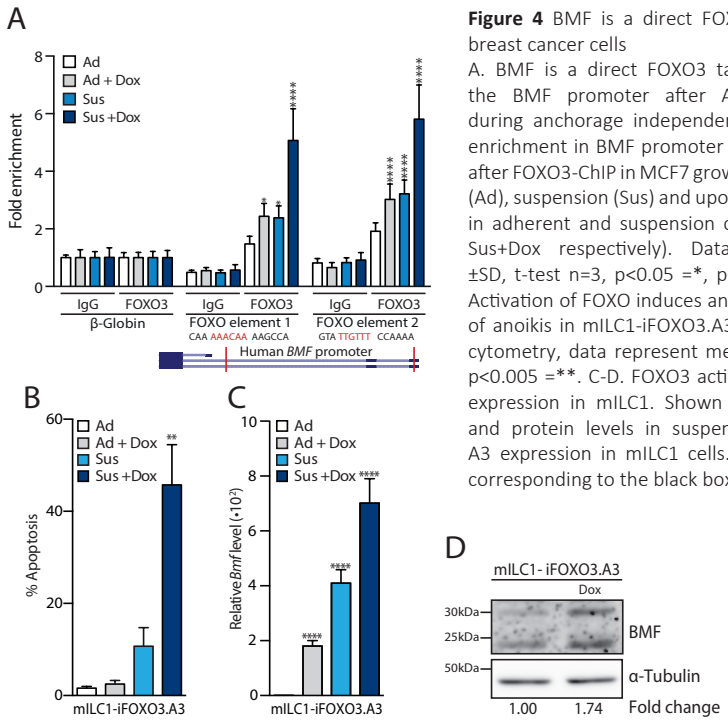

Figure 4 BMF is a direct FOXO3 target gene in breast cancer cells
A. BMF is a direct FOXO3 target. FOXO3 binds the BMF promoter after AKT inhibition and during anchorage independent growth. Average enrichment in BMF promoter chromatin recovery after FOXO3-ChIP in MCF7 growing under adherent (Ad), suspension (Sus) and upon FOXO3 expression in adherent and suspension conditions (Ad+Dox, Sus+Dox respectively). Data represent mean ±SD, t-test n=3, p<0.05 =*, p<0.00005 =****. B. Activation of FOXO induces anoikis. Quantification of anoikis in mILC1-iFOXO3.A3 measured by flow cytometry, data represent mean ±SD, n=3, t-test p<0.005 =**. C-D. FOXO3 activation induces BMF expression in mILC1. Shown are relative mRNA and protein levels in suspension upon FOXO3. A3 expression in mILC1 cells. Blots are cropped corresponding to the black box.

To determine whether FOXO3 activation was sufficient to induce anoikis in E-cadherin-negative cells, we cultured mILC1-iFOXO3.A3 and MDA-MB-231-iFOXO3.A3 in suspension and assayed anchorage-independent survival. Addition of Dox triggered anoikis in mILC1 (Figure 4b), confirming that FOXO activation is indeed sufficient to prevent anchorage independence in E-cadherin-negative breast cancer cells. Although MDA-MB-231-iFOXO3.A3 cells showed a modest increase in BMF expression upon expression of FOXO3 (Supplementary Figure S4B), this did not lead to anoikis, which indicates that the induced BMF levels were insufficient to cause apoptosis in these anchorage-independent breast cancer cells.

Activation of the PI3K/AKT pathway by GFR signalling and ectopic expression of either oncogenic PI3KE545K or myristoylated AKT1 results in repression of anoikis in mammary epithelial cells [75]. Interestingly, we have previously shown that inactivation of E-cadherin function in cancer cells results in hypersensitisation of GFR signalling without activating mutations [56]. To confirm that active PI3K/AKT signalling, which is an established upstream inhibitor of FOXO, controls anoikis resistance, we cultured mILC1 cells and the MCF7-ΔCDH1 cells in suspension and inhibited AKT activation using AKTi, and observed that AKTi resulted in a twofold increase in anoikis (Figures 5a and b). More important, we could show that AKT inhibition resulted in a 2–3-fold upregulation of BMF mRNA and protein expression in anchorage-independent cells (Figures 5c–e).

In conclusion, our data show that E-cadherin-negative metastatic breast cancer cells restrain anoikis through PI3K/AKT signalling, a cue that subsequently inhibits FOXO3-dependent transcriptional activation of its pro-apoptotic target BMF.

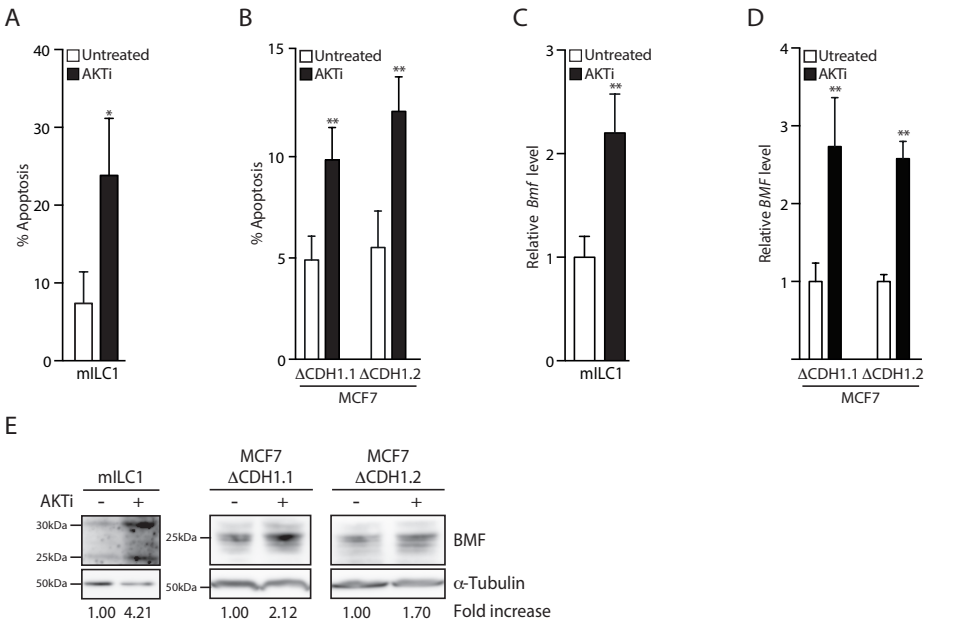

Figure 5 Growth factor receptor signals restrain BMF expression through PI3K/AKT-dependent signals
A-B. Anoikis resistance in E-cadherin negative breast cancer cells is AKT-dependent. Shown is the quantification of anoikis induction in mILC1, MCF7-ΔCDH1.1 and MCF7-ΔCDH1.2 grown in suspension measured by flow cytometry. Data represent the mean ±SD, n=3, t-test p<0.05 = *, p<0.005 = **. C-E. AKT inhibition results in BMF expression. Shown are qPCR analyses of Bmf/BMF mRNA and western blot analyses of Bmf/BMF protein levels in mILC1, MCF7-ΔCDH1.1 and MCF7-ΔCDH1.2 cultured in suspension and after treatment with AKTi. Data represent the mean ±SD, n=3, t-test p<0.05 = *, p<0.005 = **. Blots are cropped corresponding to the black box

Upregulation of BMF expression restrains anchorage-independent tumour growth and metastasis of E-cadherin-negative mammary cancer in mice

Because BMF was the major pro-apoptotic factor upregulated in anoikis-sensitive breast cancer cell lines, we determined whether induction of BMF expression was sufficient to induce anoikis in E-cadherin-negative breast cancer cells. To this end, we stably introduced a Dox-inducible BMF cDNA expression system (iBMF) in mILC1 and MDA-MB-231 cells (Figure 6a) and assayed anoikis resistance. Expression of BMF was indeed sufficient to cause a marked increase in apoptosis in both cell types (Figures 6b and c). Moreover, treating mILC1 and MDA-MB-231 cells with increasing concentrations of the BH3-mimetic drug ABT-199 induced a dose-dependent execution of apoptosis (Figure 6d), suggesting that anchorage-independent E-cadherin-deficient breast cancer cells have a lower threshold for the BH3-only protein-dependent execution of anoikis. Together, these results show that increased levels of BMF or inhibition of BCL2 using the BMF-mimetic ABT-199 is sufficient to induce apoptosis in E-cadherin-negative cells, especially in an anchorage-independent setting.

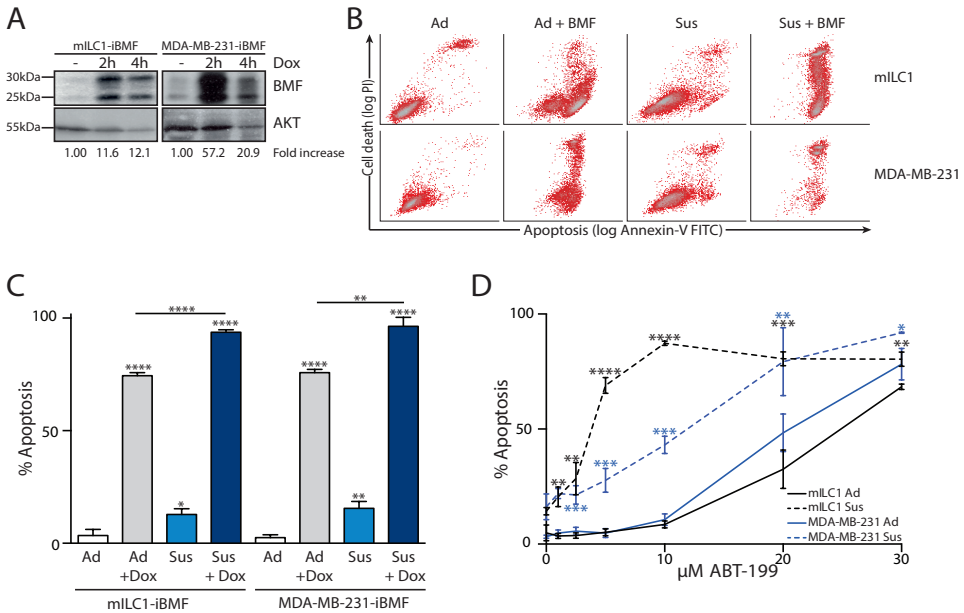

Figure 6 BMF expression is sufficient to induce apoptosis in E-cadherin negative breast cancer cells
A. Inducible expression of BMF in mILC1-iBMF and MDA-MB-231-iBMF before and after doxycycline treatment. Blots are cropped corresponding to the black box. B-C. BMF expression induces apoptosis in mILC1 and MDA-MB-231 cells. Flow cytometric analysis of anoikis induction by Annexin-V-FITC and Propidiumiodide staining of mILC1-iBMF and MDA-MB-231-iBMF cells (B). (C) Depicts a quantification of the anoikis induction of mILC1-iBMF and MDA-MB-231-iBMF measured in (B) data represent mean ±SD, n=3, t-test p<0.05 =*, p<0.005 =**, p<0.0005 =***, p<0,00005 =****. D. Induction of apoptosis and anoikis by the BMF mimetic ABT-199. FACS analysis of apoptosis induction using Annexin-V-FITC and Propidiumiodide staining of mILC1 and MDA-MB-231 cells after 24 hours of treatment with ABT-199 in adherent (Ad) and suspension (Sus) conditions. Data represent mean ±SD, n=3, p<0.05 =*, p<0.005 =**, p<0.0005 =***, p<0,00005 =****.

As anoikis resistance is an excellent prognosticator of E-cadherin-negative breast cancer growth and metastasis [79,80], we investigated the effect of BMF expression on tumour growth in vivo. To this end, we orthotopically transplanted 10,000 mILC1 cells carrying either an empty vector or the iBMF expression vector in recipient mice and monitored tumour growth. Once tumours reached an average volume of 100mm^3, we induced BMF expression by feeding mice Dox-containing chow. Treatment of mILC1 cells carrying the empty expression vector with Dox either at a 100mm^3 or when metastasis was detected using bioluminescence imaging (BLI) did not result in significant changes in tumour growth (Figure 7a). In contrast, BMF expression induced a significant reduction in tumour growth (Figure 7b). Moreover, induction of BMF expression when metastases were detected led to a robust 19-fold decrease in primary tumour volume (Figure 7c). Importantly, we observed a reduction in metastasis formation based upon BMF expression on thoracic BLI in Dox-fed mice when compared with control mice (Figures 7d–h).

In closing, our data establish that restriction of FOXO3-dependent BMF expression underpins anchorage-independent tumour growth and metastasis of E-cadherin-negative breast cancer cells.

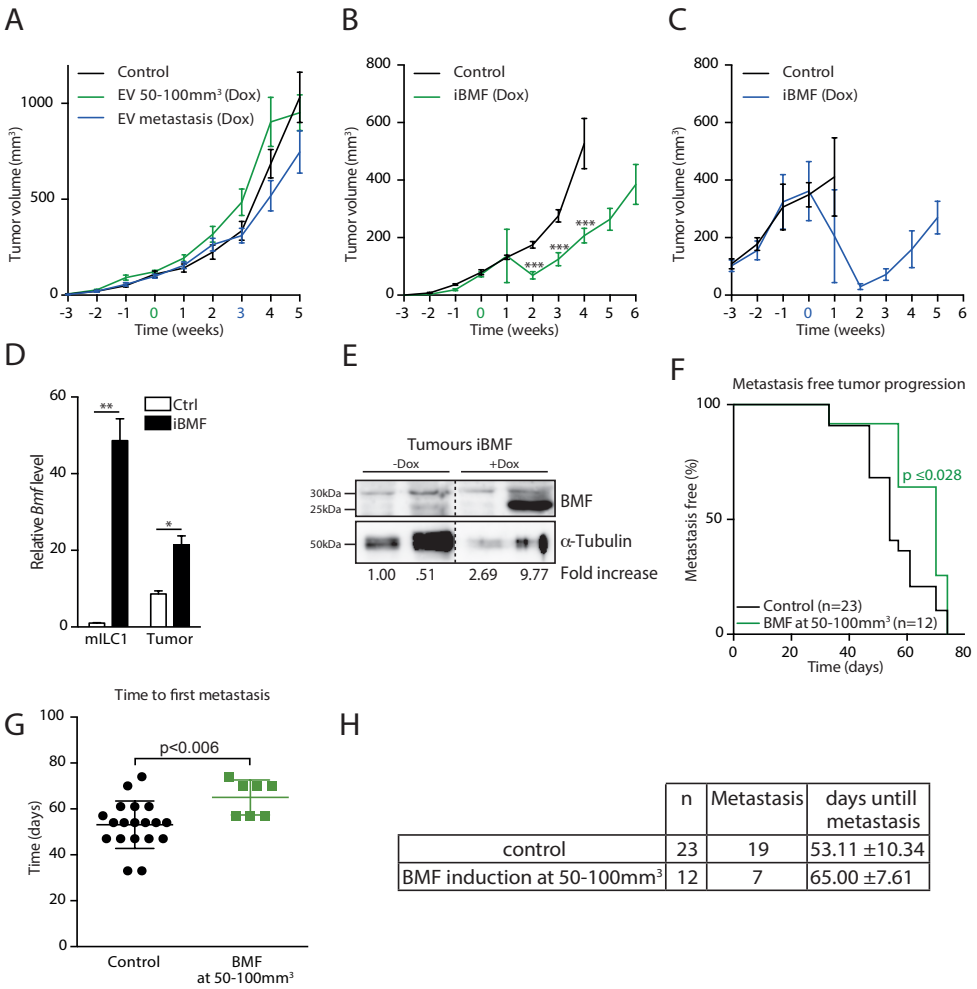

	n	Metastasis	days untill metastasis
control	23	19	53.11 ±10.34
BMF induction at 50-100mm³	12	7	65.00 ±7.61

Figure 7 BMF expression restrains anchorage-independent tumour growth and metastasis of E-cadherin negative breast cancer cells

A. Doxycycline treatment does not influence tumour growth of mILC1 cells carrying the empty doxycycline-inducible expression vector (EV). B. BMF expression inhibits mammary tumour growth in mice. Primary tumour growth of control mice (n=10) and mice treated with doxycycline (n=12), which was started when tumours reached a volume of 100mm3. Data represent the mean tumour volume ±SEM, Holm-Sidak corrected t-test p<0.0005=***. C. BMF expression inhibits mammary tumour growth in mice with metastatic disease. Primary tumour growth of control (n=10) and mice treated with doxycycline (n=13), which was started when lung metastasis were detected by bioluminescent imaging (>2x10³ photons/s/cm²/sr), data represent the mean tumour volume ±SEM. D. Successful BMF expression after Dox treatment was determined by qPCR analysis of the parental mILC1-iBMF and in primary tumours derived from either untreated or Dox-treated mice. Data represent mean ±SD, n=3, t-test p<0.05 =*, p<0.005. E. Western blot analysis of tumour lysates shows Bmf induction upon dox treatment of mice. Two untreated (-Dox) and treated (+Dox) tumours are shown respectively. F. BMF expression inhibits metastasis formation of mILC1 cells. Kaplan-Meier curve representing metastasis free tumour progression, measured in days until metastasis were detected by bioluminescent imaging in control mice (n=23) and mice treated with doxycycline at a primary tumour volume of 50-100mm³ (n=12), Mantel-Cox test p=0.028. G-H. Time until first metastasis are detected by bioluminescence imaging in control mice (n=19) and mice treated with doxycycline at a primary tumour volume of 50-100mm3 (n=7). Data represent individual mice with detected metastasis (>2x10³ photons/s/cm²/sr) ±SD, Welch's corrected t-test p<0.0062.

Discussion

Acquisition of anchorage independence through evasion of apoptosis is a hallmark of cancer [86]. Metastatic cells have shifted the regulation of pro-apoptotic and anti-apoptotic mechanisms toward survival and have thereby gained the possibility to bypass the induction of anoikis during dissemination.

Activation of growth factor signalling in cancer cells is essential for anoikis resistance owing to modulation of expression and activity of apoptotic factors [219]. Others and we have demonstrated that inactivation of E-cadherin underpins anoikis resistance in breast cancer cells, a finding that appears to depend on hyper-sensitisation of GFR signalling through AKT/PKB and ERK upon dismantling of the AJ complex [51,56,57,79,80]. As these mechanisms confer constitutive activation of GFR signals in breast cancer cells, it provides a clear rationale for the maintenance of anoikis resistance in E-cadherin-deficient breast cancer cells. Although AKT/PKB and ERK can control the posttranslational modulation of BAD, BIM and BAX, our current data show that anoikis-resistant breast cancer cells restrain *BMF* transcription, the main pro-apoptotic factor uniformly expressed in E-cadherin-expressing breast cancer cells upon transfer to anchorage independence [215,216,222]. Elegant studies by the Brugge laboratory have identified BIM and BMF as key anoikis regulators of luminal mammary cells, a process counterbalanced by constitutive activation of growth factor-induced PI3K/AKT pathways [75,77]. However, the underlying mechanism that prevented metastatic breast cancer cells from expressing *BMF* upon loss of anchorage remained unclear. As we detected clear changes in *BMF* mRNA levels upon transfer to anchorage independence when comparing breast cancer cells in the context of E-cadherin expression, we probed for transcriptional upstream cues, which resulted in our finding that FOXOs are key players in the regulation of *BMF* expression in breast cancer.

BMF can directly compete for BAK/BAX binding with BCL2 and thereby drive apoptosis. Our data indicate that the increase in BMF expression, rather than the levels of BLC2, is the rate-limiting factor driving breast cancer cell survival. First, the robust upregulation in *BMF* mRNA expression in anoikis-sensitive cells combined with reduced *BMF* expression in anoikis-resistant cells led us to think that a specific BMF threshold should be reached to induce anoikis. Second, although anoikis-resistant cells induced *BMF* transcription in the absence of anchorage, this did not trigger anoikis, despite expressing comparable levels of BCL2 when compared with anoikis-sensitive cells. In line with this, we did not detect differences in the expression levels of BCL2 upon transfer to anchorage independence between cell lines. Finally, we could force anoikis-resistant cells to undergo apoptosis by ectopic expression of BMF or treatment with ABT-199. Together, our data show that loss of the AJ leads to GFR-induced signals that block FOXO-dependent BMF expression, a feature that is essential for survival in breast cancer cells during metastasis.

Our results indicate that FOXO-dependent transcription of *BMF* may be subject of epigenetic regulation as well. Although we have ectopically activated FOXO3 under anchorage-dependent and-independent conditions, we detected further enhanced FOXO3 binding at the *BMF* promoter in suspension. The chromatin state of the BMF locus is expected to influence FOXO3 binding, as it is known that FOXO3 prefers to bind genomic regions associated with activating epigenetic marks [223,224]. Histone deacetylase (HDAC) activity has been reported as a negative regulator of *BMF* expression, because inhibition of HDACs results in BMF expression in multiple human cancer cell lines [225,226]. How BMF is regulated post-transcriptionally remains to be fully characterised, but it was previously described that phosphorylation of ERK2 can inactivate BMF function [227,228]. In line with these findings, complementing HDAC inhibition with inhibitors of mitogenic signalling, that is, B-RAF, augments the pro-apoptotic effect of BMF [229]. This might also explain why BMF induction does not directly lead to apoptosis in anchorage-independent MDA- MB-231 cells that show a constitutively elevated growth factor signalling owing to oncogenic KRAS and B-RAF mutations [230].

Loss of BMF has been linked to tumour suppression in several cancer types [231]. Preclinical intervention strategies using BH3-only mimetics as monotherapy have been successful but mostly in lymphoid malignancies [232,233]. Recent studies indicated that BH3-mimetics can be used to treat non-lymphoid cancers but mostly in combination with oestrogen antagonists, proteasome inhibitors, specific PI3K-mTOR inhibitors or chemotherapy [218,234–239]. As previous findings from our laboratory demonstrated that E-cadherin-negative lobular breast cancer depends on p120-catenin-mediated activation of RhoA, Rock and subsequent actomyosin contraction [112], we anticipate that dual inhibition of these pathways might be successful in E-cadherin-negative cancers that are not driven by oncogenic activation of GFR pathways. Although we do not yet know whether RhoA–Rock signals converge onto the GFR–AKT–FOXO axis in the regulation of anoikis resistance, the fact that FOXO expression had no effect on survival of B-RAF/KRAS-mutated MDA-MB-231 cells seems to be in line with this assumption. Moreover, given that human invasive lobular carcinoma mostly expresses ER and responds to oestrogen antagonists, our findings provide an additional option to improve current treatment regimens in lobular breast cancer by using a combination BH3-mimetics and ER-targeted drugs.

In conclusion, we have linked activation of GFR pathways to inhibition of FOXO3-dependent BMF expression and the regulation of anchorage-independent tumour growth and metastasis in E-cadherin-negative metastatic breast cancer cells.

Materials and methods

Cell lines

Mouse breast cancer cell lines $Trp53^{\Delta/\Delta}$-4 (KP8) and mILC1 (KEP1) were derived from tumours that developed in female K14cre;$Trp53^{F/F}$ and K14cre;$Cdh1^{F/F}$;$Trp53^{F/F}$ mice and cultured as described previously [79]. Human breast cancer cell lines MCF7 and MB-MDA-231 were verified by STR analysis and cultured as described [56].

Constructs, lentiviral transduction and transfections

Lentiviral cDNA expression vectors expressing iBMF, iFOXO3 and iFOXO3.A3 were generated using Gateway cloning in the pINDUCER20 Dox-inducible expression system [240]. Guide RNAs for Cdh1.1 and Cdh1.2 CRISPR were cloned into the lentiviral pSicoR CRISPR/Cas9 vector [241] using BsmBI restriction sites (Supplementary Table S1). After lentiviral transduction, cells were selected for incorporation using puromycin and subsequently FACS-sorted based on E-cadherin expression (DECMA-1, 1:2000; Abcam no. 11512, Cambridge, UK). BMF and BIM knockdown in Trp53$^{\Delta/\Delta}$-4 cells was achieved by lentiviral transduction of pLKO1-shBMF (TRCN0000009716 (shBMF #1) and TRCN0000009717 (shBMF #2)) and pLKO1-shBIM (TRCN0000231244 (shBIM #1) and TRCN0000231246 (shBIM #2), Sigma-Aldrich, Zwijndrecht, The Netherlands), followed by puromycin selection. For MCF7, siRNA smartpools targeting BMF, BIM or control siRNA (Dharmacon M-004393-04-0005 and M-004383-02-0005, Lafayette, CO, USA) were reverse-transfected using HiPerfect (Qiagen, Venlo, The Netherlands) at a final siRNA concentration of 40 nM. Forty-eight hours after transfection, cells were harvested and seeded for anoikis assays.

Immunoblotting and antibodies

Proteins were detected using SDS-PAGE and subsequent western blotting analysis with primary antibodies recognising BAD (CST-9292, Cell Signaling Technology, Leiden, The Netherlands), BIM (CST-2819) BMF (human: CST-5889, mouse: ENZO-17A9), BID (SC-11423 Santa Cruz, Heidelberg, Germany), AKT/PKB (CST), FOXO1 (CST- 29H4), FOXO3 (H144 Santa Cruz), NOXA (SP7122p Acris, Herford, Germany), PUMA (CST-4976) and BCL2 (CST-2876) used at 1:2000. Primary antibodies were detected by secondary HRP-conjugated antibodies targeting mouse, rabbit and rat IgG and visualised using chemiluminescence (Bio-Rad, Veenendaal, The Netherlands).

Immunofluorescence

Cells were grown on glass coverslips, fixed using ice-cold methanol and blocked with 2% BSA (Invitrogen, Breda, The Netherlands) and 0.1% normal goat serum (Invitrogen). Cells were stained with mouse anti-p120 (BD616134, 1:500 overnight), Alexa Fluor 555-conjugated mouse anti-E-cadherin, (1:200, BD560064, 2 h at room temperature) and DAPI (Sigma-Aldrich). Secondary 563-conjugated goat anti-mouse antibodies were used for visualisation on a Zeiss LSM700 confocal microscope (Sliedrecht, The Netherlands).

Quantitative real-time PCR

mRNA was isolated from live cells using the Qiagen RNeasy Kit (Qiagen). cDNA synthesis was performed using the iScript cDNA Synthesis Kit (Bio-Rad). Real-time PCR was performed using SYBR green FastStart master mix (Roche, Woerden, The Netherlands) in the CFX Connect Real-time PCR detection system (Bio-Rad). Target genes were amplified using the specific primer pairs (data not shown), and specificity was confirmed by analysis of the melting curves. Target gene expression levels were normalised to GAPDH, PBDG and TUBA1A levels.

Anoikis assays

Anoikis resistance was analysed by seeding six-well ultra-low cluster polystyrene culture dishes (Corning, Corning, NY, USA) with 50 000 cells/ml. After 24 h, cells were harvested and resuspended in 100 ml of Annexin-V buffer supplemented with Annexin-V (IQ Products, Groningen, The Netherlands) and propidium iodide (Sigma-Aldrich). Anoikis was defined as the Annexin-V and propidium iodide–positive population and quantified using a FACSCalibur (BD Biosciences, Breda, The Netherlands).

Chromatin immunoprecipitation

MCF7-iFOXO3 cells were grown under adherent (Ad) or suspension (Sus) conditions in the absence or presence of Dox and treated with the allosteric AKT inhibitor VIII 1 h prior to harvesting to ensure full FOXO activation. Immunoprecipitations were performed on 20 × 106 cells with 5 µg rabbit anti-FOXO3 (Santa Cruz H144) and 5 µg of normal rabbit IgG (Santa Cruz). ChIPs were performed as previously described [242].

Orthotopic transplantations and tumour watch

For longitudinal tumour growth and dissemination experiments, 10 000 mILC1 cells were transplanted in the fourth inguinal mouse mammary gland of Nude-recipient mice as described previously [112]. Primary tumours were allowed to develop to a volume of 100 mm3 at which point expression of BMF was induced by feeding Dox-containing chow (Ssniff, Soest, Germany). Alternatively, BMF expression was induced when lung metastasis were detected using BLI of the thorax (42×103 photons/s/cm2/sr). Tumour volumes and lung metastases were followed in time as described using a Biospace ϕ imager (Nesles la Vallée, France) [112]. All animal experiments were approved by the Utrecht University Animal Experimental Committee (DEC-ABC no. 2012.III.05.044).

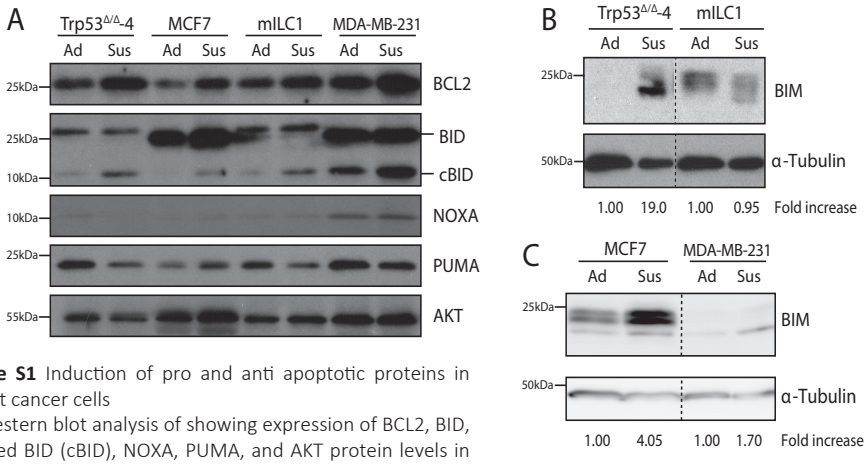

Figure S1 Induction of pro and anti apoptotic proteins in breast cancer cells

A. Western blot analysis of showing expression of BCL2, BID, cleaved BID (cBID), NOXA, PUMA, and AKT protein levels in Trp53$^{\Delta/\Delta}$-4, MCF7, mILC1 and MDA-MB-231 cells grown under adherent (Ad) and suspension (Sus) conditions. B. BIM levels are increased in Trp53$^{\Delta/\Delta}$-4 cells upon transfer to suspension shown by Western blot analysis of BIM protein levels in Trp53$^{\Delta/\Delta}$-4 and mILC1 cells. C. BIM levels are increased in MCF7 cells upon transfer to suspension shown by Western blot analysis in MCF7 and MDA-MB-231 cells grown under adherent (Ad) and suspension (Sus) conditions.

Acknowledgements

We thank S Elledge from the HHMI Boston and R Lebbink of the Molecular Microbiology Department, UMC, Utrecht for kindly providing the pINDUCER20 and pSicoR CRISPR/Cas9 constructs and the UMC Utrecht Cell Biology Department for help with confocal imaging. The Derksen, van Diest, Dansen and Burgering laboratories are acknowledged for support and suggestions. Research was supported by grants from the Netherlands Organization for Scientific Research (NWO/ZonMW-VIDI 016.096.318), Foundation Vrienden UMC Utrecht (11.081) and the Dutch Cancer Society (KWF-UU-2011-5230 and KWF-UU-2009-4490)

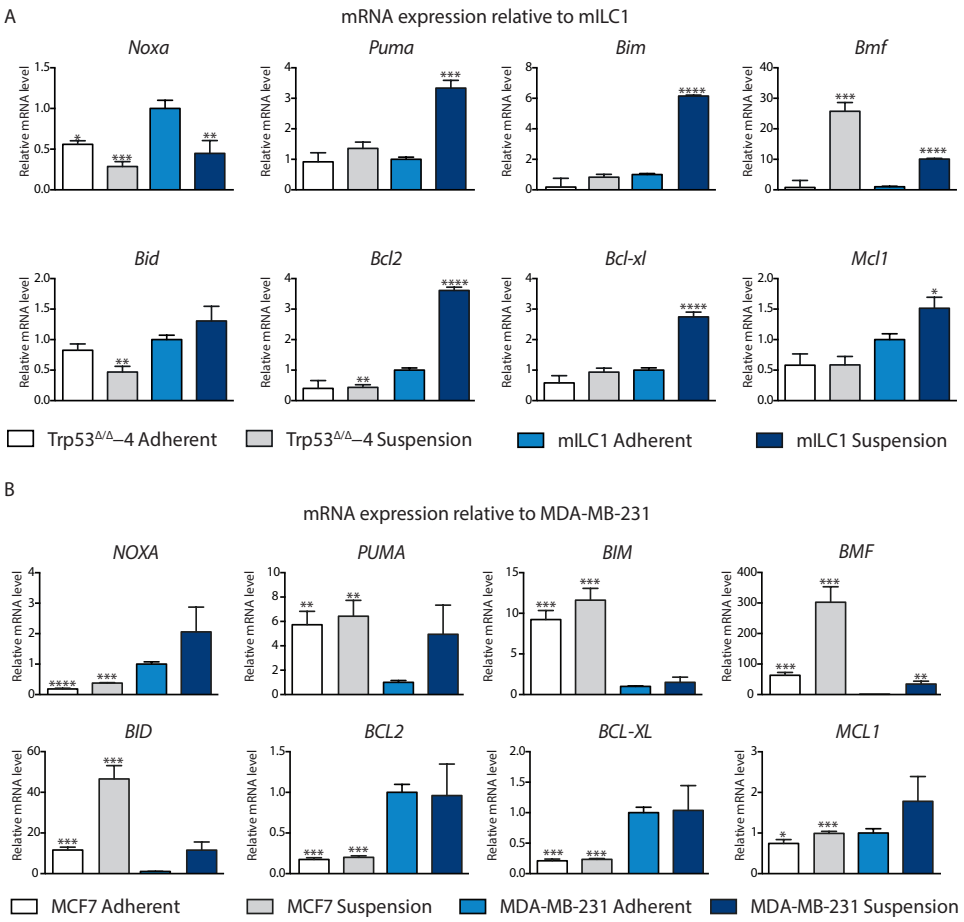

Figure S2 Transcriptional regulation of pro and anti apoptotic proteins in breast cancer cells
A. qPCR analysis of Noxa, Puma, Bim, Bmf, Bid, Bcl2, Bcl-xl, Mcl1 mRNA expression in Trp53$^{\Delta/\Delta}$-4 relative to mILC1 adherent cells. Data represent the mean ±SD, n=3, t-test p<0.05 =*, p<0.005 =**, p<0.0005=***). B. qPCR analysis of NOXA, PUMA, BIM, BMF, BID, BCL2, BCL-XL, MCL1 mRNA expression in MCF7 relative to MDA-MB-231 adherent cells. Data represent the mean ±SD, n=3, t-test p<0.05 =*, p<0.005 =**, p<0.0005=***).

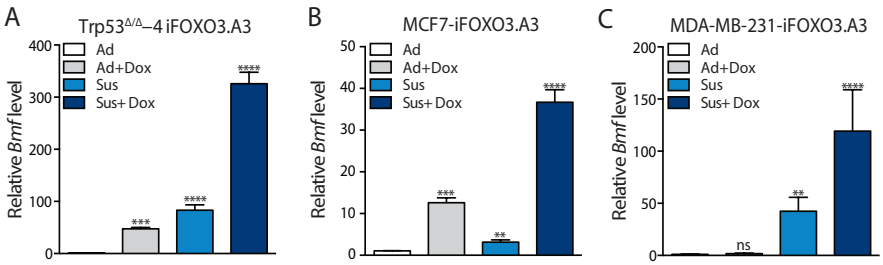

Figure S3 FOXO3 activation induces Bmf/BMF expression
A-C. FOXO3 activation induces Bmf expression in Trp53$^{\Delta/\Delta}$-4, MCF7 and MDA-MB-231. Shown are qPCR analyses of Bmf /BMF mRNA before and after doxycycline treatment. Data represent the mean ±SD, n=3, t-test p<0.05 =*, p<0.005 =**, p<0.0005 =***, p<0,00005 =****).

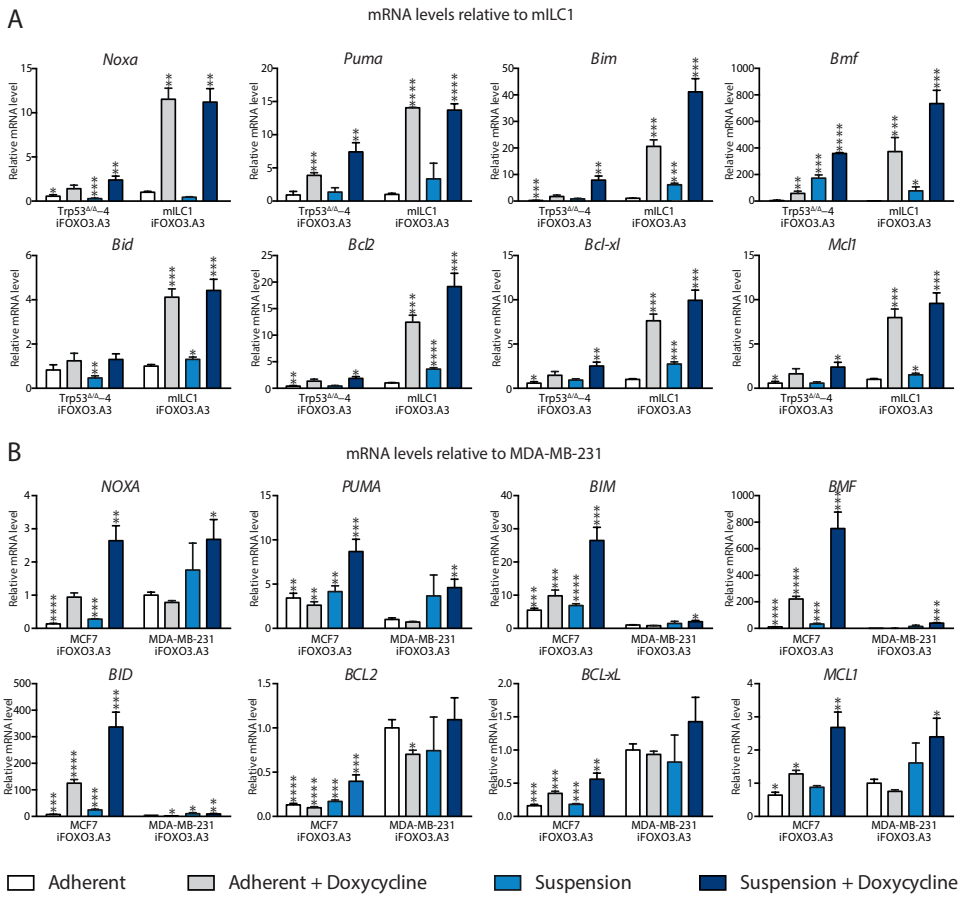

Figure S4 Transcriptional regulation of pro and anti-apoptotic proteins by FOXO3
A. qPCR analysis of Noxa, Puma, Bim, Bmf, Bid, Bcl2, Bcl-xl, Mcl1 mRNA expression in mILC1-iFOXO3.A3 and Trp53$^{\Delta/\Delta}$-4 cells cultured in under adherent (Ad) and suspension (Sus) conditions in the presence or absence of Doxycycline (Dox). B. qPCR analysis of NOXA, PUMA, BIM, BMF, BID, BCL2, BCL-XL, MCL1 mRNA expression in MDA-MB-231- iFOXO3.A3 and MCF7-iFOXO3.A3 cells cultured in under adherent or suspension conditions in the presence or absence of Doxycycline. Data represent mean ±SD levels in mRNA expression relative to MDA-MB-231 cultured under adherent conditions, n=3, t-test p<0.05 =*, p<0.005 =**, p<0.0005=***).

Chapter 4

E-cadherin loss induces targetable autocrine activation of oncogenic growth factor signalling in metastatic lobular breast cancer

Milou Tenhagen [1,*], Katy Teo [2,*], Adam Byron[2], Natalie ter Hoeve [1], Eric Strengman [1], Amit Mandoli[3], Ana M. Sotoca[3], Abhishek A. Singh[3], Joost H. A. Martens [3], Hendrik G. Stunnenberg [3], Matthias Christgen[4], Paul J. van Diest[1], Valerie G. Brunton[2], Patrick W.B. Derksen[1]

* Equal contribution
[1] Department of Pathology, University Medical Center Utrecht, Utrecht, The Netherlands.
[2] Edinburgh Cancer Research Centre, Institute of Genetics and Molecular Medicine, University of Edinburgh, Edinburgh, United Kingdom.
[3] Department of Molecular Biology, Faculty of Science, Nijmegen Centre for Molecular Life Sciences, Radboud University, Nijmegen, The Netherlands.
[4] Institute of Pathology, Hannover Medical School, Hannover, Germany

Manuscript in preparation

Abstract

Despite the fact that loss of E-cadherin is causal to the development and progression of invasive lobular breast cancer (ILC), no targeted therapy is available to treat this major breast cancer subtype. To identify the pathways that can be clinically targeted, we performed a reverse phase protein array (RPPA) on breast cancer cells in the context of E-cadherin loss. We demonstrate that E-cadherin loss leads to increased activation of PI3K/AKT signalling. Moreover, autocrine activation of growth factor receptor signalling and its downstream PI3K/AKT hub was a direct consequence of E-cadherin loss, independent of activating mutations in either *PIK3CA*, *AKT* or *PTEN*. Additionally, analysis of human ILC samples confirmed pathway activity, and pharmacological inhibition of AKT using AZD5363 and MK2206 resulted in robust inhibition of cell growth and survival of ILC cells in anchorage-dependent and -independent conditions. In conclusion, our data demonstrate that E-cadherin loss evokes additional PI3K/AKT activation independent of oncogenic mutations in this pathway. We propose clinical intervention of PI3K/AKT in ILC based on functional E-cadherin inactivation, irrespective of activating pathway mutations.

Introduction

Invasive lobular breast cancer (ILC) is a major luminal breast cancer subtype accounting for approximately 15% of all breast cancers. Loss of E-cadherin expression is a hallmark of ILC, and is already evident in lobular carcinoma *in situ* (LCIS), a lesion that most probably precedes ILC formation [99,103]. Conditional mouse models have demonstrated that E-cadherin loss is causal to the development and progression of lobular breast cancer [79,80]. Subsequent studies using mouse and human ILC models have shown that tumour progression is in part due to anchorage independence triggered by p120-catenin (p120)-dependent activation of RhoA and Rock [111,112]. Loss of E-cadherin expression is observed in the vast majority of lobular breast cancers, due to inactivating *CDH1* frame-shift mutations and subsequent loss of heterozygosity, or transcriptional silencing through E-cadherin promoter methylation [91,94]. As a result of E-cadherin inactivation, the adherens junction (AJ) is no longer functional, leading to disruption of epithelial integrity and acquisition of tumour-promoting events such as anchorage independence, angiogenesis and tumour cell invasion (reviewed in [194]).

Another major driver in breast cancer is the PI3-kinase (PI3K) pathway, which can be activated through loss of PTEN function or activating mutations in PI3K subunits or their downstream effectors. ILCs represent a subgroup of tumours in which the mutation rate of *PIK3CA* (48%) and genomic loss of *PTEN* (8%) is higher than in matched invasive ductal carcinomas (IDCs) (33% and 3%, respectively) [97,129,135]. Additionally, although the underlying activation cue remains unknown, high activation of PI3K signalling was linked to specific subtypes such as basal-type, HER2-positive and ILC tumours [135,243]. These findings have triggered an increase in clinical trials to target PI3K, AKT or mTOR [107,109,244]. Given the broad occurrence of PI3K/AKT pathway mutations [129,130], clinical intervention of this pathway has not been tailored for a specific breast cancer subtype. Also, despite the recent insight into the oncogenic pathways

underpinning ILC (reviewed in [194]), there is no targeted intervention strategy to treat metastatic ILC. Although next-generation sequencing and mRNA expression profiling have provided a comprehensive and detailed genomic and transcriptional landscape of lobular and ductal breast cancers [123–126,198,245], these data have not provided direct insight into pathway and protein activation. Moreover, while recent studies have coupled protein expression to patient survival [246–248], they did not specifically report on ILC or the role of E-cadherin loss in this context.

Here, we have studied human and mouse models of ILC to delineate the consequences of E-cadherin loss in ILC to the activation of signalling pathways. We find that growth factor-dependent PI3K/AKT signals are activated upon E-cadherin loss, even in the presence of somatic activating mutations.

Results

Pathway analysis reveals activation of PI3K/AKT signalling in ILC cells

To study the effect of E-cadherin loss on downstream pathway activation, we made use of well-characterized cell lines from metastatic mouse and human ILC and their non-metastatic E-cadherin-positive counterparts (Figure 1).

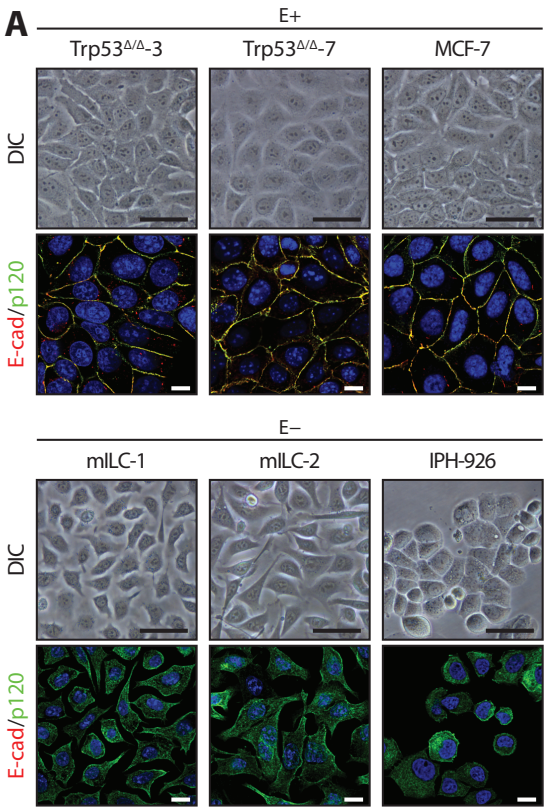

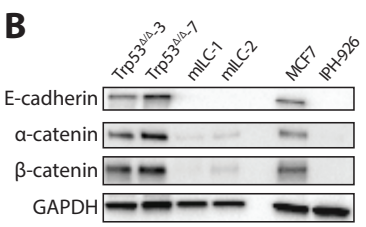

Figure 1 Breast cancer cells used in this study
A. DIC (top) and merged immunofluorescence (IF) images (bottom) for E-cadherin (red) and p120 (green) expression in the mouse (left and middle panels) and human breast cancer cell lines (right panels). E-cadherin-expressing (E+) and E-cadherin mutant (E–) are grouped accordingly. Scale bars DIC. 20 µm, Scale bars IF: 10 µm. B. Expression of the adherens junction components E-cadherin, α-catenin and β-catenin were assessed by western blotting. GAPDH served as a loading control.

These included mouse ILC (mILC) lines which were derived from E-cadherin- and p53-deficient mammary tumours [79,80] and cell lines derived from non-invasive tumours that developed in mammary-specific p53 conditional knock-out mice (Trp53$^{\Delta/\Delta}$ cells). As a model of human ILC, we used IPH-926 cells [249]. MCF7 cells were used to model E-cadherin-expressing non-metastatic human breast cancer cells (Figure 1).

To examine the effect of E-cadherin inactivation on protein expression, post-translational modifications and downstream pathway activation, we used an RPPA to provide a relatively high throughput antibody-based platform for the analysis of protein expression and phosphorylation status (Figure 2A). Expression and phosphorylation of key signalling proteins was assayed using a panel of 122 antibodies directed against established oncogenic pathways

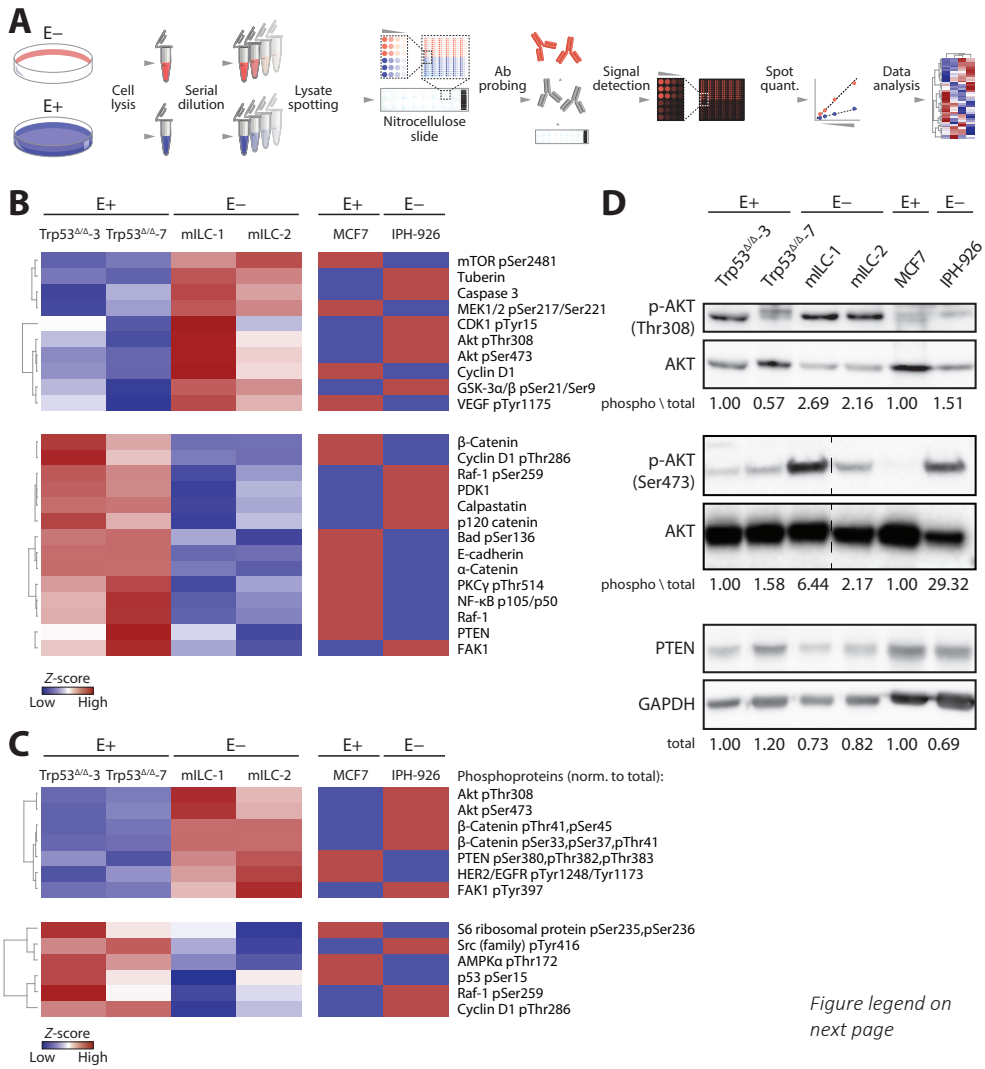

Figure legend on next page

Figure 2 Differential protein expression and phosphorylation in the context of E-cadherin expression
A. Experimental workflow for the RPPA analysis. After collection, dilution and spotting of the cell lysates, each of 16 sub-arrays (pads) per nitrocellulose slide were probed with a different validated primary antibody (Ab). A fluorescent secondary antibody was used for signal detection and quantification. Mean intensity of the biological replicates was used to perform cluster analysis. B-C. Heat map showing the levels of proteins and phosphoproteins (B) and phosphoproteins relative to respective total protein levels (C) in whole cell lysates from mouse ($Trp53^{\Delta/\Delta}$-3, $Trp53^{\Delta/\Delta}$-7, mILC-1, mILC-2) and human (MCF7, IPH-926) cell lines as determined by RPPA. The normalized intensity values were standardized as Z-scores and subjected to unsupervised hierarchical cluster analysis. Heat maps display the relative enrichment of selected clusters of proteins or phospho-proteins (red, up-regulated; blue, down-regulated). Human data are displayed as the difference of expression in IPH-926 over MCF7 (red, up-regulated in IPH-926; blue, down-regulated in IPH-926). D. Western blot analysis of the differentially regulated proteins and phospho-proteins identified by RPPA. Phosphorylation levels of AKT (Thr308 and Ser473) were assessed and normalized over the corresponding total protein levels, while PTEN expression levels were normalized over GAPDH levels. For mouse cells, phospho levels of $Trp53^{\Delta/\Delta}$-3 were set to 1. MCF7 phospho levels were also set to 1 to compare to IPH-926 cells. E+ = E-cadherin-expressing cells, E– = E-cadherin-negative cells.

such as growth factor receptor (GFR) signalling, stress response, cell adhesion and apoptosis. Unsupervised hierarchical cluster analysis of the RPPA data identified a distinct separation of the E-cadherin-expressing cell lines and the E-cadherin mutant ILC cell lines in terms of both protein expression and phosphorylation (Additional figures 1 and 2). As reported previously [112], we noted that expression levels of α-catenin and β-catenin were decreased in ILC cells (Figure 2B, lower panel), a finding that served as an internal control for the RPPA (see also Figure 1B). E-cadherin-negative cells showed higher activation of distinct pathways and their effectors, including PI3K pathway components AKT, GSK3-α/β, and mTOR (Figure 2B–D), while expression of PTEN was lower in mouse and human ILC cells when compared to E-cadherin-expressing breast cancer cells (Figure 2B, D). Finally, we analyzed expression of the proteins that showed elevated expression in ILC cells using TMAs containing 129 primary ILC samples and 30 LCIS samples (Table 1).

In agreement with the RPPA and western blotting data from the human and mouse cell line panel, we observed that levels of active (phosphorylated) AKT were common in LCIS and ILC (Table 2, Figure 3A). Interestingly, PTEN expression was reduced or lost in IPH-926 and the majority of ILC samples when compared to E-cadherin-expressing cells (Table 2, Figure 3B), suggesting that inactivation of PTEN may be induced during ILC progression.

In conclusion, using a comprehensive set of mouse and human cell lines and primary tumour samples, we have identified increased activation of a distinct set of oncogenic pathways and proteins in ILC.

Table 1 Clinicopathologic characteristics of 129 ILC patients studied for pAKT (Ser473) and PTEN expression

		Number	%
Age (years)	Mean	57	
	range	32-83	
Histological grade	1	12	9.3
	2	76	58.9
	3	35	27.1
Lymph node status	negative	68	52.7
	positive	57	44.2
Metastasis	negative	86	66.7
	positive	9	7
ER status (10%)	negative	12	9.3
	positive	107	82.9
PR status (10%)	negative	35	27.1
	positive	83	64.3
Her2 (3+)	negative	86	66.7
	positive	7	5.4

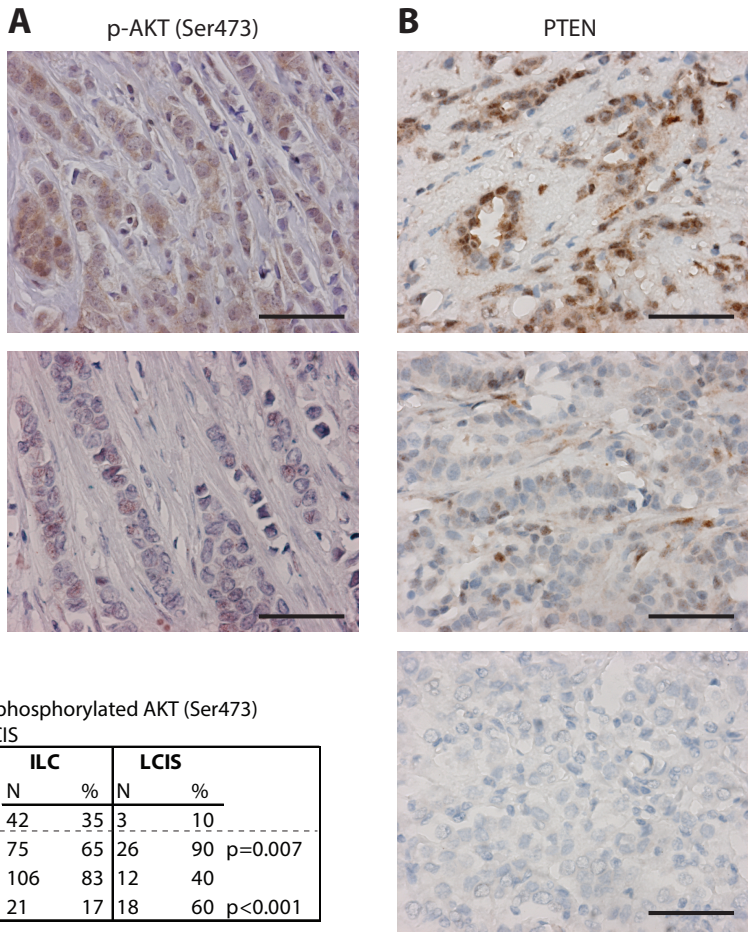

Figure 3 PI3K/AKT signalling is active in ILC patients
A. Representative images of high (top) and low (bottom) expression of phosphorylated AKT (Ser473) in ILC patients. B. IHC of PTEN in ILC shows normal (top), reduced (middle) or absence (bottom) of PTEN expression. Scale bars: 50 µm.

Table 2 Expression of phosphorylated AKT (Ser473) and PTEN in ILC and LCIS

		ILC		LCIS		
		N	%	N	%	
pAkt	Negative	42	35	3	10	
(Ser473)	Positive	75	65	26	90	p=0.007
PTEN	Low/absent	106	83	12	40	
	Positive	21	17	18	60	p<0.001

PI3K/AKT pathway activation is a consequence of E-cadherin loss

Enhanced PI3K/AKT signalling is a tumour-promoting event that is widely observed in several types of cancer. Activation of this pathway can be induced by either mutational activation or aberrant GFR-dependent signals. To study if AKT pathway activation could be induced by autocrine growth factor-dependent signals, we initially cultured our cell lines without serum and assayed phosphorylation of AKT (pSer473 and pThr308). Interestingly, both mouse and human ILC cells displayed elevated AKT activation when compared to the E-cadherin-expressing cells. This trend was also observed for the downstream target mTOR, while expression of PTEN, a negative regulator of PI3K signalling, remained lower (Figure 4A). To assess if mutational activation of core PI3K pathway components was underpinning pathway activation, we performed next-generation sequencing on mILC cell lines, which did not reveal somatic mutations in the GFR-PI3K-AKT pathway members *Igf1r, Pik3ca, Akt1, Akt2, Akt3, Pten* and *Mtor* (data not shown). In contrast, the human ILC cell line IPH-926 harboured a heterozygous deletion in *PTEN* (c.950_953delTACT) that probably contributes to the observed AKT activation under serum-free conditions. The high basal levels of phospho-AKT in human

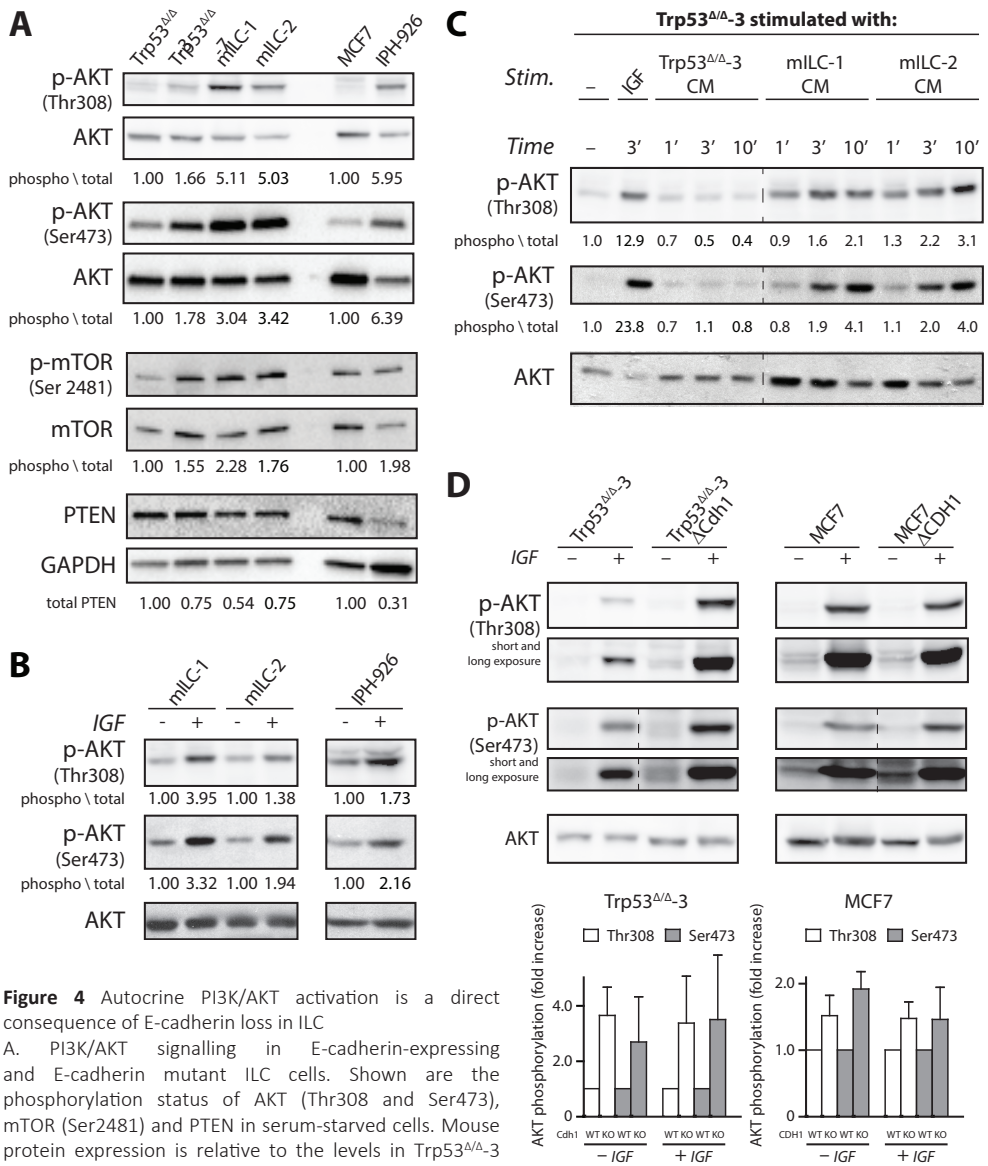

Figure 4 Autocrine PI3K/AKT activation is a direct consequence of E-cadherin loss in ILC

A. PI3K/AKT signalling in E-cadherin-expressing and E-cadherin mutant ILC cells. Shown are the phosphorylation status of AKT (Thr308 and Ser473), mTOR (Ser2481) and PTEN in serum-starved cells. Mouse protein expression is relative to the levels in Trp53$^{\Delta/\Delta}$-3 and human protein expression is relative to the levels in MCF7. B. Phosphorylation of AKT (Thr308 and Ser473) is induced upon IGF stimulation of E-cadherin-negative cells. Quantification of protein levels is relative to the levels in unstimulated cells. C. Stimulation (Stim.) of Trp53$^{\Delta/\Delta}$-3 cells with IGF and mILC-conditioned medium induces phosphorylation of AKT. AKT phosphorylation levels in unstimulated cells were set to 1. D. E-cadherin knock-out (ΔCDH1) in Trp53$^{\Delta/\Delta}$-3 and MCF7 cells increases basal levels of pAKT. Stimulation of serum-starved cells with IGF (+IGF) induces an increase in AKT phosphorylation in ΔCDH1 cells. Graph shows the fold increase of Thr308 (white) and Ser473 (grey) in Trp53$^{\Delta/\Delta}$-3 (left) and MCF7 (right) cells upon E-cadherin knock-out in serum-starved conditions (–IGF) and growth factor-stimulated (+IGF) conditions. Data represent the average fold increase ± SD of three independent experiments. For each experiment, phospho levels of wild type cells were set to 1. KO = knock-out, WT = wild type. Phosphorylation of AKT (Thr308 and Ser473) and mTOR (Ser2481) were normalized over total protein levels, PTEN levels were normalized over GAPDH levels.

ILC cells, however, did not represent maximal activation, since administration of recombinant *IGF* induced a further increase (Figure 4B). These results indicated that loss of E-cadherin promotes constitutive AKT activation, even in the presence of PTEN-inactivating mutations.

Because we did not detect activating somatic mutations in PI3K pathway members in the mouse breast cancer cell lines, and E-cadherin loss induced an increase in phosphorylation of AKT under serum-free conditions, we hypothesized that an autocrine loop might underlie GFR-dependent AKT activation. To test this, we harvested conditioned medium from mILC cell lines (mILC-CM) that were cultured under serum-free conditions for 3 days. Similar experiments using the human ILC cells could not be performed due to the extensive doubling time (approximately 14 days) and low metabolic activity *in vitro* (data not shown). Therefore, culture supernatant from serum-starved mILC cells was used to stimulate serum-starved $Trp53^{\Delta/\Delta}$-3 cells, and AKT phosphorylation was assessed. Interestingly, mILC-CM induced a robust increase in phospho-AKT, while stimulation with $Trp53^{\Delta/\Delta}$-CM did not affect AKT phosphorylation (Figure 4C). These data thereby confirm our assumption that GFR-dependent signalling is subject to autocrine activation upon mutational inactivation of E-cadherin. Subsequent mRNA expression profiling of the mouse and human ILC cell lines demonstrated that a number of growth factor-receptor pairs were concomitantly expressed, such as TGFβR/TGFβ, ACVR/INHB and FGFR/FGF (Additional table 3), which could underlie the autocrine activation observed. In summary, we conclude that autocrine GFR activation contributes to PI3K/AKT pathway activation in E-cadherin mutant ILC cells.

To establish causality and uncouple autocrine-induced growth factor-dependent signalling from oncogenic mutations, we performed a CRISPR/Cas9-based knock-out strategy to ablate E-cadherin in mouse $Trp53^{\Delta/\Delta}$ and human MCF7 cells. We could indeed show that phospho-AKT levels were increased up to 3-fold upon knock-out of E-cadherin (ΔCDH1; Figure 4D and Additional figure 3). Moreover, stimulation with *IGF* resulted in a further increase in phospho-AKT (Figure 4D), indicating a direct link between E-cadherin loss and PI3K pathway activation in mouse and human breast cancer.

Because induction of PI3K/AKT signals in MCF7-ΔCDH1 cells occurred in the presence of an activating somatic *PIK3CA* mutation and genomic *AKT* amplification [250], these findings confirm our observation that loss of E-cadherin confers an additive effect onto GF-dependent activation of PI3K/AKT in the presence of constitutively activating oncogenic mutations. Finally, our data indicate that loss of E-cadherin provokes an autocrine cue that induces GFR pathway activation in ILC.

ILC cells are sensitive to inhibition of AKT

Given the increase in AKT activity, we wondered whether E-cadherin mutant breast cancer cells were sensitive to pharmacological inhibition of the PI3K/AKT pathway. To inhibit AKT, we made use of the ATP competitor AZD5363 and two allosteric inhibitors, MK2206 and VIII. The latter is being used *in vitro* to target AKT1/2 with high specificity, while AZD5363 and

MK2006 are currently being tested in clinical trials [108,251,252]. We cultured the ILC cell lines in adherent and non-adherent (suspension) settings, which we employ as a surrogate readout for cell survival during metastatic dissemination [79,80]. Using VIII, MK2206 or AZD5363, we observed a dose-dependent inhibition of growth and survival in adherent and non-adherent conditions (Figure 5A–C). Although all inhibitors induced a reduction in growth and survival, the strongest inhibition was observed for MK2206, with a 50% growth inhibition (GI50) observed at concentrations below 500 nM in all cell types (Figure 5C). In conjunction with previous results defining 0.5 μM to mark sensitivity to MK2206 [253], our results show that mouse and human ILC cells are among the most responsive anoikis resistant breast cancer cell lines reported. Overall, these results advocate the use of AKT inhibitors in the targeted treatment of ILC.

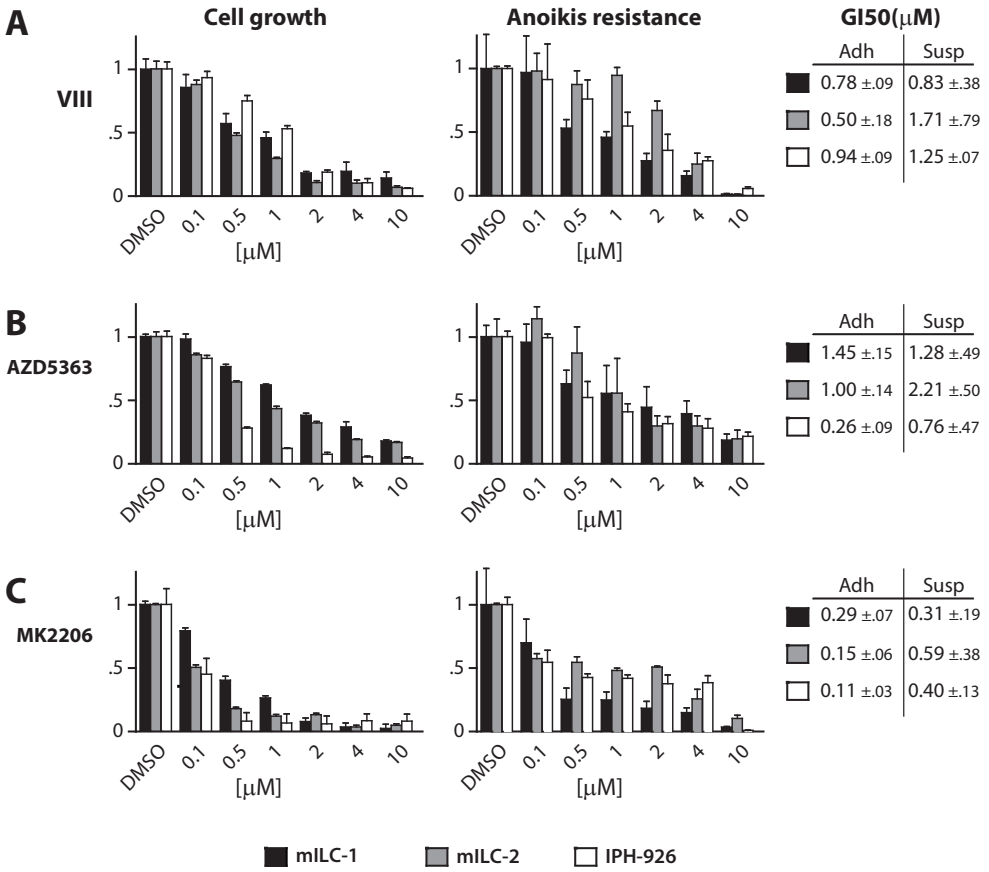

Figure 5 ILC cells are sensitive to AKT inhibition
A–C. Effect of VIII (A), AZD5363 (B) and MK2206 (C) on cell growth (left panels) and anoikis resistance (right panels) of mILC-1, mILC-2 and IPH-926 cells. The GI50 values (μM) for each inhibitor in adherent (Adh) and suspension (Susp) settings are depicted on the right side of the graph. GI50 values were calculated based on three independent experiments.

Discussion

Current treatment for ILC is mostly directed against estrogen receptors, as ER is expressed in the majority of luminal tumours. Despite the expression of these favourable prognostic markers, the overall prognosis for ILC is comparable to other types of breast cancer due to resistance to hormone receptor antagonists and low chemotherapeutic responsiveness [105,254,255]. Although targeted therapy for breast cancer is widely studied, clinical success rates have remained low, which might be largely attributed to the lack of good biomarkers that enable adequate patient stratification. Because ILC is a specific breast cancer subset that is driven by loss of E-cadherin [124–126,198,245], it is very well suited for targeted clinical intervention.

PI3K pathway inhibitors are and have been widely used as a targeted treatment option for breast cancer (reviewed in [108,256]). However, to our knowledge this treatment option has neither been specifically probed for in ILC, nor has it comprehensively been tested in ILC lacking GFR pathway mutations. We now show that loss of E-cadherin directly contributes to the activation of AKT signalling even in the presence of oncogenic *PIK3A* or inactivating *PTEN* mutations. As such, our data provide a clear ramification for use of PI3K/AKT inhibitors in the ILC spectrum. Also, because we detected differences between PTEN inactivation in non-invasive LCIS and ILC, we think our current studies provide evidence for an evolutionary scenario whereby loss of E-cadherin precedes PI3K/AKT pathway mutations.

Autocrine AKT activation upon E-cadherin inhibition can be caused by de-repression of GFR signals [50,51,57,60,257], a feature that we have recently coupled to p120-catenin loss and subsequent AJ dismantling [56]. Additionally, E-cadherin loss may promote reduced PTEN levels through MAGI2-dependent proteosomal degradation, resulting in increased AKT activation [258–261]. However, although we indeed detected reduced PTEN levels in ILC cell lines and ILC lesions when compared to the non-invasive counterparts, we have not obtained evidence for PTEN decrease as a direct result of E-cadherin knock-out. Our data indicate that AKT activation in ILC cells is instigated by an autocrine and GF-dependent PI3K/AKT activation loop. Interestingly, although GFR levels can be induced through AKT-dependent positive feedback signals [262–264], our current and published data do not support this scenario in the context of AJ inactivation [56].

Activation of PI3K signalling in cancer is often attributed to activating mutations, which are also frequently observed in ILC [97,129,130]. However, the fact that we observed increased AKT phosphorylation upon loss of E-cadherin in the presence of PI3K/AKT pathway mutations implies that two complementary modes of activation may underlie PI3K/AKT activation in ILC. An opportunity to treat primary ILC and its disseminating cancer cells arises from the ability of MK2206 to potently restrain cell survival of ILC cell lines in both adherent and non-adherent settings. As a monotherapy, MK2206 had a moderate effect on tumour growth in a breast xenograft model, while combination with paclitaxel further increased this anti-tumour effect [253,265]. In addition, phase I clinical trials combining MK2206 with paclitaxel, anastrozole or

trastuzumab in advanced solid tumours and metastatic breast cancer reported anti-tumour activity with no serious adverse effects [251,252,266]. Although the response to MK2206 *in vitro* was highly increased in cell lines harbouring *PIK3CA* or *PTEN* mutations, tumour responses could not be linked to the presence of mutations in *PIK3CA* [253,267]. Also, the low number of ILC cases in these studies generally prevents conclusions regarding efficacy of PI3K/AKT inhibition in ILC. An additional layer of complexity is added by the apparent lack of association between phospho-AKT levels in patients and mutational pathway activation [97,131,135,268]. These parameters further strengthen our assumption that AJ inactivation promotes PI3K/AKT activation. We propose therefore that inclusion criteria for clinical trials targeting PI3K/AKT should be complemented using aberrant E-cadherin localization, and/or a combination of E-cadherin loss and cytosolic p120 expression.

In conclusion we identify the PI3K/AKT pathway as a prime target for the treatment of ILC. Because AKT activation is a direct consequence of E-cadherin loss in this breast cancer subtype, functional inactivation of E-cadherin, rather than the presence of oncogenic mutations in this PI3K/AKT pathway, should be used as inclusion criteria for clinical PI3K/AKT intervention trials.

Materials and Methods

Cell culture

Mouse mammary carcinoma cells were cultured as described (Derksen 2006, 2011). MCF7 and IPH-926 cells were grown in DMEM-F12 (Sigma-Aldrich) containing 12% FCS (Sigma-Aldrich) supplemented with 100 IU/mL penicillin, 100 µg/mL streptomycin and 2.5 mM Ultraglutamine (Lonza). To generate E-cadherin knock-out cell lines, guide RNAs targeting human *CDH1* (GCTGAGGATGGTGTAAGCGATGG) and mouse *Cdh1* (CGTGTCATCAAATGGGGAAGCGG) were cloned into the pSicoR CRISPR/Cas9 vector using *BsmB*I restriction sites [241].

Reverse-phase protein array analysis

Cells were washed with ice-cold phosphate-buffered saline and lysed in 50 mM HEPES (pH 7.4), 1% Triton X-100, 10% glycerol, 150 mM sodium chloride, 1.5 mM magnesium chloride, 1 mM EGTA, 100 mM sodium fluoride, 10 mM sodium pyrophosphate, 1 mM sodium ortho-vanadate, supplemented with cOmplete ULTRA protease inhibitor and PhosSTOP phosphatase inhibitor cocktails (Roche), on ice. Lysates in biological triplicate were cleared by centrifugation (18,000 × *g*, 10 minutes, 4°C), adjusted to 1 mg/mL concentration and serially diluted to produce a dilution series comprising four serial 2-fold dilutions of each sample. Sample dilution series were spotted onto nitrocellulose-coated slides (Grace Bio-Labs) in technical triplicate under conditions of constant 70% humidity using an Aushon 2470 arrayer (Aushon Biosystems). Slides were hydrated in blocking buffer (Thermo Fisher Scientific) and incubated with validated primary antibodies (Additional table 1, not shown). Bound antibodies were detected by incubation with anti-IgG DyLight 800-conjugated secondary antibodies (New England BioLabs). Slides were read using an InnoScan 710-IR scanner (Innopsys), and

images were acquired at the highest gain without saturation of the fluorescence signal. The relative fluorescence intensity of each sample spot was quantified using Mapix software (Innopsys). The linear fit of the dilution series of each sample was determined for each primary antibody, from which median relative fluorescence intensities were calculated for each technical replicate. Signal intensities were normalized across the panel of antibodies using global sample median correction [269], and mean normalized intensities were calculated for each biological replicate (Additional table 2, not shown).

Western blotting

Protein samples were analyzed by SDS-PAGE and western blotting as previously described (Derksen 2004). In addition to the antibodies used for RPPA (Additional table 1, not shown), the following antibodies were used for western blotting: rabbit anti-phospho-AKT (Ser473) (1:1000; 5158, Cell Signaling Technologies), goat anti-AKT (1:1000; SC-1618, Santa Cruz Biotechnology) and mouse anti-GAPDH (1:10000; mAb374, Millipore). Secondary antibodies were swine anti-rabbit-PO (p217, DAKO), goat anti-mouse-PO (170-6516, Biorad), goat anti-rabbit-PO (170-6515, Biorad) and rabbit anti-goat-PO (p160, DAKO). When total protein and phospho-protein antibodies were used, samples were either run on different blots using GAPDH as a normalizer or stripped of their primary antibodies using 62.5 mM Tris-HCl (pH 6.7), 2% SDS, 0.7% β-mercaptoethanol (10 minutes, 50°C), or (when the primary antibodies were of two different species) treated with 1 mM NaN_3 to inhibit peroxidase activity.

Hierarchical cluster analysis

Mean normalized intensities were standardized by *Z*-score transformation. Normalized intensity values for phospho-proteins were further normalized to intensities of respective total proteins prior to standardization. Unsupervised hierarchical cluster analysis of standardized protein abundances for mouse samples was performed using Euclidean distance and Cluster 3.0 (C Clustering Library, version 1.37) [270], computing distances using a complete-linkage matrix. Clustering results were visualized using Java TreeView (version 1.1.1) [271]. Differences between protein abundances or $\log_2$-transformed ratios (phospho-protein/total protein) were assessed by *t*-tests with Benjamini–Hochberg *post hoc* correction to set the false discovery rate at 5%.

Conditioned medium stimulation assays

Cells were seeded in 6-well plates, serum-starved overnight and treated with serum of growth factors when cultures were approximately 80% confluent. Next, cells were lysed directly in lysis buffer containing 70 mM Tris-HCl (pH 7.4), 2% SDS, 4% glycerol and 0.5% β-mercaptoethanol. Cells were stimulated with 100 ng/mL recombinant *IGF* (Gibco Life Technologies). For the collection of conditioned medium, cells were grown without serum for at least 48 hours. Supernatant was harvested and cleared using a 45-µm filter.

Immunohistochemistry

Tissue microarrays (TMAs) were collected and constructed as previously described [272,273] or as follows: hematoxylin and eosin stained sections from primary ILC tumours were reviewed by a consultant breast pathologist and representative areas were identified. Construction of the TMA took place by extracting three individual tissue cores (0.6 mm) from these designated areas in the original paraffin embedded tissue blocks which were re-embedded into a recipient paraffin block. Approval was granted by the local tissue governance committee. Immunohistochemical stainings were performed as described before [272]. Primary antibody incubation was done for 2 hours at room temperature or at 4°C overnight (rabbit anti-phospho-AKT (Ser473), (1:10; D9E, 4060, Cell Signaling Technologies), rabbit anti-PTEN (1:100; 9559, Cell Signaling Technologies) in 1% BSA in PBS. HRP-conjugated secondary antibodies were Powervision poly-HRP anti-mouse, -rabbit and -rat (DPVO500-HRP, Immunologic) and poly-HRP anti-rabbit (DPVR500-HRP, Immunologic). These were incubated for 30 minutes at room temperature, followed by development using DAB and hematoxylin for counterstaining. Immunohistochemistry scoring took place blinded to patient characteristics and previous staining results. Scoring for phospho-AKT was done based on the presence of cytoplasmic staining. Cytoplasmic PTEN intensity was scored on a scale from 0 to 3 in which 2–3 were considered normal expression and 0–1 were low or absent.

Immunofluorescence

For immunofluorescence, cells were grown on glass cover-slips, washed with Ca^{2+}/Mg^{2+}-containing PBS and fixed with 4% PFA/PBS for 5 minutes at room temperature. Cells were permeabilized for 3 minutes using 0.3% Triton X-100 in PBS and blocked in 2% normal goat serum in PBS for 10 minutes. Blocking was performed by incubation in 10% normal goat serum in PBS for 10 minutes. Fixed samples were incubated overnight at 4°C with primary antibodies in 1% BSA in PBS using the following antibodies: mouse anti-p120 (1:500; 610134, BD Biosciences) and Alexa Fluor 555-conjugated anti-E-cadherin (1:100; 560064, BD Biosciences). Goat anti-mouse-Alexa Fluor 488 (A11029, Invitrogen) was used as a secondary antibody and incubated for 1 hour at room temperature. Samples were stained with DAPI for 3 minutes and mounted using Immu-Mount (Thermo Scientific). Samples were imaged using a Zeiss LSM 700 (Carl Zeiss) and processed using ImagesJ and Photoshop CS6 (Adobe).

Pharmacological inhibitors

The following AKT inhibitors were used: AZD5363 (ITK Diagnostics), MK2206 (MedChemExpress) and VIII (Santa Cruz Biotechnology). All inhibitors were prepared as 10 mM stock solutions in DMSO. The final DMSO concentration did not exceed 0.1%.

Anoikis assay

Anoikis assays were performed as previously described [79]. In short, cells were grown in suspension for 4 days, stained for apoptotic cells using AnnexinV-FITC (IQ products) and propidium iodide and analyzed by flow cytometry (FACSCalibur, BD Biosciences).

Colony formation assay

Anchorage-dependent cell growth was assessed as described before [112]. In short, cells were grown on 12-well plates incubated with the indicated inhibitors. When untreated cells reached confluence, the cells were fixed using methanol and stained with 0.2% crystal violet. After scanning the plates using an Epson perfection 4490 scanner, ImageJ was used to quantify the surface area containing stained cells.

mRNA sequencing

Cells were seeded into a 6-well plate and grown to 80% confluence in serum-containing medium. After washing in Ca^{2+}/Mg^{2+}-containing PBS, RNA was isolated and purified using the RNeasy kit (Qiagen), followed by DNase treatment (Qiagen). After measurement of the concentration with a Qubit fluorometer (Invitrogen), 250 ng of total RNA was treated by Ribo-Zero rRNA removal kit (Epicentre) to remove ribosomal RNAs. 16 µl of purified RNA was fragmented by addition of 4 µl 5× fragmentation buffer (200 mM Tris acetate (pH 8.2), 500 mM potassium acetate and 150 mM magnesium acetate) and incubated at 94°C for exactly 90 s. After ethanol precipitation, fragmented RNA was mixed with 5 µg random hexamers, followed by incubation at 70°C for 10 minutes and chilling on ice. From this RNA primer mix, first-strand cDNA was synthesized by adding 4 µl 5× first-strand buffer, 2 µl 100 mM DTT, 1 µl 10 mM dNTPs, 132 ng of actinomycin D and 200 U SuperScript III in a total volume of 20 µl, followed by 2 hours incubation at 48°C. First strand cDNA was purified using a Qiagen MinElute column to remove dNTPs and eluted in 34 µl elution buffer. Second-strand cDNA was synthesized by adding 91.8 µl H_2O, 5 µg random hexamers, 4 µl of 5× first-strand buffer, 2 µl of 100 mM DTT, 4 µl of 10 mM dNTPs with dTTP replaced by dUTP, 30 µl of 5× second-strand buffer, 40 U of *Escherichia coli* DNA polymerase, 10 U of *E. coli* DNA ligase and 2 U of *E. coli* RNase H, and incubated at 16°C for 2 hours, followed by incubation with 10 U T4 polymerase at 16°C for 10 minutes. Double-stranded cDNA was purified using a Qiagen MinElute column and used for Illumina sample preparation and sequencing according to the Illumina protocol. Before the final PCR, a band corresponding to ~300 bp (DNA+Adaptor) was collected and incubated with 1 U USER enzyme (NEB) at 37°C for 15 minutes followed by 5 minutes at 95°C. The 300-bp libraries were used for cluster generation on a HiSeq 2000 (Illumina). RNA-seq reads were uniquely mapped to the human (hg19) and mouse (mm9) reference genome using the ELAND or BWA program, allowing 1 mismatch, and subsequently used for bioinformatic analysis. RPKM (reads per kilobase of gene length per million reads) [274] values for RefSeq genes were computed using tag counting scripts and used to analyze the expression level of genes. The RNA sequencing data are deposited in GEO under accession number GSE81977

Mutation analysis

Genomic DNA was isolated by standard proteinase K digestion and column purification (QIAamp DNA mini kit). Control DNA was obtained from a female *Wcre;Cdh1$^{F/F}$;Trp53$^{F/F}$* mouse liver [80]. Gene panels were designed using the Ion AmpliSeq Designer website (v4.2 Ampliseq.com) and mapped to the human (hg19) and mouse (mm10) genome. Amplicon

libraries were synthesized using standard Ampliseq protocols (Thermo Fisher). In short, amplicons were amplified followed by digestion of the primers using FuPa reagent (Thermo Fisher). Sequence adapters and barcodes were ligated to the digested amplicons and a short amplification and size selection was performed using AMPure beads (Beckman Coulter) to select complete and specific libraries. All libraries were pooled equimolarly and used for emulsion PCR on a OneTouch™ 2 system using the Ion PMG template OT2 400 kit (Thermo Fisher). After loading the live ISPs on an Ion 318™ chip, sequencing was performed on an Ion Torrent PGM using Ion PGM 400 sequencing chemistry (Thermo Fisher), after which standard coverage analysis and variant-caller settings were used to detect variations. After variant calling, functional consequences were analyzed using the Variant Effect Predictor (Ensembl). For mouse variants predicted to have a functional consequence, the corresponding human sequence was analyzed for the presence of known somatic mutations in cancer (COSMIC).

Statistical analysis

For the calculation of GI50s (50% growth inhibition or 50% anoikis), GraphPad Prism 5 was used. For statistical analysis of inhibitor assays, Student's *t*-tests were performed. *P*-values of < 0.05 were considered significant.

Availability of data and materials

The datasets supporting the conclusions of this article are included within the article and its additional files. The RNA sequencing data are deposited in GEO under accession number GSE81977.

Authors' contributions

VGB, PWBD, KT and MT conceived and designed the study. KT, MT, AB, NH, JHAM, ES, AM, AAS, PvG and PJvD conducted the experiments. AB, ES and AAS performed bioinformatics analysis. KT, MT and AB analyzed and interpreted the data. MC contributed material. MT and PWBD wrote the initial version of the paper, VGB, KT and AB revised follow-up versions and all authors critically reviewed the final manuscript.

Acknowledgements

Members of the Derksen, Brunton and Van Diest labs are acknowledged for support and suggestions. We thank Corlinda ten Brink and the UMC Utrecht Cell Microscopy Center for imaging support and Kenneth MacLeod for RPPA data acquisition.

Additional Table 3 (A) Autocrine growth factor - receptor expression in mILC

Gene name Receptor	Gene-ID	Expression in mILC-1	Expression in mILC-2
Acvr1	NM_001110204	2,390	3,3406
Acvr1b	NM_007395	5,724	7,7359
Acvr2a	NM_007396	5,881	4,9895
Bmpr1a	NM_009758	14,554	30,737
Bmpr1b	NM_007560	3,202	0,64146
Bmpr2	NM_007561	5,766	5,002
Csf1r	NM_001037859	2,738	10,186
Egfr	NM_007912	11,458	15,857
Erbb2	NM_001003817	18,224	20,096
Erbb3	NM_010153	10,892	9,1797
Fgfr1	NM_001079908	11,841	14,584
Fgfr2	NM_010207	0,141	1,1318
Igf1r	NM_010513	4,189	6,0724
Igf2r	NM_010515	0,118	17,93300
Insr	NM_010568	4,884	6,1629
Met	NM_008591	47,713	36,518
Pdgfra	NM_001083316	4,148	0,87915
Pdgfrb	NM_001146268	1,148	0,35569
Tgfbr1	NM_009370	14,327	20,275
Tgfbr2	NM_009371	45,771	100,84
Tgfbr3	NM_011578	0,000	8,0404
Vegfr3	NM_008029	0,000	7,639

Gene name Ligand	Gene-ID	Expression in mILC-1	Expression in mILC-2
Inha	NM_010564	0,781	1,170
Inhba	NM_008380	18,305	40,715
Inhbb	NM_008381	21,076	17,873
Bmp1	NM_009755	31,778	50,594
Bmp4	NM_007554	1,603	4,240
Bmp7	NM_007557	22,226	31,502
Csf1	NM_001113529	33,225	35,265
Csf3	NM_009971	9,246	13,263
Areg	NM_009704	8,579	19,270
Btc	NM_007568	0,662	3,422
Epgn	NM_053087	1,101	0,439
Ereg	NM_007950	7,008	37,577
Hbegf	NM_010415	13,894	26,122
Nrg1	NM_178591	4,306	3,764
Nrg4	NM_032002	2,022	1,831
Fgf13	NM_010200	0,012	4,248
Fgf2	NM_008006	0,337	1,231
Irs1	NM_010570	6,582	4,261
Irs2	NM_001081212	3,718	6,665
Hgf	NM_010427	1,574	3,650
Pdgfa	NM_008808	20,211	44,472
Pdgfb	NM_011057	18,459	19,269
Pdgfc	NM_019971	0,292	13,462
Tgfa	NM_031199	5,052	5,109
Tgfb1	NM_011577	1,442	1,839
Tgfb3	NM_009368	8,026	4,424
Vegfa	NM_001025250	18,331	66,330
Vegfb	NM_001185164	6,725	6,974
Vegfc	NM_009506	15,284	41,739
Figf	NM_010216	0,625	1,939

Additional Table 3 (B) Autocrine growth factor - receptor expression in human ILC

Gene name Receptor	Gene-ID	Expression in IPH-926
Acvr1	NM_001105	4,396
Acvr1b	NM_004302	8,470
Acvr2a	NM_001616	7,976
Acvr2b	NM_001106	1,240
Bmpr1a	NM_004329	6,75
Bmpr2	NM_001204	6,353
Erbb2	NM_004448	93,260
Erbb3	NM_001982	68,480
Erbb4	NM_001042599	3,635
Fgfr1	NM_001174067	15,297
Fgfr3	NM_022965	9,263
Fgfr4	NM_002011	52,922
Tgfbr1	NM_004612	101,310
Tgfbr3	NM_001195683	14,840

Gene name ligand	Gene-ID	Expression in IPH-926
Inhbb	NM_002193	39,668
Bmp6	NM_001718	8,980
Bmp7	NM_001719	73,514
Btc	NM_001729	5,089
Egf	NM_001963	2,213
Hbegf	NM_001945	1,545
Fgf13	NM_001139500	3,084
Tgfb2	NM_001135599	2,687
Tgfb3	NM_003239	42,879

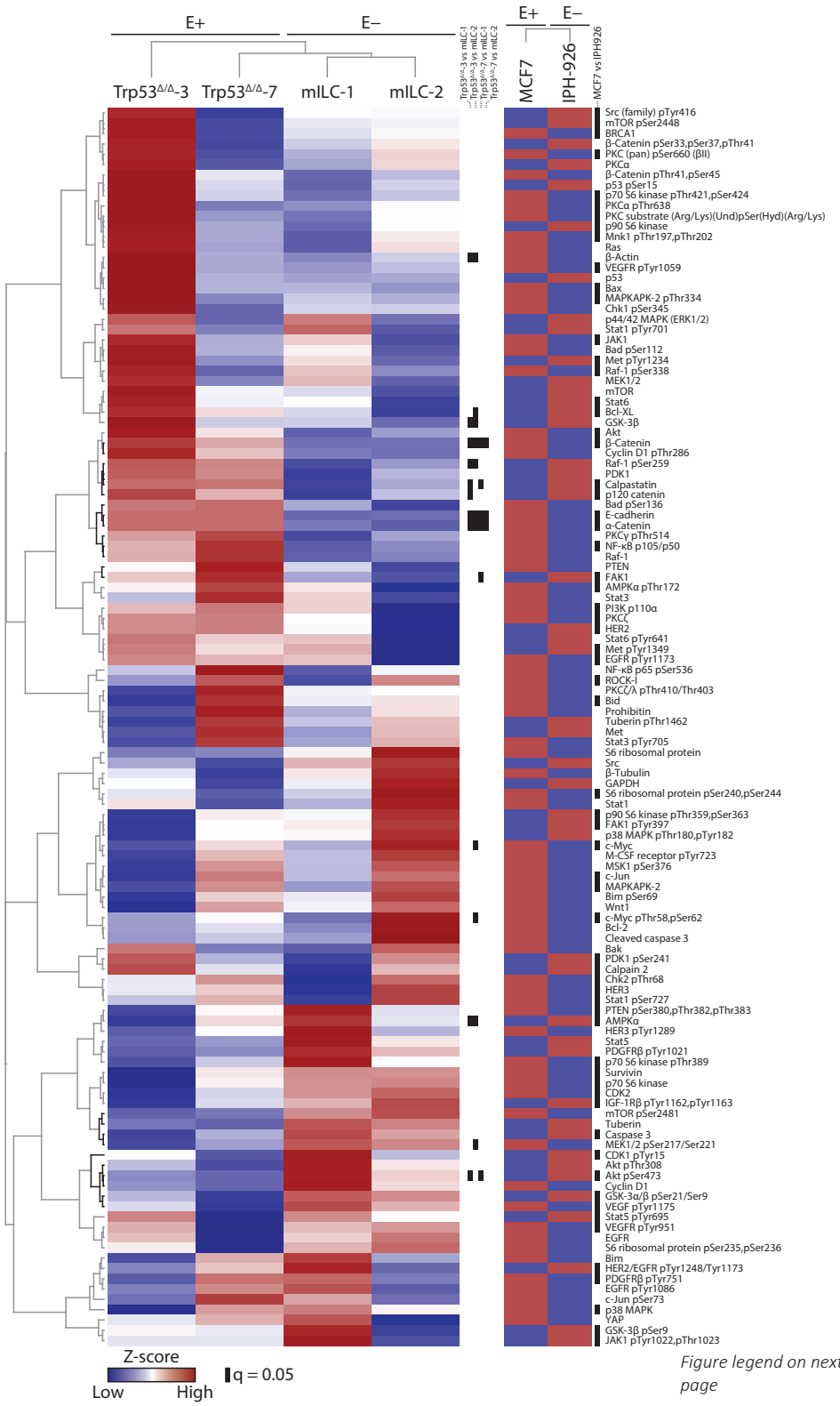

Figure legend on next page

Figure S1 *(previous page)* Protein expression and phosphorylation in the context of E-cadherin expression
Hierarchical clustering of RPPA data revealed phosphorylated and total protein expression differences comparing E-cadherin-positive (E+) and E-cadherin-negative (E–) human and mouse breast cancer cell lines. Normalized intensity values were standardized as Z-scores and subjected to hierarchical cluster analysis. Data from mouse and human cell lines were standardized separately owing to different antibody affinities to proteins from different species. Heat maps display the relative enrichment of proteins or phospho-proteins (red, up-regulated; blue, down-regulated). Human data were aligned with hierarchically clustered mouse data. Dendrograms for protein or phospho-protein clusters selected in Figure 2 are highlighted in black. Significantly differentially regulated proteins or phospho-proteins are indicated by a black bar (false discovery rate (q), 5%).

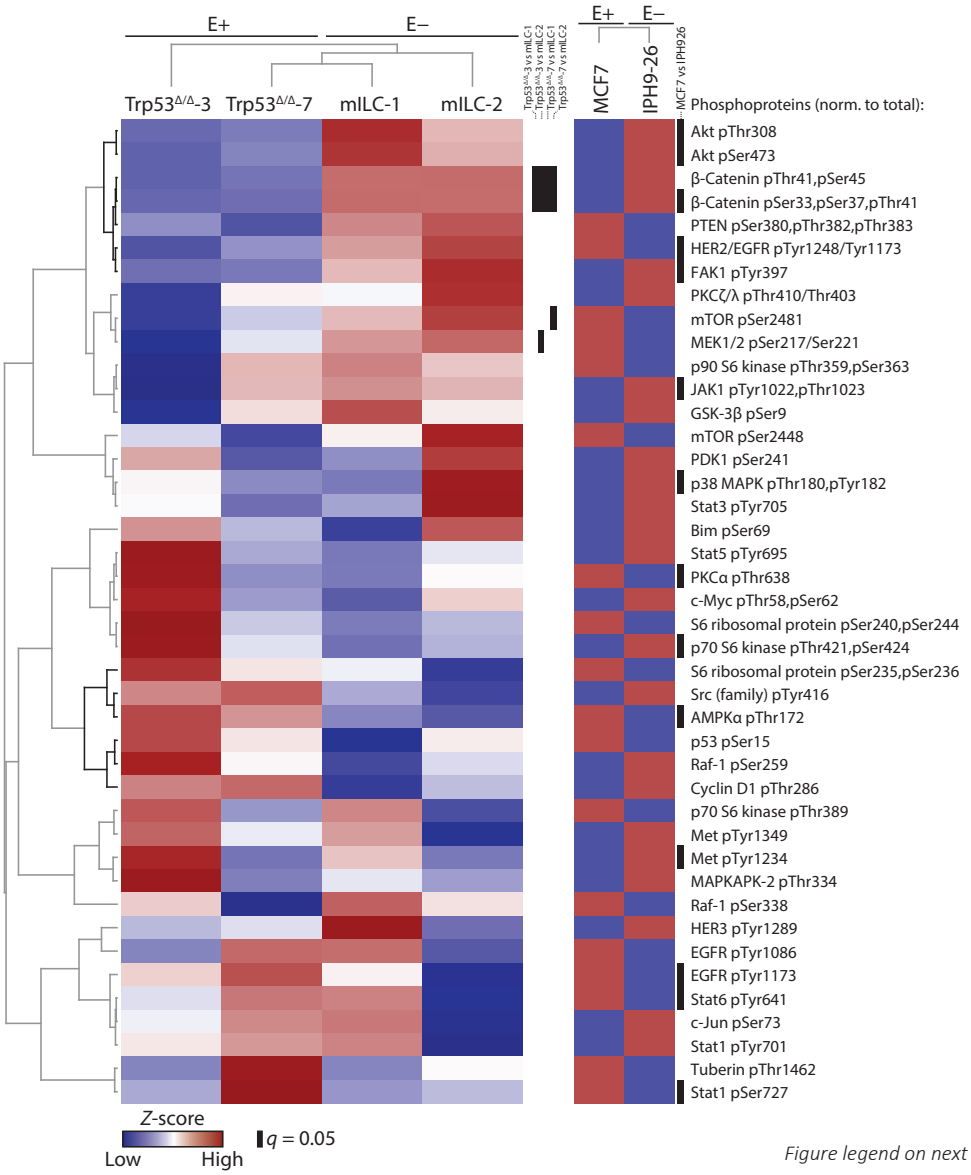

Figure legend on next page

Figure S2 *(previous page)* Hierarchical clustering reveals differences in normalized phospho-protein levels upon loss of E-cadherin expression.
Levels of phospho-proteins relative to respective total proteins levels in whole cell lysates from E-cadherin-positive (E+) and E-cadherin-negative (E−) cells were determined by RPPA. Normalized intensity values for phospho-proteins were further normalized to intensities of respective total proteins as log2-transformed ratios (phospho-protein/total protein), standardized as Z-scores and subjected to hierarchical cluster analysis. Data from mouse and human cell lines were standardized separately owing to species-dependent antibody affinity differences. Heat maps display the relative enrichment of phospho-proteins (red, up-regulated; blue, down-regulated). Human data are displayed as the difference of expression in IPH-926 over MCF7. Significantly differentially regulated phosphorylated proteins are indicated by a black bar (false discovery rate (q), 5%).

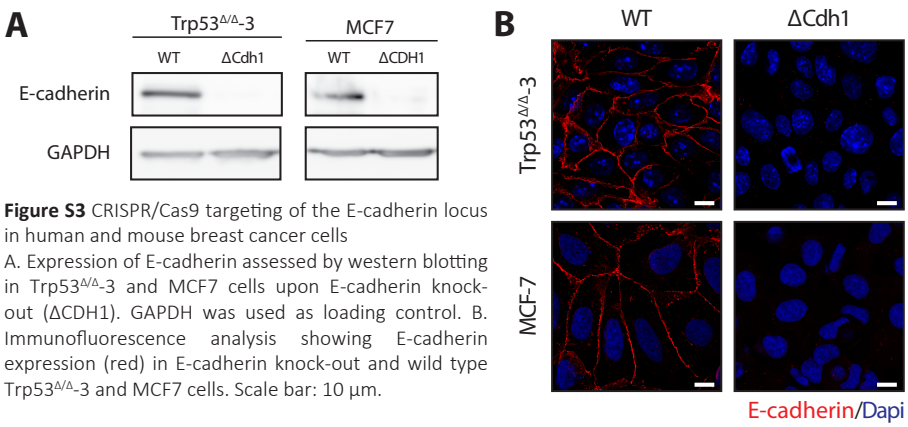

Figure S3 CRISPR/Cas9 targeting of the E-cadherin locus in human and mouse breast cancer cells
A. Expression of E-cadherin assessed by western blotting in Trp53$^{\Delta/\Delta}$-3 and MCF7 cells upon E-cadherin knock-out (ΔCDH1). GAPDH was used as loading control. B. Immunofluorescence analysis showing E-cadherin expression (red) in E-cadherin knock-out and wild type Trp53$^{\Delta/\Delta}$-3 and MCF7 cells. Scale bar: 10 µm.

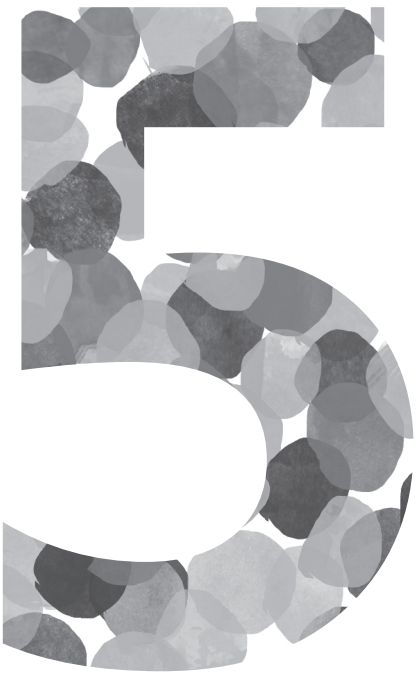

Chapter 5

Kaiso modulates transcriptional repression to control key biological processes through a CpG-containing consensus site

Milou Tenhagen[1], Robert A.H. van de Ven[1], Stephin J. Vervoort[2], Tobias M. Franks[3], Chris Benner[3], Amit Mandoli[4], Abhishek A. Singh[5], Martin W. Hetzer[3], Joost H. Martens[4], Hendrik G. Stunnenberg[4], and Patrick W.B. Derksen[1]

[1] Department of Pathology, University Medical Center Utrecht, Utrecht, The Netherlands.
[2] University Medical Center Utrecht, Department of Cell Biology, Utrecht, The Netherlands.
[3] Laboratory of Molecular and Cellular Biology, Salk Institute for Biological Studies, La Jolla, California
[4] Department of Molecular Biology, Faculty of Science, Nijmegen Centre for Molecular Life Sciences, Radboud University, Nijmegen, The Netherlands.

Manuscript in preparation

Abstract

Transcriptional repression by Kaiso (ZBTB33) occurs through binding to a sequence specific classical consensus Kaiso binding sequence (cKBS) and methylated CpGs. Although cKBS-specific Kaiso target genes have been identified, it is still unknown if and how Kaiso modulates transcriptional repression on a genome-wide scale. Using a combination of Kaiso-specific chromatin immunoprecipitation (ChIP) and Dam methyltransferase identification (DamID) approaches, we have mapped Kaiso binding sites to active promotor regions in breast cancer cells. Here, Kaiso preferentially binds to a methylation-prone CpG-containing Kaiso binding sequence TCTCGCGAGA (mKBS). We find that mKBS target genes are actively transcribed and linked to processes such as metabolism, cell cycle regulation and DNA damage repair. Our data thus favors a model in which Kaiso dampens transcriptional activation that drives key biological cues through binding to the CGCG-containing mKBS.

Introduction

Kaiso (*ZBTB33)* is a member of the zinc finger and broad-complex, tramtrack and bric-à-brac or poxvirus and zinc finger (BTB/POZ-ZF) transcription factor family that was initially identified in a yeast-two-hybrid screen as a p120-catenin (p120) binding partner [23]. Kaiso functions as a transcriptional repressor and interaction between Kaiso and p120 results in displacement of Kaiso from the DNA and subsequent transcription of genes. Kaiso binds to a specific DNA sequence, *TCCTGCNA*, called the classical Kaiso Binding Sequence (cKBS) [26]. Binding of Kaiso to the cKBS in promotors results in transcriptional repression of *Wnt11* [27], Cyclin D1 (*CCND1*) [175] and Matrix metalloproteinase 7 (*MMP7*) [26]. Derepression of Kaiso at the cKBS by p120 is dependent on nuclear translocation of p120 through a conserved NLS signal [18,111]. Kaiso has also been implicated in transcriptional activation by binding to a cKBS in the promotor of Rapsyn (*RPSN).* However, transcription of Rapsyn was regulated by Kaiso binding to the p120 family member δ-catenin instead of p120 [165].

Kaiso can also directly affect transcription through a non-cKBS-dependent DNA interaction by binding to methylated CpG (mCpG) sites in the promotor of Metastasin (*S100A4*) [160], Metastasis associated 1 family member 2 (*MTA2*) [154] and Cyclin-dependent kinase inhibitor 2A (*CDKN2A*) [162]. More recently, a CpG-containing consensus binding site was identified based on Kaiso chromatin immunoprecipitation (ChIP) available through ENCODE and subsequent *in silico* analyses [166,167], although the physiological significance of this interaction awaits further functional confirmation. Binding of Kaiso to the cKBS and mCpGs occurs through three zinc finger domains that recognize specific bases in the major groove of the cKBS and mCpG sites through both classical and methyl hydrogen bonds [25,160]. In addition, residues in the Kaiso C-terminus are required for high-affinity Kaiso-DNA interactions through binding to the opposing minor groove [24]. Apart from direct interactions with cKBS and mCpG residues, Kaiso can also modulate transcription indirectly through complex formation with other transcription factors. First, increased expression of Kaiso upon DNA damage strengthened

a Kaiso-p53 interaction at p53-responsive DNA elements [153], a process that augmented p53-DNA binding resulting in enhanced expression of apoptotic p53 target genes [275]. Second, a POZ domain-dependent Kaiso interaction with the transcriptional repressor CTCF controlled de-repression of the enhancer-blocking activity of CTCF at the insulator of the β-*globin* gene [152,177].

Loss of Kaiso resulted in major developmental defects at the gastrulation stage in *Xenopus* and zebrafish embryos, which has been coupled to aberrant regulation of canonical and non-canonical Wnt target genes [27,175,180,183] Given the assumed convergence of parallel p120/Kaiso and canonical TCF/LEF target genes in vertebrate development, these studies suggested a possible role for Kaiso in cancer (reviewed in: [204]). Initial studies in cancer showed that Kaiso expression was indeed aberrant in cancers [148]. Thymic carcinoma, non-small cell lung cancer and colon cancer displayed increased cytoplasmic expression when compared to healthy tissues, which associated with decreased overall survival and high stage tumors [29,187,188,190,193]. Interestingly, prostate tumors and ductal breast carcinoma were characterized by distinct and elevated expression of nuclear Kaiso, a feature that was associated with a high grade and poor prognosis [159,189]. Studies in cancer cells also suggested that Kaiso function may be regulated by external cues, because Kaiso expression and localization appeared to be strongly influenced by culture conditions and the tumor microenvironment [148].

Because Kaiso was initially identified as a transcriptional repressor of oncogenes, its role in cancer pointed towards that of a tumor suppressor. However, loss of Kaiso in the Wnt-driven $APC^{Min/+}$ mouse model of intestinal cancer delayed tumor development, suggesting an unexpected oncogenic role for Kaiso in cancer [186]. Also, ectopic Kaiso overexpression in the $APC^{Min/+}$ mouse model enhanced tumorigenesis, a feature that was accompanied by a paradoxical increase in Wnt target genes [187]. Recent findings in breast cancer have functionally implicated Kaiso as a tumor suppressor. In these studies, relief of Kaiso-dependent *Wnt11* repression by p120 resulted in autocrine and constitutive actomyosin contraction, which underpinned anchorage-independent survival of tumor cells [111].

Because of the suggested involvement of Kaiso in cancer and the ambiguous reports on Kaiso-DNA binding *in vivo,* we set out to perform a comprehensive analysis to identify the genome-wide Kaiso binding sites in breast cancer using two complementary approaches. A combination of Kaiso chromatin immunoprecipitation (ChIP) and DNA adenine methyltransferase identification (DamID) followed by next-generation sequencing revealed that Kaiso preferentially binds to active promotor regions. Our data identified a Kaiso-specific CGCG-containing consensus site that is linked to genes implicated in fundamental processes such as metabolism, cell cycle control and DNA damage repair.

Results

Identification of Kaiso binding sites by ChIP-seq and DamID-seq

Although it is evident that Kaiso can modulate transcriptional processes through binding to a sequence specific cKBS and/or mCpG, the identification of the genome wide binding sites in cancer remained unclear. We therefore performed Kaiso-specific ChIP-seq and DamID-seq (Fig. 1). We used p53 knockout cells from a conditional mouse model that model human breast cancer ($Trp53^{\Delta/\Delta}$-3 cells; [79]), because we have recently used these cells to identify p120-dependent Kaiso repressor-activity at the cKBS of *Wnt11* [111].

After Kaiso ChIP and subsequent next-generation sequencing, we performed genome-wide analysis and identified 6713 peaks with an average width of 822 basepairs (bp) (Fig. 2A). In parallel, we performed Kaiso DamID to partly corroborate our ChIP findings and complement them with transient Kaiso-DNA interaction that may be missed by conventional ChIP approaches. To minimize a-specific methylation by the DAM methylase Kaiso fusion proteins (Dam-Kaiso) we made use of retroviral transduction ensuring low expression levels (Fig. S1). After extraction of DNA from cells expressing Dam-Kaiso and (control) Dam-GFP, methylated sequences were PCR-amplified for detection by next-generation sequencing (Fig. 1). During analysis, DamID-peaks were identified by calculating the ratio of normalized Dam-Kaiso reads over Dam-GFP reads using a cutoff of a 3-fold increase in Dam-Kaiso reads. This computational analysis identified a total of 16,288 DamID-peaks that had an average width of 3391 bp (Fig. 2A). Comparison of Kaiso ChIP-peaks with DamID-peaks revealed a positive correlation between Kaiso ChIP tags and the ratio of normalized Dam-Kaiso tags over Dam-GFP tags (r=0.342, Fig. 2B-C). Moreover, we observed a positive correlation between the number of Kaiso ChIP and Dam-Kaiso tags (r=0.310, Fig. S2A), while there was no correlation

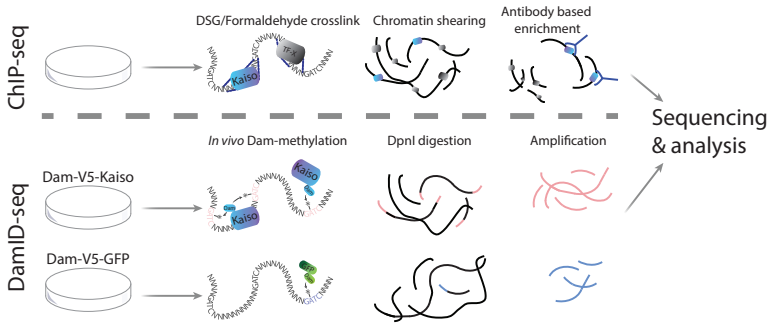

Figure 1 Kaiso binding site identification by ChIP- and DamID-sequencing

Schematic representation of ChIP (top) and DamID procedures (bottom). For ChIP-sequencing, protein-DNA interactions were cross-linked, followed by nuclear extraction and sonication to obtain 200 to 600 bp DNA fragments. Kaiso-specific monoclonal antibodies were used to immunoprecipitate the Kaiso-DNA complexes, followed by next-generation sequencing. DamID analyses were done after stable low-level expression of Dam-Kaiso or Dam-GFP. DNA-adenine-methyltransferase (Dam) methylated GATC sequences on the adenine-N6 position. Expression of Dam-GFP fusion proteins was used as a control for background methylation. After DNA isolation, DpnI fragments were prepared and used for sequencing. The ratio of Dam-V5-Kaiso (Dam-Kaiso) over Dam-V5-GFP (Dam-GFP) was then used to map specific binding sites.

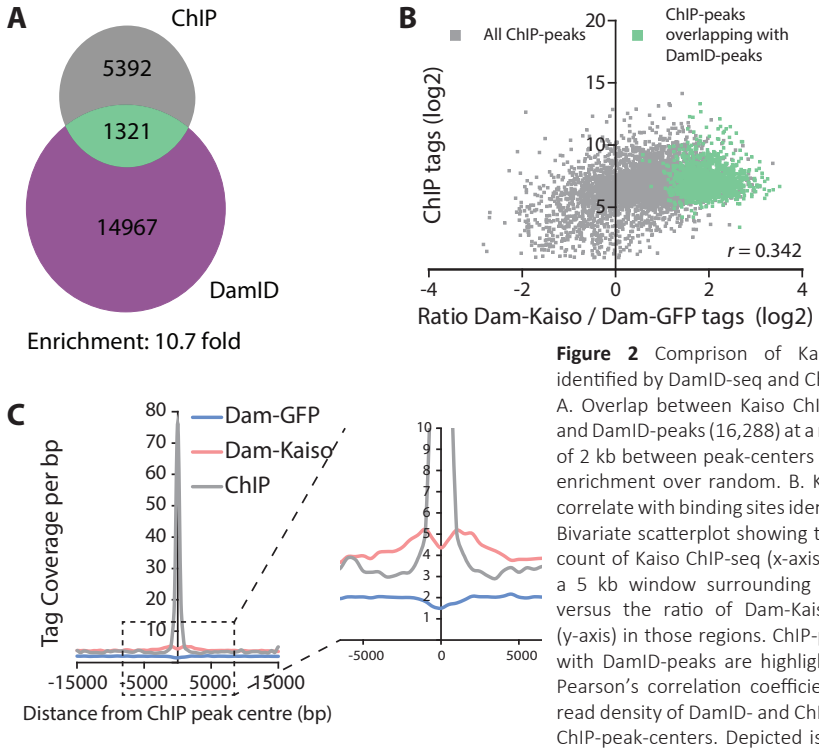

Figure 2 Comprison of Kaiso binding sites identified by DamID-seq and ChIP-seq
A. Overlap between Kaiso ChIP-peaks (n=6,713) and DamID-peaks (16,288) at a maximum distance of 2 kb between peak-centers display a 10.7-fold enrichment over random. B. Kaiso DamID ratios correlate with binding sites identified by ChIP-seq. Bivariate scatterplot showing the normalized tag count of Kaiso ChIP-seq (x-axis, grey dots) within a 5 kb window surrounding ChIP-peak-centers versus the ratio of Dam-Kaiso over Dam-GFP (y-axis) in those regions. ChIP-peaks that overlap with DamID-peaks are highlighted in green, r = Pearson's correlation coefficient. C. Sequencing read density of DamID- and ChIP-seq surrounding ChIP-peak-centers. Depicted is the tag coverage in 500 bp bins.

between Kaiso ChIP tags and Dam-GFP tags (r=0.155, Figure S2B). We mapped 1321 overlapping regions between Kaiso ChIP-peaks and DamID-peaks, which is roughly 20% of all ChIP-peaks identified (Fig. 2A and Fig. S2C-F). Overall, ChIP-seq identified 5392 Kaiso binding sites that did not overlap with those mapped using DamID. Conversely, DamID yielded 14967 potential Kaiso binding sites that were not identified using ChIP.

Kaiso binds to promotor-regions at a CGCG-containing recognition site

Analysis of Kaiso binding sites identified by ChIP-seq revealed a high occupancy of Kaiso in promotors and 5-prime UTR regions, representing a 34- and 48-fold enrichment over random respectively (Fig. 3A). Kaiso binding sites identified by DamID-seq were also enriched at these genomic locations surrounding the transcription start site (TSS), although less pronounced than seen for ChIP-seq (Fig. 3A). Kaiso-binding was focused at regions within 1 kb up- and downstream from the TSS, which represented approximately 50% of all ChIP-peaks identified (Fig. 3B and 3D). Since Kaiso is known to bind mCpGs, we assessed whether Kaiso binding sites overlapped with CpG islands. Interestingly, Kaiso binding primarily occurred in CpG-rich regions. We observed an overall 57-fold increase in ChIP and DamID peaks that overlapped with a CpG-island (Fig. 3C). Although this can be explained by abundant Kaiso binding in promotor regions, which are generally rich in CpG islands, 90.6% of all ChIP-peaks in promotors overlapped with a CpG island, while only 53% of all mouse promotors contained a

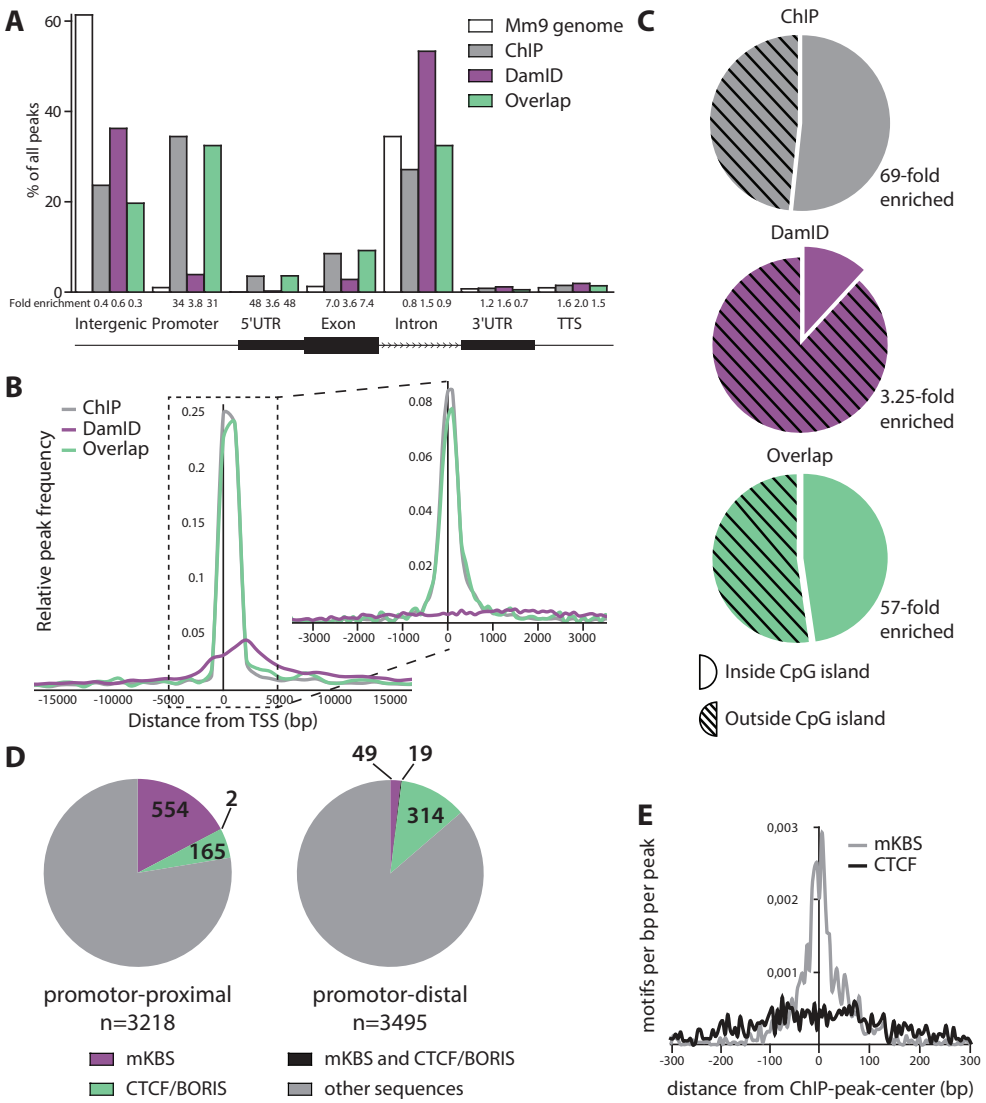

Figure 3 Kaiso binds to a CGCG-containing consensus binding site in promotors

A. Genomic regional distribution of ChIP and DamID peaks. Shown are the location of Kaiso binding in the ChIP-seq (grey), DamID-seq (purple) and overlapping (green) datasets. White bars indicate the relative distribution of the depicted regions over the entire mouse genome (mm9). The fold increase in peak presence at a given region as compared to the whole mouse genome is depicted below the x-axes. Promotors are defined as the region from -1000 to +100 bp from the TSS. The transcription termination site (TTS) encompasses a region from -100 to + 1000 bp relative to the termination codon. B. ChIP-seq peaks are enriched within a region of 1 kb up- or downstream of the TSS. Relative peak frequencies within a given distance from the TSS were calculated and plotted in 1000 bp (left) and 100 bp bins (inset; right). C. Kaiso binding is enriched in regions that contain CpG islands. Pie charts depict the percentage of ChIP-seq, DamID-seq and overlapping regions that show overlap with a CpG islands. D. mKBS sites are enriched within 1 kb up- and downstream of the TSS (promotor-proximal), while CTCF and Boris recognition sites are enriched in promotor-distal elements. E. Histogram of motif density showing the enrichment of the mKBS at the center of ChIP-peaks, while CTCF recognition sites are more evenly distributed within 100 bp up- and downstream of the ChIP-peak-center.

CpG island. This preferential binding of Kaiso to CpG rich regions indicates that (methylated) CpGs could indeed represent a Kaiso binding site. Additional motif analysis revealed a palindromic CGCG-containing motif that was previously mapped as a Kaiso binding sequence based on publicly available (ENCODE) ChIP data in myeloid (K562) and lymphoid (GM12878) cells [166,167]. The identified motif consisted of ten core nucleotides (TCTCGCGAGA) that we have now designated the methyl-Kaiso Binding Sequence (mKBS) (Fig. S3A). The fact that the mKBS is a common promotor element occurring in 5% of all human TATA-less promotors [276] strengthens our finding that approximately 90% of our mKBS sites were located within 1 kb up- or downstream of the TSS (Fig. 3D). Interestingly, 234 of the total 6713 Kaiso ChIP-peaks contained the previously identified cKBS, which is not a significant enrichment over the genome-wide occurrence of this sequence. Finally, de novo motif discovery did not identify additional novel motifs aside from a truncated version of the mKBS (Fig. S3C).

Kaiso binding co-occurs with CTCF binding sites enabling modulation of enhancer activity

Next to the mKBS we identified CTCF and its close relative Boris as two other significantly enriched motifs (Fig. 3D and Fig. S3A). In contrast to the location of the mKBS we did not observe an enrichment of CTCF or Boris motifs in promotor-proximal regions flanking the TSS (Fig. 3D). This is in line with the established role of CTCF in insulators to establish chromatin loops that mediate long-range interactions between enhancers and promotors [176]. Closer examination of the positioning of CTCF and mKBS motifs relative to the site of Kaiso-binding, revealed an interesting pattern. Whereas the mKBS displayed a sharp enrichment at the ChIP-peak centers, the CTCF motif was more broadly located around the median peak signal (Fig. 3E). These findings suggested that Kaiso and CTCF could function as co-regulators of a common gene, as has been observed for β-*globin* [152].

Motif analysis on DamID data also identified several members of the AP1 transcription factor family in close vicinity of Kaiso binding sites (Fig. S3A). However, inspection of the regions flanking the Kaiso binding sites from the ChIP assays did not reveal an enrichment of AP1 family member or any other known or novel motifs (data not shown). In conclusion, we have identified two subsets of Kaiso binding sites using ChIP and DamID; promotor-proximal mKBS-containing sites, and sites in close vicinity of the CTCF motif distal to the TSS.

Kaiso target genes are involved in processes linked to cancer progression

To assess which pathways could be affected by Kaiso repression through the mKBS, we started by characterizing the chromatin landscape of Kaiso-bound regions. For this we performed ChIP-seq for histone 3 lysine 4 tri-methylation (H3K4me3), a feature that is enriched at promotor regions with an open chromatin state. Additionally, we identified active enhancers and promotors of transcribed genes by performing ChIP-seq for histone 3 lysine 27 acetylation (H3K27Ac) and regions of active transcription by RNA polymerase II (Pol2) ChIP-seq [277,278]. Kaiso binding sites were divided into two groups; sites present within a promotor (defined as peaks occurring within 1 kb up- or downstream from the TSS without an apparent consensus site) and sites present within a promotor containing the mKBS motif (mKBS Kaiso

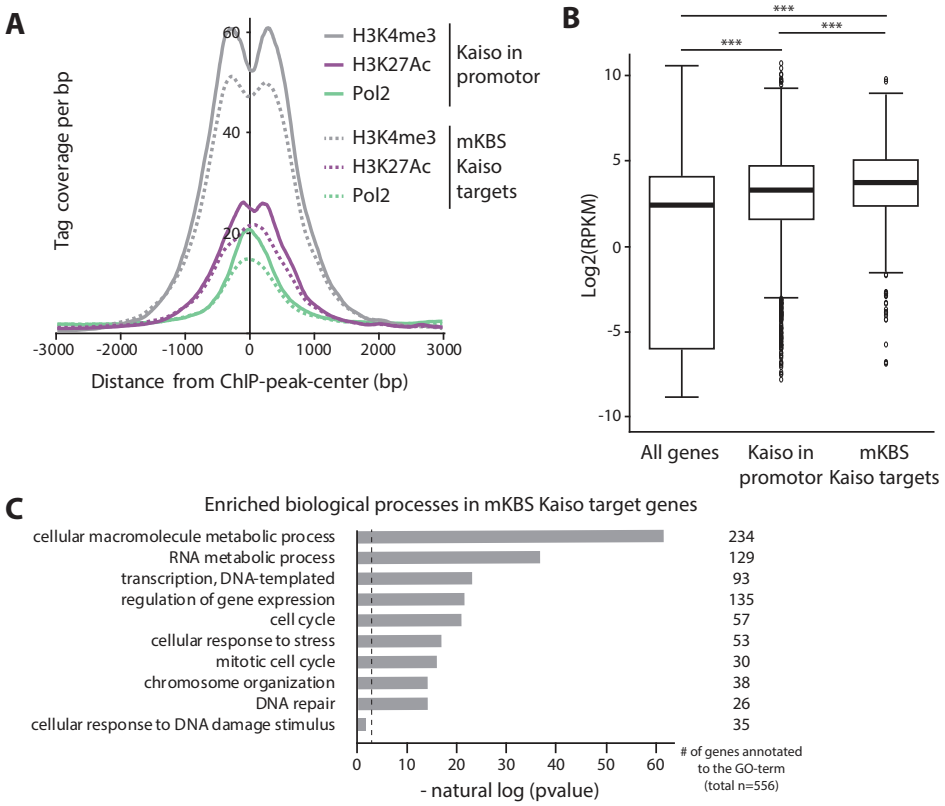

Figure 4 Binding of Kaiso occurs in transcriptionally active regions
A. Active promotor elements are enriched at Kaiso binding sites. ChIP-seq of RNA polymerase 2 (Pol2, green line), H3K27Ac (purple line) and H3K4me3 (grey line) revealed an enrichment of the active transcription marks around the ChIP-peak-center of Kaiso binding sites within the promotor without a consensus site (dashed lines) and mKBS Kaiso targets (filled line). Depicted is the fragment coverage in 5 bp bins. B. Kaiso target genes are expressed. mRNA-sequencing analysis revealed a significant increase in mRNA expression levels of genes containing a ChIP-peak in their promotor compared to all expressed mRNAs. Note the increase in mRNA expression levels of mKBS Kaiso targets. RPKM: reads per kilobase of gene length per million reads, *** $p<0.00001$. C. Pathways and processes regulated by Kaiso. Selection of the top enriched GO-terms linked to active genes harboring a mKBS. The numbers behind each bar represent the number of genes annotated to each category. Dashed line marks $p = 0.05$.

targets). Although both Kaiso targets were accompanied by a high occupancy of all three markers of active transcription (Fig. 4A), this was particularly evident at mKBS Kaiso target sites. The presence of Pol2 at Kaiso target genes was substantiated by an increase in mRNA expression levels, particularly of the genes harboring the mKBS (Fig. 4B). To gain insight into the pathways and biological function processes linked to mKBS target genes we performed Gene Ontology analysis, which revealed a significant enrichment of genes controlling cellular metabolism, cell cycle processes and DNA damage repair responses (Fig. 4C). We did not find a correlation between mKBS Kaiso targets and the specific stages of cell cycle regulation or types of DNA damage response. Taken together, our data show that Kaiso binds to the mKBS in promotor regions of actively transcribed genes that control basic cellular processes and are linked to cancer progression.

Discussion

Kaiso was initially implicated in cancer by acting as a p120-dependent transcriptional repressor of oncogenes such as *CCND1*, *MMP7* and *S100A4* (reviewed in [204]). While it still remained unclear how Kaiso subcellular localization is controlled and what its implications are in the context of transcriptional derepression, functional studies showed that Kaiso can play a tumor-suppressive role in breast cancer. Here, nuclear-localized p120 partially drives tumor progression through a cKBS-dependent repression of the non-canonical *Wnt11* gene and possibly other target genes [111]. Conversely, in mouse models of intestinal cancer Kaiso appears to function as an oncogene [186,187]. This inverse role may be explained by a difference in context such as cell-type or hyperactivation of Wnt signaling, which results in binding to distinct DNA responsive elements. Interestingly, our data revealed that many of the identified Kaiso binding sites contained the methyl-responsive CGCG nucleotides within a consensus mKBS (*TCTCGCGAGA*). These findings are in full agreement with previously published studies that have used publicly-available ENCODE data to map Kaiso binding sites [166]. Of interest is our finding that the cKBS was not significantly enriched on a genome-wide scale, suggesting that the known bi-modal DNA recognition by Kaiso (cKBS *versus* methyl-dependent/mKBS) might elicit dual and/or non-related biological responses. Also, binding sites containing a cKBS did not coincide with the mKBS in our data set, suggesting that stabilization of Kaiso-mKBS binding by the cKBS is not a common phenomenon. However, because a cKBS directly downstream of methylated CpGs in the *CCND1* promoter can stabilize Kaiso binding to methylated CpGs [192], in principle, the two modes of Kaiso-DNA binding can functionally coincide. In conclusion, genome-wide Kaiso binding to the cKBS is a less frequently occurring event, and the majority of Kaiso-dependent transcription responses might be dependent on non-cKBS target genes. Together, our data and that of others suggest that Kaiso-dependent transcriptional repression is a mostly methylation-dependent event.

Coupling of our Kaiso ChIP data to mRNA transcription profiles leads to our hypothesis that mKBS-dependent gene regulation by Kaiso is controlled through a repression or dampening of active genes that control key biological processes. In contrast, cKBS-dependent genes appear to mediate highly specialized functions in canonical and non-canonical Wnt signaling [26,27,175]. Wnt signals are essential for vertebrate development, driving patterning in the developing embryo and differentiation of tissues and organs (for detailed reviews see [178,279]). Interestingly, in colon cancer, aberrant canonical Wnt signals are the underpinning oncogenic cue [280], whereas in breast cancer only a specific basal (triple negative) subtype shows activated Wnt signals [281]. Although it is not clear how Kaiso localization impacts on repression or activation of Wnt signals in cancer, a cancer-specific dependency of canonical Wnt signals coincides with elevated expression of nuclear Kaiso. In breast cancer this is illustrated by high grade and triple negative breast cancer associating with nuclear Kaiso [159], whereas invasive lobular breast cancer is characterized by low-level nuclear Kaiso expression and has undetectable levels of canonical Wnt signaling [111,112,159]. Although the interplay between p120/Kaiso and β-catenin/TCF has been demonstrated in elegant data from the McCrea lab [27,175,183], it remains

unclear how Kaiso expression and localization affect cKBS and mKBS-mediated transcriptional repression. Future efforts will be needed to delineate the interplay between Kaiso, TCF/LEF and the role of methylation-dependent modulation of target gene expression in cancer.

Our setup yielded a 20% overlap in between ChIP and DamID, which is comparable to previous studies [282,283]. We found that Kaiso was strongly linked to the *TCTCGCGAGA* consensus sequence, which we have designated as the mKBS due to the presence of a CGCG methylation-responsive core [167]. Previous studies had reported high methylation levels at CpG sites surrounding Kaiso binding sites in the promotors of *CDKN2A*, xOCT19 and *MTA2* [154,185,284]. From these experiments it was concluded that methylation increased transcriptional repression through enhancing Kaiso-DNA binding. In contrast, genome-wide analysis on *ENCODE* data demonstrated that methylation levels of the mKBS core or other CGCG-sites bound by Kaiso are relatively low [166]. The latter may however be due to trivial differences in cell type, culture conditions, or transient methylation of CpGs within the mKBS. Transient methylation of distinct CpGs in promotors can indeed regulate temporal expression of hormone receptor target genes [285–287]. Additionally, although hyper-methylation of CpG islands in promotors of transcriptional repressors frequently occurs in cancer, the majority of CpG islands is unmethylated *in vivo* [288]. This fact, combined with our observation that Kaiso preferentially binds to the mKBS in transcriptionally active regions, suggests that transient methylation of the mKBS likely occurs in largely un-methylated promotor regions.

Aside from the classical model in which Kaiso functions as a direct transcriptional repressor, it has become clear that Kaiso can confer transcriptional regulation indirectly through interaction with other transcription factors. For instance, Kaiso controls β-*globin* expression by binding 30 basepairs upstream from CTCF, thereby inhibiting the enhancer blocking function of CTCF [152]. Our observation that the CTCF motif coincides with Kaiso binding sites suggests that modulation of CTCF transcriptional activity by Kaiso distal from promotors might be an alternative mode of derepression. Second, Kaiso interacts with p53 at p53-responsive DNA elements, a phenomenon that is overtly induced in response to DNA damage [153,275]. Because we have used p53 knockout cancer cells, this prevented us from mapping p53-mediated Kaiso binding sites. Unfortunately, we have found no evidence for additional DNA binding sites that could provide an alternative mode of indirect and Kaiso-dependent gene regulation.

Finally, we hypothesize that binding of Kaiso to the mKBS dampens transcription of active genes that control key biological processes such as cell metabolism, cell cycle regulation and DNA damage responses. Our genome-wide data identified these processes after a combination of ChIP/DamID and mRNA profiling in a noninvasive p53 knockout breast cancer cell line. In cancer, aberrant control of cell metabolism, cell cycle regulation and DNA damage responses underpin tumor progression. We therefore envisage a scenario in which Kaiso acts as a tumor suppressor that negatively modulates expression of the aforementioned biological processes. Through either impingement of indirect or direct mechanisms such as methylation and/or complex formation with repressors or activators, Kaiso will be inhibited

in its repressive role and expression of the target genes will be increased. Supporting this is the finding that induction of double strand breaks by chemotherapeutics induced Kaiso expression, which enhanced the expression of pro-apoptotic p53 target genes [153]. In closing, the presence of Kaiso binding sites in transcriptionally active regions suggests that Kaiso functions to control subtle attenuation of gene transcription rather than forming a 'stop and go' function. Because of the abundant occurrence of mKBS sites in genes driving key biological processes, aberrant function of Kaiso could unleash transcriptional activity leading to tumor progression.

Materials and methods

Cell culture

Trp53$^{\Delta/\Delta}$-3 Cells were cultured as described [79]. Phoenix cells were grown in DMEM-F12 (Sigma-Aldrich) containing 6% fetal bovine serum (Sigma-Aldrich), 100 IU/ml penicillin and 100 µg/ml streptomycin (Lonza).

Immunofluorescence

For immunofluorescence, cells were grown on glass cover-slips to 70% confluence and washed with Ca2+/Mg2+-containing PBS. Cells were fixed with 4% PFA in PBS for 10 minutes at room temperature. Permeabilization was performed using 0.3% Triton X-100 in PBS for 3 minutes, followed by blocking in 4% BSA/PBS for 15 minutes. Samples were incubated with the primary antibody mouse anti-V5 (1:1000, 46-0705, Invitrogen) overnight at 4°C and rabbit anti-GFP (SC-8334, Santa Cruz) for 2 hours at room temperature. Secondary antibody incubation with goat anti-mouse-Alexa Fluor 568 (1:600, A11031, Invitrogen) and goat anti-rabbit-Alexa Fluor 488 (1:600, A11034, Invitrogen) took place at room temperature for 1 hour. Samples were stained with DAPI for 5 minutes and mounted with Immu-Mount (Thermo Scientific). Slides were imaged using a Zeiss LSM 700 (Carl Zeiss) and processed using ImageJ and Photoshop CS6 (Adobe).

Cloning and transduction

To generate the pMSCV-EcoDam-V5-Kaiso-puro expression vector, Gateway Cloning was used to recombine mouse Kaiso cDNA (provided by P. McCrea, M.D. Anderson Cancer Center, Houston, Texas [27]) into pMSCV-EcoDam-V5-puro [282] by LR reaction. Next, Phoenix cells were transfected with pMSCV-EcoDam-V5-GFP-puro [282] and pMSCV-EcoDam-V5-Kaiso-puro using X-tremeGene 9 (Roche). After 48 hours, supernatant containing the virus was collected and filtered through a 45 µm filter before transducing Trp53$^{\Delta/\Delta}$-3 cells in the presence of 4 µg/ml polybrene (Sigma-Aldrich). After 72 hours, transduced cells were selected using puromycin.

Chromatin immunoprecipitation

ChIP was performed as described previously [289]. In short, Trp53$^{\Delta/\Delta}$-3 cells were cross-linked with 2 mM DSG (Thermo Fisher Scientific) and 1% formaldehyde. Incubation with nuclear extraction buffer (20 mM Tris, 10 mM NaCl, 2 mM EDTA, 0.5% NP-40) was performed to

lyse the cells and enrich for nuclei. Lysates were collected in sonication buffer (20 mM Tris, 150 mM NaCl, 2 mM EDTA, 1% NP-40 and 0.3% SDS) and chromatin was sheared to 200 to 600 bp fragments by ultrasonication at maximum power for 8 minutes (M220, covaris). Immunoprecipitation was performed using antibodies directed against the following proteins: Kaiso (10 µg, 6F, 12723, Abcam), RBP1 (5µg, PB-7C2, Euromedex), H3K4me3 (5µg, ab8580, Abcam) and H3K27Ac (5µg, ab4729, Abcam). DNA was purified using phenol/chloroform extraction and used for library preparation as previously described [290] and used for sequencing on a HiSeq2000 (Illumina).

RNA sequencing

Cells were seeded into a 6-well plate and grown to 80% confluence in serum-containing medium. After washing in Ca2+/Mg2+-containing PBS, RNA was isolated and purified using the RNeasy kit (Qiagen), followed by DNase treatment (Qiagen). RNA library preparation was performed as previously described [290] and used for cluster generation on a HiSeq 2000 (Illumina).

Computational analysis

For RNA-sequencing, reads were uniquely mapped to the mouse (mm9) reference genome using the ELAND or BWA program, allowing 1 mismatch, and subsequently used for bioinformatic analysis. RPKM (reads per kilobase of gene length per million reads) [274] values for RefSeq genes were computed using tag counting scripts and used to analyze the expression level of genes. ChIP sequencing reads were processed and mapped to the mouse (mm9) reference genome using BWA programming allowing 1 mismatch. ChIP-peaks were identified using Model based Analysis of ChIP-seq (MACS1.3.3) with a cutoff p-value of 10-7 for peak detection [291,292]. DamID sequencing reads were aligned to the mouse genome (mm9) using Bowtie. Only reads aligning uniquely to a single genomic location were kept for further analysis. In addition, only reads aligning just downstream from a GATC sequence were used for downstream analysis. Putative DamID-peaks were identified using HOMER [293] using an initial peak-size of 2500 bp and a 3-fold enrichment of normalized DamID-Kaiso reads over DamID-GFP control reads. In addition, peaks were required to contain at least 100 normalized reads per peak (per 10 million reads sequenced) to remove low magnitude sites. For comparison between ChIP-peaks and DamID-peaks, the 'mergepeaks' function of HOMER was used, applying a maximal distance between the peak centers of 2000 bp. HOMER was also used to determine the location of Kaiso binding sites in the genome, the overlap of Kaiso binding sites with CpG islands, and (de novo) motif analysis. Additionally, using the 'annotatepeaks' function, tag enrichment histograms of Kaiso ChIP, DamID, RNA polymerase and histone marks were generated. DAVID gene ontology database [294] was used to identify enriched functional annotations. In addition to statistical analysis included in the aforementioned software packages, R (2.15.3, R Core team 2011) and Excel (Microsoft) were used to analyse RNA-seq data and perform Pearson's correlation testing.

Acknowledgements

Members of the Derksen, Hetzer and Martens are acknowledged for support and suggestions. We thank Corlinda ten Brink and the UMC Utrecht Cell Microscopy Center for imaging support and Juliet Daniel for providing the ChIP-grade Kaiso antibody and suggestions.

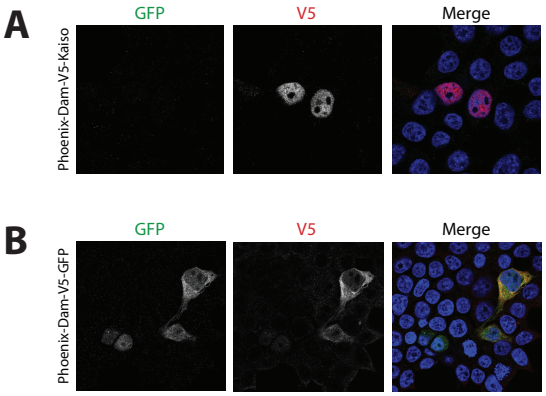

Figure S1

A-B. Immunofluorescent analysis of Phoenix cells transfected with Dam-V5-Kaiso (A) and Dam-V5-GFP (B) stained for GFP (green) and V5 (red). Dam-Kaiso properly localized to the nucleus, while Dam-GFP was diffusely expressed throughout the cell as expected.

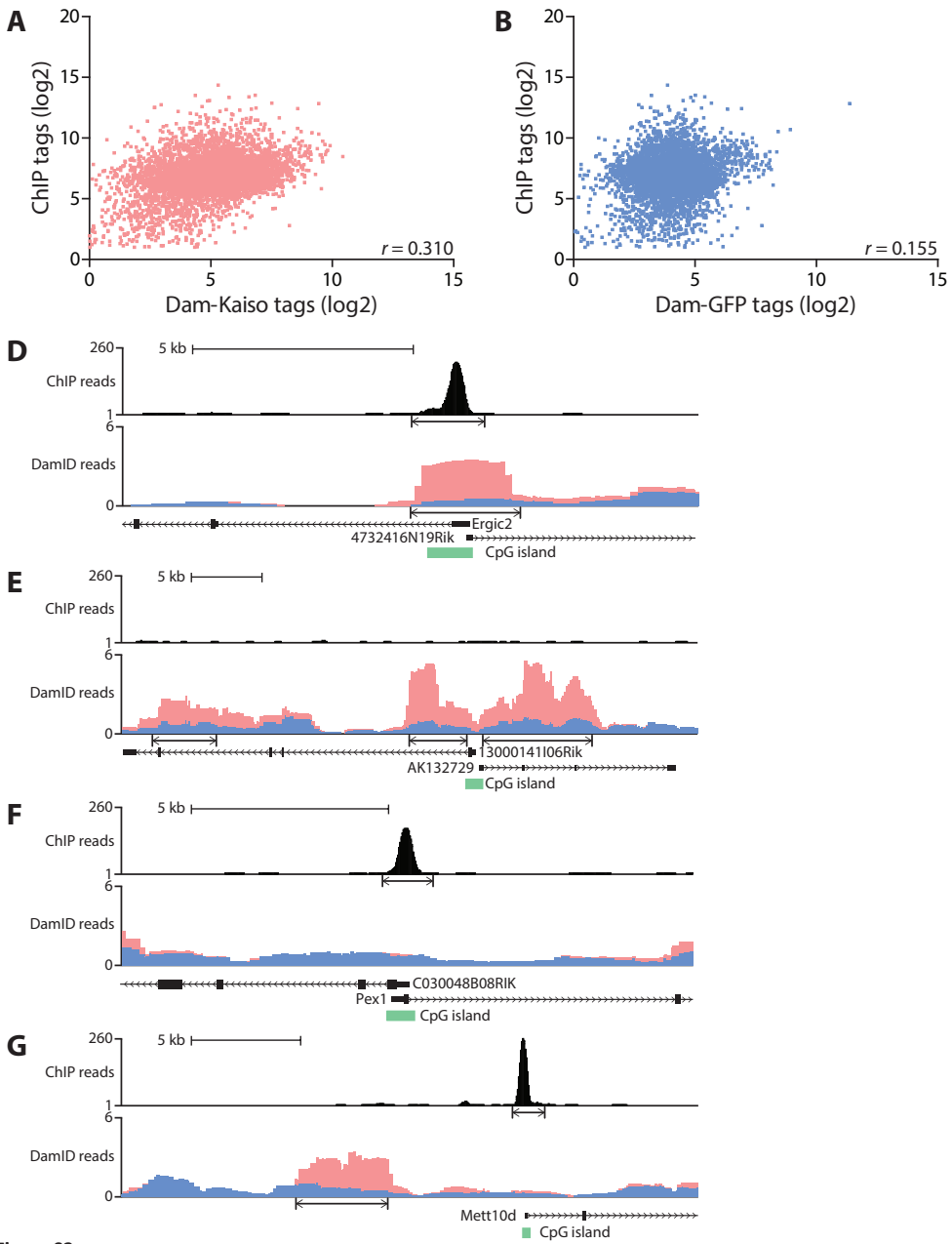

Figure S2

A-B. Overlap between DamID and ChIP-seq binding sites. Bivariate scatterplot showing the normalised tag count of Kaiso ChIP-seq within a 5 kb window surrounding ChIP-peak-centers versus the presence of Dam-Kaiso (A) and Dam-GFP tags (B). r = Pearson's correlation coefficient. C-F: Examples of genomic locations showing Kaiso binding sites detected by both ChIP and DamID (C), exclusively by DamID (D), exclusively by ChIP (E) or by discontinuous ChIP and DamID signals (F). ChIP reads are presented in black, Dam-GFP is depicted in blue and Dam-Kaiso is depicted in pink. At the bottom, the presence of RefSeq genes and CpG islands according to the UCSC genome browser is depicted schematically.

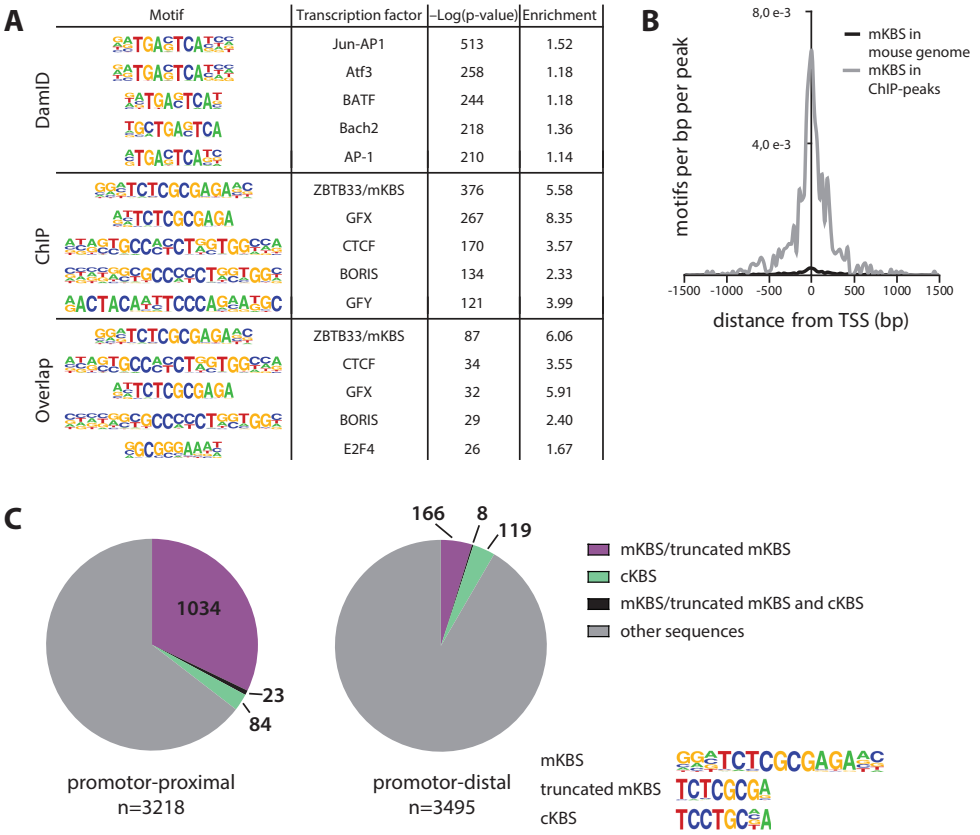

Figure S3

A. Motif analysis of Kaiso binding sites. Top 5 enriched motifs for DamID, ChIP and overlapping peaks are depicted. B. mKBS motifs are primarily located around the TSS. Presence of the mKBS motif was assessed in ChIP-peaks (grey) and in the mouse genome (black) located 500bp up- and downstream of the TSS in a 30 bp bins. C. Distribution of mKBS, incomplete mKBS motifs and the cKBS in ChIP-peaks within promotors (promotor proximal) and outside promotors (promotor distal). Promotors were defined as localized 1 kb up- and downstream of the TSS.

Chapter 6

Summarizing Discussion

Summary

In this thesis we focused on breast cancer progression cues driven by loss of the adherens junction. **Chapter 1** provides a comprehensive overview of the epithelial adherens junction (AJ), its downstream and neighboring effectors and the contribution of AJ inactivation upon E-cadherin loss to cancer development and progression. This chapter also elaborates on the ties between the AJ, p120 and the transcriptional repressor Kaiso. An overview is given on how Kaiso may control transcriptional processes in the nucleus and its involvement in cancer progression. In **chapter 2** we studied the contribution of the E-cadherin binding partner p120 to the development of ILC. For this, we made use of a mammary-specific conditional mouse model of ILC, in which E-cadherin and p53 were inactivated. Introduction of the p120 conditional allele into this model mostly prevented mILC formation and instead led to the formation of basal EMT-like carcinosarcomas. These results showed that p120 is critical for mILC development and that p120 loss is dominant over the loss of E-cadherin in this mouse model. In **chapter 3** we demonstrated that E-cadherin negative breast cancer cells evade anoikis by preventing transcriptional upregulation of the BH3-only pro-apoptotic protein BMF, an essential player during mammary gland homeostasis. We identified that BMF is a direct target of FOXO3, an established transcription factor that is inhibited by PI3K-AKT activation upon loss of E-cadherin. Because we could show that the BH3-only mimetic ABT199 re-sensitized E-cadherin mutant breast cancer cells to anoikis, we propose the use of BH3-only mimetics in the clinical management of ILC. In **chapter 4** we aimed at a comprehensive analysis of the pathways that are activated upon loss of E-cadherin. For this we performed a reverse phase protein array on E-cadherin negative breast cancer cells, which showed that loss of E-cadherin leads to an autocrine activation of the GFR-PI3K-AKT pathway. Interestingly, our data demonstrated that loss of E-cadherin induced an increase in AKT activation both in the presence and absence of activating mutations in the PI3K pathway. We subsequently showed that AKT inhibition in these cells leads to a strong inhibition of cell growth and survival. Based on this, E-cadherin negative ILC is likely to also be sensitive to treatment with PI3K pathway inhibitors. **Chapter 5** focused on the genome-wide identification of Kaiso target genes. These analyses revealed that Kaiso preferentially binds to a CpG-containing 10 nucleotide consensus sequence (mKBS) in active promotors. The data presented suggested that Kaiso attenuates active transcription of multiple genes and pathways through a methyl-dependent KBS (mKBS). Finally, we showed that mKBS target genes are involved in cancer-related processes, including metabolism, cell cycle progression and DNA damage repair.

General discussion

1: Targeted therapy for ILC patients

Detection of invasive lobular breast cancer (ILC) is difficult due to its diffuse growth pattern that hinders detection by palpation or mammography [102]. Also, surgical resection is challenging and often does not achieve clean margins. Follow-up treatment usually consists of estrogen antagonists because most ILCs express ER [103,105]. There is however an unmet need for alternative treatment options, due to the fact that approximately 30% of all ILCs are or will become refractory for endocrine therapy. This non-responsiveness is a clinical problem as ILC tends to harbor an intrinsic resistance to standard chemotherapy regimens [104,254]. ILC represents a relatively homogeneous group of tumors that is driven by inactivation of E-cadherin [79,98,99,125]. Novel targeted intervention based on the effects of AJ inactivation can therefore improve the outcome of the non-responsive ILC patients.

Targeting the PI3K pathway in ILC

In chapter 4 we presented evidence that loss of E-cadherin enhances autocrine GFR-PI3K-AKT signaling. The mechanisms through which E-cadherin can directly influence growth factor receptor (GFR) signaling are based on the proximity of the AJ to GFRs and their downstream interactors. Due to this spatial organization, E-cadherin can interfere with receptor-ligand interaction and reduce receptor mobility, thereby increasing growth factor sensitivity [51,56]. This GFR mobility may be restricted by AJs forming a diffusion barrier providing apical-basal polarity, thereby physically separating receptors from their ligands [295]. E-cadherin can also sequester the EGFR via neurofibromatosis type 2 tumor suppressor (NF2, also known as Merlin). Recruitment of Merlin by E-cadherin stabilizes the junction while inducing a conformational change in Merlin. This active conformation of Merlin is able to sequester EGFR into a membrane component in which internalization and binding to downstream effectors cannot take place [57,296]. Loss of E-cadherin potentially releases this sequestration leading to increased GFR activity. Currently, several clinical trials are ongoing that target GFRs like IGFR and FGFR in hormone receptor positive breast cancer [297]. However, unless a tumor strongly depends on a single GFR, proximal monotherapy is likely inadequate to reduce tumor growth.

In ILC, hyper-activation of the PI3K pathway downstream of GFRs frequently occurs as a result of activating mutations in PI3K subunits, *AKT1* and inactivation of *PTEN* [97,127,129]. Our data directly linked E-cadherin loss to increased AKT activation independent of activating PI3K pathway mutations. Moreover, our *in vitro* results indicated that inhibition of AKT using MK2206 is a promising approach to treat ILC (Chapter 4). However, the effect of MK2206 as a mono treatment in preclinical mouse models ranged from ineffective to almost complete tumor regression, depending on the cell line and treatment regimen used [253,265,298]. Nonetheless, combining MK2206 with cytotoxic drugs like docetaxel, carboplatin, paclitaxel or

doxorubicin resulted in synergistic induction of cell death *in vitro* and greatly enhanced tumor growth inhibition compared to mono treatment *in vivo* [253,265]. To predict response to MK2206, protein expression levels were linked to the ability of MK2206 to inhibit cell growth *in vitro.* This revealed that cell lines with low levels of total and phospho-AKT1/2 or high levels of the close AKT relative SGK1 displayed reduced sensitivity to MK2206 [253,299]. Both AKT and SGK1 are regulated by PI3K signaling via activating phosphorylation events induced by mTORC2 and PDK1 [300,301]. Also, several downstream substrates, such as FOXO, are shared between AKT and SGK1 [302] which explains possible redundancy. Response to AKT inhibition was also linked to mutations in the PI3K pathway; cell lines displaying high sensitivity to MK2206 all contained a *PIK3CA* and/or *PTEN* mutations [253] while knockdown of PTEN or introduction of *PIK3CA* activating mutations in MCF10A and breast cancer cells increased sensitivity to MK2206 inhibition [253,267,298]. Interestingly however, several cell lines containing PTEN or PIK3CA mutations were resistant to MK2206 suggesting that mutation status is not a definitive marker of sensitivity [253]. Phase I clinical trials using MK2206 and compounds targeting other PI3K pathway components showed that mutations in the PI3K pathway were inconsistently associated with clinical response [251,266,303,304]. An association between phospho-AKT levels and sensitivity to MK2206 was also absent in these trials; neither baseline phosphorylation levels of AKT nor the degree of reduction in AKT phosphorylation associated with tumor response [251,266]. Since there is only limited clinical data on the association between mutation status, expression levels of PI3K pathway components and response to PI3K pathway targeted therapy, analysis on these associations should be continued. We propose that inactivation of the AJ should be implemented as a key inclusion criterion for ILC-specific clinical trials, since this subgroup of tumors is likely to respond to AKT inhibition independent of mutations leading to activation of the PI3K pathway.

Over time, numerous inhibitors have been developed that target several kinases in the PI3K pathway including mTor, AKT and PI3K. In fact, the allosteric mTor inhibitor Everolimus is an FDA-approved drug for the treatment of hormone-receptor positive advanced breast cancer after secondary resistance to non-steroidal aromatase inhibitors (AI) [305,306]. Resistance to PI3K pathway targeted therapy however can limit clinical success. Mechanisms of resistance do not only include mutations in pathway components, but also involve the relief of negative feedback, which results in a net increase in PI3K pathway activation [307,308]. Moreover, PI3K and AKT-independent ways to activate downstream components of the PI3K pathway may confer resistance (reviewed in [309] and [310]). Finally, activation of other oncogenic pathways like RAS-MAPK and Jak-Stat provide alternative pathways leading to tumor progression [311,312]. A comprehensive overview of the molecular mechanisms behind resistance to PI3K targeted therapy is provided by Fruman *et al.* [309] and Paplomata *et al.* [256].

Targeting the executors of cell death: BH3-only mimetics to tip the balance towards apoptosis

As an alternative to inhibition of key upstream nodes in survival pathways, direct targeting of distal components like the apoptosis pathway could enhance tumor eradication. In chapter 3 we showed that the BH3-only mimetic ABT199 effectively inhibits PI3K-AKT-FOXO dependent

survival of metastatic E-cadherin negative breast cancer cells. Initially, BH3-only mimetics were designed to sequester the anti-apoptotic family members BCL2, BCL-XL and BCL-W, thereby releasing pro-apoptotic family members leading to caspase-dependent apoptosis [313]. Unfortunately, due to the involvement of BCL-XL in platelet survival, administration of the BH3-only mimetic ABT737 induced thrombocytopenia, a severe side-effect that prevented clinical success [314,315]. Because of this toxicity, ABT199 was developed to specifically target BCL2 [316]. Compared to ABT737, ABT199 showed equal effectiveness in the treatment of mouse lymphoma without reducing platelet counts [317]. Since BCL2 is a key oncogenic driver in lymphoid malignancies, clinical trials using BH3-only mimetics have led to FDA-approval for the use of ABT199 as a single agent for the treatment of refractory chronic lymphoid leukemia [318]. Interestingly, BCL2 is also expressed in the vast majority of breast tumors, particularly in luminal and ER positive tumors such as ILC [218,237]. BCL2-expressing ILC therefore represents a large group of tumors that could benefit from ABT199 treatment. We propose to include BCL2 levels and loss of the AJ leading to AKT-FOXO-dependent repression of BMF as parameters to select patients for clinical trials to test the efficacy of ABT199 in breast cancer.

Since ABT-199 is only able to sequester BCL2, it is not surprising that resistance to this BH3-only mimetic in lymphoid malignancies was found to occur through redundancy by the BCL-2 family members BCL-XL and the structurally less related MCL1 [235,319,320]. However, although MCL1 and BCL-XL are ubiquitously expressed in breast cancer [237], the presence of these proteins in breast cancer xenografts did not affect the ability of ABT-199 to inhibit tumor growth suggesting a dominance of BCL2 in the regulation of apoptosis in breast cancer [218,237]. Oncogenic PI3K signaling also provides a mechanism of resistance to BH3-only mimetics [321]. We (chapter 3) and others [75] have shown that activation of this oncogenic pathway is causal to the development of anoikis resistance as it prevents upregulation of pro-apoptotic BH3-only family members thereby preventing luminal clearance of mammary ducts. As a result, BH3-only mimetics would be ineffective as their efficacy depends on the presence of endogenous pro-apoptotic factors. Inhibition of PI3K signaling in combination with BH3-only mimetics however could provide an opportunity for synergistic tumor eradication as will be discussed below.

Targeted therapy in the mix: finding a lethal cocktail

Previous research has shown that inhibition of PI3K signaling increased the sensitivity of ER positive breast cancer cells to endocrine therapy [322–324] even in cells displaying primary or acquired resistance to endocrine therapy [325,326]. Also, baseline hyper-activation of the PI3K pathway predicted poor outcome after endocrine therapy in breast cancer patients [324]. Moreover, an increase in phospho-AKT was observed in recurrent breast tumors after endocrine therapy [326]. Finally, PI3K signaling could directly activate the transcriptional activity of ERα [327,328]. In short, it appears that activation of the PI3K pathway triggers or facilitates resistance to endocrine therapy. Since E-cadherin negative ILC are mostly ER/PR positive and display an intrinsic high activation of GFR signaling, this group of patients should be included in clinical trials targeting the PI3K pathway in hormone receptor positive breast cancer, or as independent group retrospectively analyzed in these studies.

As described above, E-cadherin negative breast cancers could also benefit from treatment with BH3-only mimetics. Although ABT199 mono treatment is ineffective in treating BCL2-expressing breast cancer xenografts in mice, combining ABT199 with docetaxel or tamoxifen increased tumor responses and improved survival [218,237]. So far, it is unclear how docetaxel and ABT199 are able to synergize. Tamoxifen treatment however is known to induce BCL2 expression, thereby possibly increasing the sensitivity of breast cancer cells to BH3-only mimetics [218,329]. Interestingly, the response to BH3-only mimetic treatment in breast cancer xenografts showed an inverse correlation with phospho-AKT levels [218]. Also, combination of ABT-199 and a PI3K pathway inhibitor *in vitro* resulted in a synergistic reduction in viability, even in cells with acquired or primary resistance to ABT-199 [218,235]. Moreover, combining a BH3-only mimetic with a PI3K pathway inhibitor in breast cancer xenografts resulted in a significant increase in survival compared to BH3-only mimetic or PI3K pathway inhibitor mono treatment [218]. Apparently, this dual inhibition has synergistic outcomes despite the fact that PI3K acts directly upstream of the apoptotic machinery by regulating *BMF* expression (chapter 3). This can be explained the fact that combination therapy inhibits anti-apoptotic proteins and enhances the activity of pro-apoptotic proteins. BH3-only mimetics suppress the activity of the anti-apoptotic protein BCL2, while PI3K pathway inhibitors relieve the inhibitory function of PI3K signaling on pro-apoptotic pathway players like BMF. In other words, PI3K pathway inhibitors might prime cells for apoptosis by inducing transcription of BH3-only genes such as BIM and/or BMF [309,330].

As an alternative to combining PI3K pathway targeted therapy with endocrine therapy or distal BH3-only mimetics, inhibitors of actomyosin contractility could be applied. ILC patients could benefit from this combination treatment as ILC cells greatly depend on Wnt-induced and p120-dependent Rho/ROCK signaling for anchorage independent survival [111,112]. Also, we have already shown that administration of the ROCK inhibitor Fasudil inhibits ILC tumor growth *in vivo* (Schackmann *et al.*, manuscript in preparation) and it would be interesting to test whether MK2206 can enhance this effect *in vitro* and *in vivo*. In melanoma cells, a dual inhibitor of ROCK and AKT (CCT129254) impaired invasion *in vitro* and *in vivo* while an analogue only able to inhibit AKT (CCT130293) was ineffective at inhibiting cell movement. Also, although both inhibitors were able to reduce primary tumor outgrowth, only dual ROCK and AKT inhibition reduced metastatic outgrowth suggesting that inhibiting both kinases may provide a benefit over mono treatment [331].

In closing, our results suggest that ILC patients might benefit from a combined treatment with MK2206, ABT199 and/or Rock inhibitors (Figure 1). Also, both PI3K pathway inhibitors and BH3-only mimetics have shown synergistic effects on cell death when combined with chemotherapeutics and endocrine therapy. PI3K pathway and BH3-only targeted therapies could therefore sensitize ILC patients to chemotherapeutics and endocrine therapy, even after resistance to these standard therapies has occurred. Clinical trial data however have made increasingly clear that promising preclinical results are not always recapitulated in patients. It is therefore key to employ critical inclusion criteria based on biochemical evidence

to select patients that are likely to respond, while continuously monitoring expression of marker proteins and mutation status of the targeted pathways.

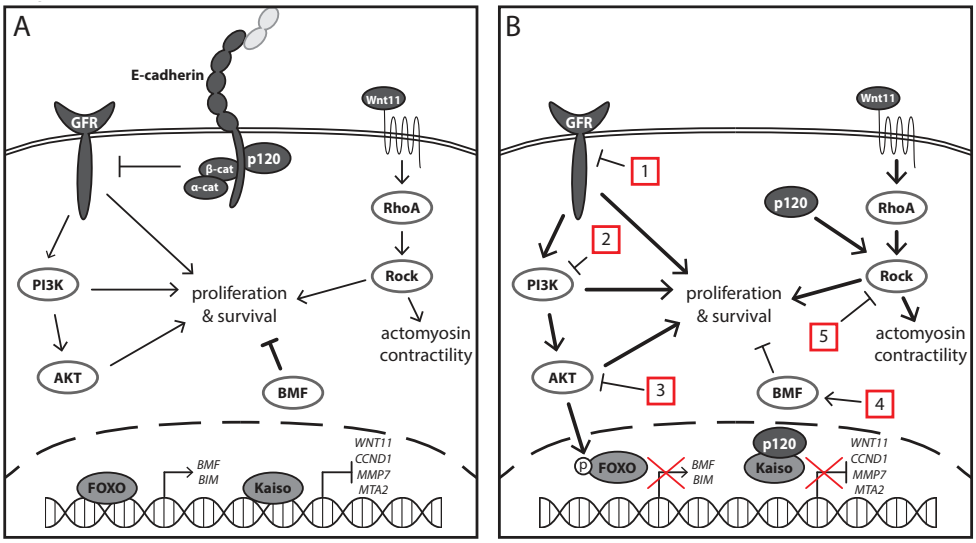

Figure 1 AJ-dependent growth factor receptor (GFR) activation and the consequences for downstream signals: options for intervention?
AJ-driven survival signaling in non-malignant E-cadherin-expressing cells (A) and E-cadherin negative breast cancer cells (B). Repression of GFRs by E-cadherin is relieved upon loss of E-cadherin (B) resulting in enhanced PI3K-AKT-dependent and -independent proliferation and survival (B). This enhanced activation of AKT increases phosphorylation of FOXO, thereby inhibiting the transcriptional activity of FOXO and repressing the transcription of the pro-apoptotic BH3-only molecules *BMF* and *BIM*. Inhibition of PI3K signaling by GFR (1), PI3K (2) and/or AKT inhibition (3) and apoptosis by BH3-only mimetics (4) can counteract increased proliferation and survival signaling in these E-cadherin deficient cells (B). In E-cadherin expressing cells Kaiso functions as a transcriptional repressor of several oncogenes including *WNT11, CCND1, MTA2* and *MMP7* (A). Nuclear localization of p120 in E-cadherin negative cells derepresses these Kaiso targets (B). Finally, Rho-ROCK signaling is enhanced by cytosolic p120 and autocrine WNT11 in E-cadherin negative cells. This signal promotes actomyosin contractility and anoikis resistance, which can be restrained by inhibition of ROCK (5) (B).

2: Multifaceted regulation of transcription by Kaiso

The majority of Kaiso-binding takes place at CpGs

Transcriptional regulation by Kaiso occurs through direct binding of Kaiso to the cKBS in the promotor of several individual genes in multiple cell types [27,28,161,162,175,181,188,192,332,333]. Surprisingly, both we and others did not find an enrichment for the cKBS in genome-wide mapping of Kaiso binding sites (chapter 5). This suggests that binding of Kaiso to the cKBS is not the primary mechanism by which Kaiso regulates gene transcription. Instead, the majority of Kaiso binding occurs inside CpG islands, more specifically at the mKBS (TCTCGCGAGA). This site was not only identified in our breast cancer cells, but also in normal lymphoblasts, myelogenic leukemia cells [166] and preadipocytes [167], suggesting that the mKBS is universal binding sequence. Swapping the sites flanking the methylated CpGs in the mKBS greatly reduced the affinity of Kaiso to the mKBS *in vitro*, indicating the importance of the

structure surrounding the methylated CpGs [167]. Interestingly, *de novo* motif analysis of Kaiso binding sites in our Trp53$^{\Delta/\Delta}$-3 cells identified truncated versions of the mKBS, suggesting that variation in the flanking sequences are tolerated to a certain degree.

Is CpG methylation required for Kaiso-DNA binding?

In vitro binding experiments pointed out the high preference of Kaiso-DNA binding for methylated CpGs over unmethylated CpGs. Corresponding evidence for methylation *in vivo* came from ChIP experiments in which DNA de-methylation by 5-azacytidine treatment resulted in reduced Kaiso binding to the *CCND1* [192], *MTA2* [154] and *GR* [334] promotor. Moreover, methylation of endogenous promotors was analyzed using bisulfite sequencing and methylation-specific PCR. This revealed high methylation levels of the CpG-containing binding site of Kaiso and the surrounding CpGs in the *CDKN2A* [284], *xOct19* [185] and *MTA2* [154] promotor. Genome-wide assessment of methylation status however indicated that the majority of mKBSs and other CGCG-sites occupied by Kaiso displayed low levels of methylation (less than 20%) [166]. Interestingly, the embryonic lethality in *Xenopus* embryos upon loss of xKaiso involving axis truncation, failure to close the blastopore and increased apoptosis [335] greatly mimicked the developmental defects observed upon depletion of dna methyl transferase 1 (*DNMT1*) [336]. Moreover, in APC$^{min/+}$ mice, loss of DNMT1 or MBD2 (a member of the methyl-CpG-binding domain family of transcription factors) displayed reduced intestinal tumorigenesis [337,338], similar to Kaiso knockout APC$^{min/+}$ mice [186]. These *Xenopus* and mouse models showed that loss of Kaiso mimics the loss of proteins to do with DNA methylation, thereby suggesting that Kaiso operates in a methylation-dependent manner. At the moment there is no clear consensus on whether Kaiso can exclusively bind to CpG sites *in vivo* when these sites are methylated. However, the two schools of thought can be brought together in a model involving a variable, time and/or stimulus dependent methylation status. Transient methylation of specific CpGs has been observed in the promotor of the ER-responsive pS2 gene. Upon activation by estrogens, cyclical methylation occurred. This resulted in successive rounds of ER-promotor binding and transcription [286,287]. Such a cyclical methylation, recruitment of transcription factors and transcription rate was also observed at the androgen-receptor responsive gene SGK1 upon hormone stimulation [285]. Both at the pS2 and SGK1 promotor the transient methylation does not involve all CpGs in the promotor region. Instead, only a few CpGs displayed differential methylation upon hormone administration while the surrounding CpGs remained unmethylated [285,287]. This phenomenon of single CpGs able to regulate transcription is also observed at a genome-wide scale. These are known as traffic-light CpGs [339]. Because the chromatin landscape surrounding the mKBS contains markers of active transcription (chapter 5, [166]), methylation of the mKBS is expected to occur within a region that is generally unmethylated, similar to the pS2 and SGK1 promotor. Upon an external or internal stimulus, such as cell cycle progression, DNA damage, or hypoxia as described below, methylation of the mKBS is diminished, resulting in reduced Kaiso binding (Figure 2A). It will be very interesting to extend our findings with bisulfite sequencing on synchronized or stimulated cells to provide more insight into a possible transient methylation of the mKBS as a mechanism for transcriptional regulation by Kaiso in breast cancer.

Kaiso binding is likely to fine-tune transcription by affecting histone acetylation dynamics

Binding of Kaiso to CpG-containing binding sites induced recruitment of corepressor-complexes containing SMRT and NCoR in mouse adipocytes and HeLa cells respectively [154,167]. In contrast, at the cKBS of *MMP7* Kaiso interacted with MTG16 [171], a corepressor capable of attracting NCoR [172]. The common denominator in these corepressor-complexes is the presence of a histone deacytelase (HDAC) which mediates histone deacytelation, thereby creating an inactive chromatin environment [340]. Consistent with this, the ability of Kaiso to repress *MTA2* expression was dependent on HDAC activity [154]. Additionally, Kaiso-dependent repression of *Siamois* was mediated by acetylation of histone 3 [175]. Enrichment of histone marks of active transcription including high levels of acetylated histones at sites of Kaiso binding (chapter 5, [166]) therefore seems rather counterintuitive. The presence of HDACs at active chromatin regions containing high levels of acetylated histones however is not unusual. In fact, HDACs were shown to be highly abundant at promotors of actively transcribed genes, even more abundant than on silenced genes or genes poised for transcription [341]. These active sites of transcription also have high levels of histone acetyltransferases (HATs) and it was suggested that the co-occurrence of HATs and HDACs at these sites is needed for successive rounds of transcription [340,341]. Functionally, the presence of H3K27Ac at promotors is known to regulate transcription kinetics by increasing the recruitment of transcription factors (TFs), while also increasing the elongation rate of Pol2 without affecting initiation [342]. This implies that the transcriptional repressor Kaiso is specifically located at mKBS motifs within active promotor regions. We therefore propose a model in which Kaiso acts to fine-tune expression, rather than performing a 'stop and go' function. Although genome-wide alterations in chromatin landscape upon loss of Kaiso-DNA binding has not yet been assessed, it is likely that it is the recruitment of HDACs by Kaiso that regulates the ability of histone acetylation to enhance transcription. While a Kaiso knockout can be used as a tool to completely abolish Kaiso-DNA binding, binding of Kaiso to the cKBS and methylated CpGs can possibly be distinguished by introduction of two Kaiso point mutants which were previously shown to display mutual exclusive binding to these binding sequences *in vitro* ([343] and P. Wright, personal communication).

Collaboration with other transcription factors determines Kaiso binding to non-consensus sites

The classical idea of a sequence-specific TF is that the majority of binding takes place at the consensus site. There are however TFs, such as E2F family members, that do not have an obvious preference for consensus site binding [344]. Kaiso might group with this type of TFs as the cKBS and mKBS only covered 12% of all binding sites identified in our ChIP dataset. As described above, the absence of a consensus site in the remaining 88% can partially be explained by a variety in flanking sequences surrounding CpGs, or a mechanism similar to E2F family members. The latter involves weak binding of E2F to E2F consensus-like sites which is stabilized by surrounding transcription factors and/or certain histone modifications, a phenomenon known as assisted binding [344,345]. For Kaiso, an indication for assisted binding comes from the fact that we identified Kaiso binding ~50 bp up- and downstream of CTCF recognition sites. Our observations were in agreement with a previous finding in which CTCF

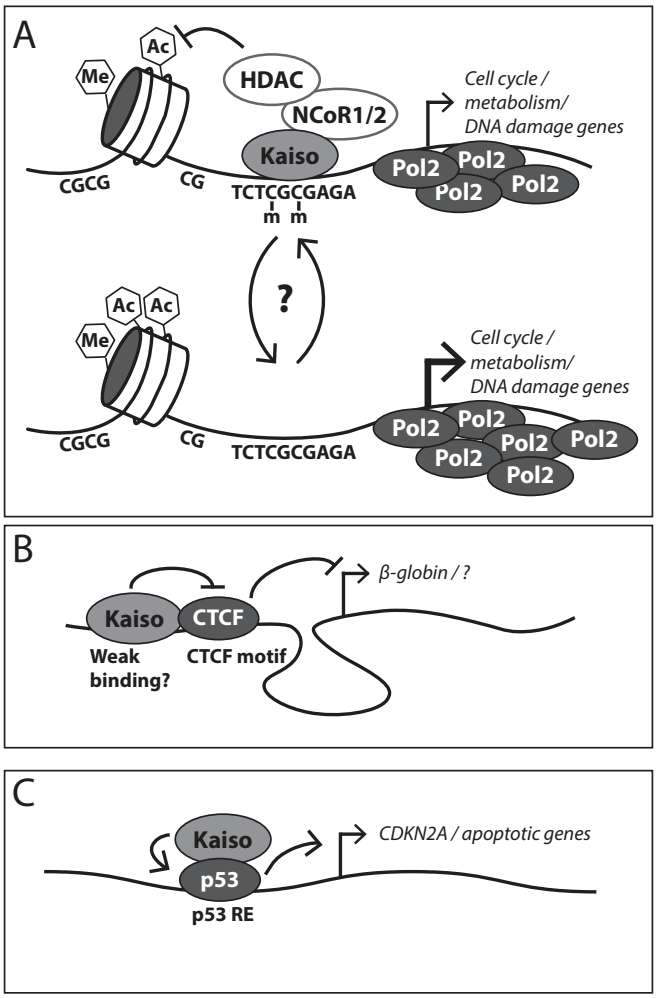

Figure 2 Models for transcriptional regulation by Kaiso
A. Transcriptional regulation at mKBS sites. Top: Kaiso binds in transcriptionally active regions characterized by generally low CpG methylation levels and H3K27Ac (Ac), H3K4me3 (Me) and Pol2 occupancy. Internal or external stimuli such as cell cycle progression, hypoxia or DNA damage induction can induce transient demethylation of the mKBS site resulting in cyclical expression of Kaiso target genes B. Transcriptional regulation at Kaiso binding sites in collaboration with CTCF outside promotors. Binding of Kaiso occurs in close proximity to CTCF. CTCF binds to the CTCF motif while binding of Kaiso to the DNA does not involve a particular consensus sequence. CTCF is likely to stabilize Kaiso binding through assisted binding. CTCF is able to inhibit expression of distal genes by enhancer blocking, while Kaiso inhibits this enhancer blocking activity. Kaiso is thereby able to induce gene transcription over a large distance. C. Transcriptional regulation of p53 target genes by Kaiso. Kaiso does not directly bind to the DNA but instead stabilizes p53. In this way Kaiso is able to induce expression of p53 target genes.

and Kaiso were found to directly interact and bind to the β-*globin* insulator within 35 bp [152]. It is possible that CTCF stabilizes weak Kaiso interactions to suboptimal binding sequences, which conforms to the concept of assisted binding (Figure 2B). An alternative method for the recruitment of transcription factors to non-consensus sites is through 'piggyback'

binding. This involves binding of a certain TF to its responsive element and the interaction of Kaiso with this TF without Kaiso binding to the DNA itself [345] (Figure 2C). Binding of Kaiso to p53 is an example of this phenomenon [153]. Unfortunately, the p53 responsive elements implicated in Kaiso-p53 interactions [153] were not identified in our cells because they are p53 knockout. Additionally, although no other TF binding site sequences were found enriched at or near a Kaiso binding site, collaboration with other TFs can still occur. This collaboration however possibly takes place at a low frequency, in a transient fashion or depends on stimuli influencing binding of these other TFs. Overall, the preferred Kaiso binding site is the mKBS consensus site, while other binding sites identified by ChIP-sequencing are likely a result of assisted binding or indirect Kaiso-DNA interaction through interaction with other TFs.

Stimuli affecting Kaiso binding to the DNA

Although post-translational modification is a well-known mechanism to affect TF function [340,346–348], this does not appear to represent a common regulatory cue for Kaiso. Interestingly however, DNA damage induction increased Kaiso mRNA and protein levels, providing a possible mechanism to influence Kaiso function [153]. Also, studies have suggested that the tumor microenvironment can regulate subcellular distribution of Kaiso [148]. Moreover, *in vitro* culture of colorectal cancer cells under hypoxic conditions induced association of Kaiso with the promotor of *HIF1α* thereby decreasing HIF1α expression [349]. Taken together, DNA damage, the microenvironment and Wnt signaling described in chapter 1 represent internal and external stimuli affecting Kaiso activity. These cues, combined with differential expression and/or activity of collaborating TFs, provide mechanisms whereby Kaiso can differentially affect target gene expression in different cell types and under different conditions.

Kaiso: oncogene or tumor suppressor?

Based on our observations, Kaiso is likely to fine-tune the expression of genes involved in basic processes and regulate p120-dependent repression of oncogenes. Depending on the presence of collaborating TFs, Kaiso can either induce or repress gene transcription. Although the signals governing the strength of Kaiso-DNA interaction are not completely clear, the sequence of the binding site and/or transient methylation of the mKBS are likely to be involved. Additionally, DNA-Kaiso affinity can be influenced by the interaction of Kaiso with other TFs like CTCF or p53, or with non-DNA binding proteins like p120 and β-catenin.

Initially, Kaiso was viewed as a tumor suppressor due to its ability to repress the transcription of several oncogenes. Loss of E-cadherin in cancer and subsequent inhibition of Kaiso by p120-binding fits into this tumor suppressive role. In contrast, an oncogenic function for Kaiso was indicated from the $APC^{min/+}$ mouse model for intestinal cancer [187]. Taken together, Kaiso function depends on multiple stimuli that appear context and environment-dependent. The complexity of this regulation probably underpins Kaiso's dual and enigmatic role as a tissue-specific tumor suppressor or oncogene.

Addenda

References
Nederlandse samenvatting
Curriculum vitae
List of publications
Dankwoord

References

1. Yoshida-Noro C, Suzuki N, Takeichi M. Molecular nature of the calcium-dependent cell-cell adhesion system in mouse teratocarcinoma and embryonic cells studied with a monoclonal antibody. Dev. Biol. 1984;101:19–27.

2. Pokutta S, Weis WI. Structure and mechanism of cadherins and catenins in cell-cell contacts. Annu. Rev. Cell Dev. Biol. 2007;23:237–61.

3. van Roy F. Beyond E-cadherin: roles of other cadherin superfamily members in cancer. Nat. Rev. Cancer. 2014;14:121–34.

4. Hülsken J, Birchmeier W, Behrens J. E-cadherin and APC compete for the interaction with β-catenin and the cytoskeleton. J. Cell Biol. 1994;127:2061–9.

5. Stappert J, Kemler R. A short core region of E-cadherin is essential for catenin binding and is highly phosphorylated. Cell Adhes. Commun. 1994;2:319–27.

6. Huber AH, Weis WI. The structure of the β-catenin/E-cadherin complex and the molecular basis of diverse ligand recognition by β-catenin. Cell. 2001;105:391–402.

7. Reynolds AB, Daniel J, McCrea P, Wheelock MJ, Wu J, Zhang Z. Identification of a new catenin: the tyrosine kinase substrate p120-cas associates with E-cadherin complexes. Mol. Celluar Biol. 1994;14:8333–42.

8. Yap AS, Niessen CM, Gumbiner BM. The Juxtamembrane Region of the Cadherin Cytoplasmic Tail Supports Lateral Clustering, Adhesive Strengthening, and Interaction with p120ctn. J. Cell Biol. 1998;141:779–89.

9. Ishiyama N, Lee SH, Liu S, Li GY, Smith MJ, Reichardt LF, et al. Dynamic and Static Interactions between p120 Catenin and E-Cadherin Regulate the Stability of Cell-Cell Adhesion. Cell. 2010;141:117–28.

10. Schackmann RCJ, Tenhagen M, van de Ven R a H, Derksen PWB. P120-Catenin in Cancer-Mechanisms, Models and Opportunities for Intervention. J. Cell Sci. 2013;126:3515–25.

11. Thoreson MA, Anastasiadis PZ, Daniel JM, Wheelock MJ, Johnson KR, Hummingbird DK, et al. Selective Uncoupling of p120ctn from E-cadherin disrupts strong adhesion. J. cell. 2000;148:189–201.

12. Ireton RC, Davis MA, van Hengel J, Mariner DJ, Barnes K, Thoreson MA, et al. A novel role for p120 catenin in E-cadherin function. J. Cell Biol. 2002;159:465–76.

13. Davis M, Ireton R, Reynolds A. A core function for p120-catenin in cadherin turnover. J. Cell Biol. 2003;163:525–34.

14. Nanes BA, Chiasson-MacKenzie C, Lowery AM, Ishiyama N, Faundez V, Ikura M, et al. P120-Catenin Binding Masks an Endocytic Signal Conserved in Classical Cadherins. J. Cell Biol. 2012;199:365–80.

15. Fujita Y, Krause G, Scheffner M, Zechner D, Leddy HEM, Behrens J, et al. Hakai, a c-Cbl-like protein, ubiquitinates and induces endocytosis of the E-cadherin complex. Nat. Cell Biol. 2002;4:222–31.

16. Hatzfeld M. The p120 family of cell adhesion molecules. Eur. J. Cell Biol. 2005;84:205–14.

17. Aho S, Levänsuo L, Montonen O, Kari C, Rodeck U, Uitto J. Specific sequences in p120ctn determine subcellular distribution of its multiple isoforms involved in cellular adhesion of normal and malignant epithelial cells. J. Cell Sci. 2002;115:1391–402.

18. Kelly KF, Spring CM, Otchere A a, Daniel JM. NLS-dependent nuclear localization of p120ctn is necessary to relieve Kaiso-mediated transcriptional repression. J. Cell Sci. 2004;117:2675–86.

19. van Hengel J, Vanhoenacker P, Staes K, van Roy F. Nuclear localization of the p120(ctn) Armadillo-like catenin is counteracted by a nuclear export signal and by E-cadherin expression. Proc. Natl. Acad. Sci. U. S. A. 1999;96:7980–5.

20. Roczniak-Ferguson A, Reynolds AB. Regulation of p120-catenin nucleocytoplasmic shuttling activity. J. Cell Sci. 2003;116:4201–12.

21. Hosking CR, Ulloa F, Hogan C, Ferber EC, Figueroa A, Gevaert K, et al. The transcriptional repressor Glis2 is a novel binding partner for p120 catenin. Mol. Biol. Cell. 2007;18:1918–27.

22. Lee M, Ji H, Furuta Y, Park J-I, McCrea PD. p120-catenin regulates REST and CoREST, and modulates mouse embryonic stem cell differentiation. J. Cell Sci. 2014;127:4037–51.

23. Daniel JM, Reynolds AB. The catenin p120(ctn) interacts with Kaiso, a novel BTB/POZ domain zinc finger transcription factor. Mol. Cell. Biol. 1999;19:3614–23.

24. Buck-Koehntop BA, Martinez-Yamout MA, Dyson HJ, Wright PE. Kaiso uses all three zinc fingers and

adjacent sequence motifs for high affinity binding to sequence-specific and methyl-CpG DNA targets. FEBS Lett. 2012;586:734–9.

25. Buck-Koehntop BA, Stanfield RL, Ekiert DC, Martinez-Yamout MA, Dyson HJ, Wilson IA, et al. Molecular basis for recognition of methylated and specific DNA sequences by the zinc finger protein Kaiso. Proc. Natl. Acad. Sci. 2012;18462:1–6.

26. Daniel JM, Spring CM, Crawford HC, Reynolds AB, Baig A. The p120(ctn)-binding partner Kaiso is a bi-modal DNA-binding protein that recognizes both a sequence-specific consensus and methylated CpG dinucleotides. Nucleic Acids Res. 2002;30:2911–9.

27. Kim SW, Park J-I, Spring CM, Sater AK, Ji H, Otchere A a, et al. Non-canonical Wnt signals are modulated by the Kaiso transcriptional repressor and p120-catenin. Nat. Cell Biol. 2004;6:1212–20.

28. Jiang G, Wang Y, Dai S, Liu Y, Stoecker M, Wang E, et al. P120-Catenin Isoforms 1 and 3 Regulate Proliferation and Cell Cycle of Lung Cancer Cells via β-Catenin and Kaiso Respectively. PLoS One. 2012;7:e30303.

29. Dai SD, Wang Y, Jiang GY, Zhang PX, Dong XJ, Wei Q, et al. Kaiso is expressed in lung cancer: Its expression and localization is affected by p120ctn. Lung Cancer. 2010;67:205–15.

30. Takeichi M. Dynamic contacts: rearranging adherens junctions to drive epithelial remodelling. Nat. Rev. Mol. Cell Biol. 2014;15:397–410.

31. Rimm DL, Koslov ER, Kebriaei P, Cianci CD, Morrow JS. α1(E)-Catenin Is An Actin-Binding And Actin-Bundling Protein Mediating The Attachment Of F-Actin To The Membrane Adhesion Complex. Proc. Natl. Acad. Sci. U. S. A. 1995;92:8813–7.

32. Drees F, Pokutta S, Yamada S, Nelson WJ, Weis WI. α-catenin is a molecular switch that binds E-cadherin-β-catenin and regulates actin-filament assembly. Cell. 2005;123:903–15.

33. Yamada S, Pokutta S, Drees F, Weis WI, Nelson WJ. Deconstructing the cadherin-catenin-actin complex. Cell. 2005;123:889–901.

34. Leckband DE, de Rooij J. Cadherin adhesion and mechanotransduction. Annu. Rev. Cell Dev. Biol. 2014;30:291–315.

35. Noren NK, Liu BP, Burridge K, Kreft B. p120 catenin regulates the actin cytoskeleton via Rho family GTPases. J. Cell Biol. 2000;150:567–80.

36. Martinez MC, Ochiishi T, Majewski M, Kosik KS. Dual regulation of neuronal morphogenesis by a δ-catenin-cortactin complex and Rho. J. Cell Biol. 2003;162:99–111.

37. Wolf A, Keil R, Götzl O, Mun A, Schwarze K, Lederer M, et al. The armadillo protein p0071 regulates Rho signalling during cytokinesis. Nat. Cell Biol. 2006;8:1432–40.

38. Zhang JY, Wang Y, Zhang D, Yang ZQ, Dong XJ, Jiang GY, et al. δ-catenin promotes malignant phenotype of non-small cell lung cancer by non-competitive binding to E-cadherin with p120ctn in cytoplasm. J. Pathol. 2010;222:76–88.

39. Anastasiadis PZ, Moon SY, Thoreson MA, Mariner DJ, Crawford HC, Zheng Y, et al. Inhibition of RhoA by p120 catenin. Nat. Cell Biol. 2000;2:637–44.

40. Wildenberg GA, Dohn MR, Carnahan RH, Davis M a., Lobdell NA, Settleman J, et al. p120-Catenin and p190RhoGAP Regulate Cell-Cell Adhesion by Coordinating Antagonism between Rac and Rho. Cell. 2006;127:1027–39.

41. Castaño J, Solanas G, Casagolda D, Raurell I, Villagrasa P, Bustelo XR, et al. Specific phosphorylation of p120-catenin regulatory domain differently modulates its binding to RhoA. Mol. Cell. Biol. 2007;27:1745–57.

42. Menke A, Giehl K. Regulation of adherens junctions by Rho GTPases and p120-catenin. Arch. Biochem. Biophys. 2012;524:48–55.

43. Grosheva I, Shtutman M, Elbaum M, Bershadsky a D. p120 catenin affects cell motility via modulation of activity of Rho-family GTPases: a link between cell-cell contact formation and regulation of cell locomotion. J. Cell Sci. 2001;114:695–707.

44. Stehbens SJ, Paterson AD, Crampton MS, Shewan AM, Ferguson C, Akhmanova A, et al. Dynamic microtubules regulate the local concentration of E-cadherin at cell-cell contacts. J Cell Sci. 2006;119:1801–11.

45. Meng W, Mushika Y, Ichii T, Takeichi M. Anchorage of Microtubule Minus Ends to Adherens Junctions Regulates Epithelial Cell-Cell Contacts. Cell. 2008;135:948–59.

46. Ichii T, Takeichi M. P120-catenin regulates microtubule dynamics and cell migration in a cadherin-independent manner. Genes Cells. 2007;12:827–39.

&

47. Ligon LA, Holzbaur ELF. Microtubules tethered at epithelial cell junctions by dynein facilitate efficient junction assembly. Traffic. 2007;8:808–19.

48. Watabe M, Nagafuchi A, Tsukita S, Takeichi M. Induction of polarized cell-cell association and retardation of growth by activation of the E-cadherin-catenin adhesion system in a dispersed carcinoma line. J. Cell Biol. 1994;127:247–56.

49. Takahashi K, Suzuki K. Density-dependent inhibition of growth involves prevention of EGF receptor activation by E-cadherin-mediated cell-cell adhesion. Exp. Cell Res. 1996;226:214–22.

50. Perrais M, Chen X, Perez-moreno M, Gumbiner BM. E-Cadherin Homophilic Ligation Inhibits Cell Growth and Epidermal Growth Factor Receptor Signaling Independently of Other Cell Interactions. Mol. Biol. Cell. 2007;18:2013–25.

51. Qian X, Karpova T, Sheppard AM, McNally J, Lowy DR. E-cadherin-mediated adhesion inhibits ligand-dependent activation of diverse receptor tyrosine kinases. EMBO J. 2004;23:1739–48.

52. Fedor-Chaiken M, Hein PW, Stewart JC, Brackenbury R, Kinch MS. E-cadherin binding modulates EGF receptor activation. Cell Commun. Adhes. 2003;10:105–18.

53. Hoschuetzky H, Aberle H, Kemler R. β-Catenin mediates the interaction of the cadherin-catenin complex with epidermal growth factor receptor. J. Cell Biol. 1994;127:1375–80.

54. Pece S, Gutkind JS. Signaling from E-cadherins to the MAPK pathway by the recruitment and activation of epidermal growth factor receptors upon cell-cell contact formation. J. Biol. Chem. 2000;275:41227–33.

55. Reddy P, Liu L, Ren C, Lindgren P, Boman K, Shen Y, et al. Formation of E-cadherin-mediated cell-cell adhesion activates AKT and mitogen activated protein kinase via phosphatidylinositol 3 kinase and ligand-independent activation of epidermal growth factor receptor in ovarian cancer cells. Mol. Endocrinol. 2005;19:2564–78.

56. Schackmann RCJ, Klarenbeek S, Vlug EJ, Stelloo S, van Amersfoort M, Tenhagen M, et al. Loss of p120-catenin induces metastatic progression of breast cancer by inducing anoikis resistance and augmenting growth factor receptor signaling. Cancer Res. 2013;73:4937–49.

57. Curto M, Cole BK, Lallemand D, Liu C-H, McClatchey AI. Contact-dependent inhibition of EGFR signaling by Nf2/Merlin. J. Cell Biol. 2007;177:893–903.

58. Mateus AR, Seruca R, Machado JC, Keller G, Oliveira MJ, Suriano G, et al. EGFR regulates RhoA-GTP dependent cell motility in E-cadherin mutant cells. Hum. Mol. Genet. 2007;16:1639–47.

59. Mateus AR, Simões-Correia J, Figueiredo J, Heindl S, Alves CC, Suriano G, et al. E-cadherin mutations and cell motility: A genotype-phenotype correlation. Exp. Cell Res. 2009;315:1393–402.

60. Bremm A, Walch A, Fuchs M, Mages J, Duyster J, Keller G, et al. Enhanced activation of epidermal growth factor receptor caused by tumor-derived E-cadherin mutations. Cancer Res. 2008;68:707–14.

61. Knudsen K a, Wheelock MJ. Cadherins and the mammary gland. J. Cell. Biochem. 2005;95:488–96.

62. Andrews JL, Kim AC, Hens JR. The role and function of cadherins in the mammary gland. Breast Cancer Res. 2012;14:203.

63. Sternlicht MD. Key stages in mammary gland development: the cues that regulate ductal branching morphogenesis. Breast Cancer Res. 2006;8:201.

64. Williams JM, Daniel CW. Mammary ductal elongation: Differentiation of myoepithelium and basal lamina during branching morphogenesis. Dev. Biol. 1983;97:274–90.

65. Ewald AJ, Brenot A, Duong M, Chan BS, Werb Z. Collective epithelial migration and cell rearrangements drive mammary branching morphogenesis. Dev. Cell. 2008;14:570–81.

66. Rudland PS, Hughes CM. Immunocytochemical identification of cell types in human mammary gland: variations in cellular markers are dependent on glandular topography and differentiation. J Histochem Cytochem. 1989;37:1087–100.

67. Visvader JE, Stingl J. Mammary stem cells and the differentiation hierarchy : current status and perspectives. 2014;1143–58.

68. Inman JL, Robertson C, Mott JD, Bissell MJ. Mammary gland development: cell fate specification, stem cells and the microenvironment. Development. 2015;142:1028–42.

69. Humphreys RC, Krajewska M, Krnacik S, Jaeger R, Weiher H, Krajewski S, et al. Apoptosis in the terminal endbud of the murine mammary gland: a mechanism of ductal morphogenesis. Development. 1996;122:4013–22.

70. Frisch SM, Francis H. Disruption of epithelial cell-matrix interactions induces apoptosis. J. Cell Biol.

1994;124:619–26.

71. Mailleux AA, Overholtzer M, Brugge JS. Lumen formation during mammary epithelial morphogenesis. Cell Cycle. 2008;7:57–62.

72. Paoli P, Giannoni E, Chiarugi P. Anoikis molecular pathways and its role in cancer progression. Biochim. Biophys. Acta. 2013;

73. Reginato MJ, Mills KR, Becker EBE, Lynch DK, Bonni A, Muthuswamy SK, et al. Bim regulation of lumen formation in cultured mammary epithelial acini is targeted by oncogenes. Mol. Cell. Biol. 2005;25:4591–601.

74. Reginato MJ, Mills KR, Paulus JK, Lynch DK, Sgroi DC, Debnath J, et al. Integrins and EGFR coordinately regulate the pro-apoptotic protein Bim to prevent anoikis. Nat. Cell Biol. 2003;5:733–40.

75. Schmelzle T, Mailleux AA, Overholtzer M, Carroll JS, Solimini NL, Lightcap ES, et al. Functional role and oncogene-regulated expression of the BH3-only factor Bmf in mammary epithelial anoikis and morphogenesis. Proc. Natl. Acad. Sci. U. S. A. 2007;104:3787–92.

76. Schuler F, Baumgartner F, Klepsch V, Chamson M, Müller-Holzner E, Watson CJ, et al. The BH3-only protein BIM contributes to late-stage involution in the mouse mammary gland. Cell Death Differ. 2016;23:41–51.

77. Mailleux AA, Overholtzer M, Schmelzle T, Bouillet P, Strasser A, Brugge JS. BIM regulates apoptosis during mammary ductal morphogenesis, and its absence reveals alternative cell death mechanisms. Dev. Cell. 2007;12:221–34.

78. Boussadia O, Kutsch S, Hierholzer A, Delmas V, Kemler R. E-cadherin is a survival factor for the lactating mouse mammary gland. Mech. Dev. 2002;115:53–62.

79. Derksen PWB, Liu X, Saridin F, van der Gulden H, Zevenhoven J, Evers B, et al. Somatic inactivation of E-cadherin and p53 in mice leads to metastatic lobular mammary carcinoma through induction of anoikis resistance and angiogenesis. Cancer Cell. 2006;10:437–49.

80. Derksen PWB, Braumuller TM, van der Burg E, Hornsveld M, Mesman E, Wesseling J, et al. Mammary-specific inactivation of E-cadherin and p53 impairs functional gland development and leads to pleomorphic invasive lobular carcinoma in mice. Dis. Model. Mech. 2011;4:347–58.

81. Wagner KU, Ward T, Davis B, Wiseman R, Hennighausen L. Spatial and temporal expression of the Cre gene under the control of the MMTV-LTR in different lines of transgenic mice. Transgenic Res. 2001;10:545–53.

82. Wagner KU, Wall RJ, St-Onge L, Gruss P, Wynshaw-Boris A, Garrett L, et al. Cre-mediated gene deletion in the mammary gland. Nucleic Acids Res. 1997;25:4323–30.

83. Shamir ER, Pappalardo E, Jorgens DM, Coutinho K, Tsai W-T, Aziz K, et al. Twist1-induced dissemination preserves epithelial identity and requires E-cadherin. J. Cell Biol. 2014;204:839–56.

84. Shamir ER, Ewald AJ. Adhesion in mammary development: Novel roles for E-cadherin in individual and collective cell migration. Curr. Top. Dev. Biol. 2015. p. 353–82.

85. Kurley SJ, Bierie B, Carnahan RH, Lobdell NA, Davis MA, Hofmann I, et al. P120-Catenin is essential for terminal end bud function and mammary morphogenesis. Development. 2012;1734:1724–34.

86. Hanahan D, Weinberg RA. Hallmarks of cancer: The next generation. Cell. 2011;144:646–74.

87. Jeanes A, Gottardi CJ, Yap AS. Cadherins and cancer: how does cadherin dysfunction promote tumor progression? Oncogene. 2008;27:6920–9.

88. Berx G, van Roy F. Involvement of members of the cadherin superfamily in cancer. Cold Spring Harb. Perspect. Biol. 2009;1:a003129.

89. Guilford P, Hopkins J, Harraway J, McLeod M, McLeod N, Harawira P, et al. E-cadherin germline mutations in familial gastric cancer. Nature. 1998;392:402–5.

90. Becker KF, Atkinson MJ, Reich U, Becker I, Nekarda H, Siewert JR, et al. E-cadherin gene mutations provide clues to diffuse type gastric carcinomas. Cancer Res. 1994;54:3845–52.

91. Berx G, Becker KF, Höfler H, Van Roy F. Mutations of the human E-cadherin (CDH1) gene. Hum. Mutat. 1998;12:226–37.

92. Yoder BJ, Wilkinson EJ, Massoll NA. Molecular and Morphologic Distinctions between Infiltrating Ductal and Lobular Carcinoma of the Breast. Breast J. 2007;13:172–9.

93. Dieci MV, Orvieto E, Dominici M, Conte P, Guarneri V. Rare Breast Cancer Subtypes: Histological, Molecular, and Clinical Peculiarities. Oncologist. 2014;19:805–13.

94. Berx G, Nollet F, Leeuw WJF De, Vijver MJ Van De, Cornelisse C, Roy F Van. E-cadherin as a tumour/invasion suppressor gene mutated in human lobular breast cancers. EMBO J. 1995;14:6107–15.

&

95. Droufakou S, Deshmane V, Roylance R, Hanby A, Tomlinson I, Hart IR. Multiple ways of silencing E-cadherin gene expression in lobular carcinoma of the breast. Int. J. Cancer. 2001;92:404–8.

96. Sarrió D, Moreno-Bueno G, Hardisson D, Sanchez-Estevez C, Guo M, Herman JG, et al. Epigenetic and genetic alterations of APC and CDH1 genes in lobular breast cancer: Relationships with abnormal E-cadherin and catenin expression and microsatellite instability. Int. J. Cancer. 2003;106:208–15.

97. Ciriello G, Gatza ML, Beck AH, Wilkerson MD, Rhie SK, Pastore A, et al. Comprehensive Molecular Portraits of Invasive Lobular Breast Cancer. Cell. 2015;163:506–19.

98. Moll R, Mitze M, Frixen UH, Birchmeier W. Differential loss of E-cadherin expression in infiltrating ductal and lobular breast carcinomas. Am. J. Pathol. 1993;143:1731–42.

99. Vos CB, Cleton-Jansen AM, Berx G, de Leeuw WJ, ter Haar NT, van Roy F, et al. E-cadherin inactivation in lobular carcinoma in situ of the breast: an early event in tumorigenesis. Br. J. Cancer. 1997;76:1131–3.

100. Reed AEM, Kutasovic JR, Lakhani SR, Simpson PT. Invasive lobular carcinoma of the breast: morphology, biomarkers and 'omics. Breast Cancer Res. 2015;17:12.

101. Arpino G, Bardou VJ, Clark GM, Elledge RM. Infiltrating lobular carcinoma of the breast: tumor characteristics and clinical outcome. Breast Cancer Res. 2004;6:R149–56.

102. Johnson K, Sarma D, Hwang ES. Lobular breast cancer series: imaging. Breast Cancer Res. 2015;17:94.

103. Vlug E, Ercan C, van der Wall E, van Diest PJ, Derksen PWB. Lobular breast cancer: pathology, biology, and options for clinical intervention. Arch. Immunol. Ther. Exp. (Warsz). 2014;62:7–21.

104. Guiu S, Wolfer A, Jacot W, Fumoleau P, Romieu G, Bonnetain F, et al. Invasive lobular breast cancer and its variants: How special are they for systemic therapy decisions? Crit. Rev. Oncol. Hematol. 2014;92:235–57.

105. Sikora MJ, Jankowitz RC, Dabbs DJ, Oesterreich S. Invasive lobular carcinoma of the breast: patient response to systemic endocrine therapy and hormone response in model systems. Steroids. 2013;78:568–75.

106. Katz A, Saad ED, Porter P, Pusztai L. Primary systemic chemotherapy of invasive lobular carcinoma of the breast. Lancet Oncol. 2007;8:55–62.

107. Hosford SR, Miller TW. Clinical potential of novel therapeutic targets in breast cancer : CDK4/6, Src, JAK/STAT, PARP, HDAC, and PI3K/AKT/mTOR pathways. Pharmgenomics. Pers. Med. 2014;7:203–15.

108. Mohamed A, Krajewski K, Cakar B, Ma CX. Targeted Therapy for Breast Cancer. Am. J. Pathol. American Society for Investigative Pathology; 2013;183:1096–112.

109. Yamamoto-Ibusuki M, Arnedos M, André F. Targeted therapies for ER+/HER2- metastatic breast cancer. BMC Med. 2015;13:15–9.

110. de Leeuw WJ, Berx G, Vos CB, Peterse JL, van de Vijver MJ, Litvinov S, et al. Simultaneous loss of E-cadherin and catenins in invasive lobular breast cancer and lobular carcinoma in situ. J. Pathol. 1997;411:404–11.

111. van de Ven RAH, Tenhagen M, Meuleman W, van Riel JJG, Schackmann RCJ, Derksen PWB. Nuclear p120-catenin regulates the anoikis resistance of mouse lobular breast cancer cells through Kaiso-dependent Wnt11 expression. Dis. Model. Mech. 2015;8:373–84.

112. Schackmann RCJ, Amersfoort M Van, Haarhuis JHI, Vlug EJ, Halim VA, Roodhart JML, et al. Cytosolic p120-catenin regulates growth of metastatic lobular carcinoma through Rock1-mediated anoikis resistance. J. Clin. Invest. 2011;121:3176–88.

113. Wetering M Van De, Barker N, Harkes IC, Wetering M Van De, Barker N, Harkes IC, et al. Mutant E-cadherin Breast Cancer Cells Do Not Display Constitutive Wnt Signaling Mutant E-cadherin Breast Cancer Cells Do Not Display Constitutive Wnt Signaling. 2001;278–84.

114. Shibata T, Kokubu A, Sekine S, Kanai Y, Hirohashi S. Cytoplasmic p120ctn regulates the invasive phenotypes of E-cadherin-deficient breast cancer. Am. J. Pathol. 2004;164:2269–78.

115. Dabbs DJ, Bhargava R, Chivukula M. Lobular versus ductal breast neoplasms: the diagnostic utility of p120 catenin. Am. J. Surg. Pathol. 2007;31:427–37.

116. Sarrió D, Pérez-Mies B, Hardisson D, Moreno-Bueno G, Suárez A, Cano A, et al. Cytoplasmic localization of p120ctn and E-cadherin loss characterize lobular breast carcinoma from preinvasive to metastatic lesions. Oncogene. 2004;23:3272–83.

117. Li X, Schwartz MR, Ro J, Hamilton CR, Ayala AG, Truong LD, et al. Diagnostic utility of E-cadherin and P120 catenin cocktail immunostain in distinguishing DCIS from LCIS. Int. J. Clin. Exp. Pathol. 2014;7:2551–7.

118. Rakha EA, Patel A, Powe DG, Benhasouna A, Green AR, Lambros MB, et al. Clinical and biological significance of E-cadherin protein expression in invasive lobular carcinoma of the breast. Am. J. Surg. Pathol. 2011;34:1472–9.

119. Perou CM, Sørlie T, Eisen MB, van de Rijn M, Jeffrey SS, Rees C a, et al. Molecular portraits of human breast tumours. Nature. 2000;406:747–52.

120. Sorlie T, Perou CM, Tibshirani R, Aas T, Geisler S, Johnsen H, et al. Gene expression patterns of breast carcinomas distinguish tumor subclasses with clinical implications. Proc. Natl. Acad. Sci. U. S. A. 2001;98:10869–74.

121. Abd El-rehim DM, Ball G, Pinder SE, Rakha E, Paish C, Robertson JF, et al. High-throughput protein expression analysis using tissue microarray technology of a large well-characterised series identifies biologically distinct classes of breast cancer confirming recent cDNA expression analyses. Int. J. Cancer. 2005;116:340–50.

122. Parker JS, Mullins M, Cheung MCU, Leung S, Voduc D, Vickery T, et al. Supervised risk predictor of breast cancer based on intrinsic subtypes. J. Clin. Oncol. 2009;27:1160–7.

123. Weigelt B, Geyer FC, Natrajan R, Lopez-garcia MA, Ahmad AS, Savage K, et al. The molecular underpinning of lobular histological growth pattern : a genome-wide transcriptomic analysis of invasive lobular carcinomas and grade- and molecular subtype-matched invasive ductal carcinomas of no special type. J. Pathol. 2010;45–57.

124. Zhao H, Langerød A, Ji Y, Nowels KW, Nesland JM, Tibshirani R, et al. Different gene expression patterns in invasive lobular and ductal carcinomas of the breast. Mol. Biol. Cell. 2004;15:2523–36.

125. Bertucci F, Orsetti B, Nègre V, Finetti P, Rougé C, Ahomadegbe J-C, et al. Lobular and ductal carcinomas of the breast have distinct genomic and expression profiles. Oncogene. 2008;27:5359–72.

126. Turashvili G, Bouchal J, Baumforth K, Wei W, Dziechciarkova M, Ehrmann J, et al. Novel markers for differentiation of lobular and ductal invasive breast carcinomas by laser microdissection and microarray analysis. BMC Cancer. 2007;7:55.

127. Michaut M, Chin S-F, Majewski I, Severson TM, Bismeijer T, de Koning L, et al. Integration of genomic, transcriptomic and proteomic data identifies two biologically distinct subtypes of invasive lobular breast cancer. Sci. Rep. 2016;6:18517.

128. Reis-Filho JS, Simpson PT, Turner NC, Lambros MB, Jones C, Mackay A, et al. FGFR1 emerges as a potential therapeutic target for lobular breast carcinomas. Clin. Cancer Res. 2006;12:6652–62.

129. Buttitta F, Felicioni L, Barassi F, Martella C, Paolizzi D, Fresu G, et al. PIK3CA mutation and histological type in breast carcinoma: high frequency of mutations in lobular carcinoma. J. Pathol. 2006;208:350–5.

130. Christgen M, Noskowicz M, Schipper E, Christgen H, Heil C, Krech T. Oncogenic PIK3CA Mutations in Lobular Breast Cancer Progression. Genes. Chromosomes Cancer. 2013;52:69–80.

131. Beelen K, Opdam M, Severson TM, Koornstra RHT, Vincent AD, Wesseling J, et al. PIK3CA mutations, phosphatase and tensin homolog, human epidermal growth factor receptor 2, and insulin-like growth factor 1 receptor and adjuvant tamoxifen resistance in postmenopausal breast cancer patients. Breast Cancer Res. 2014;16:R13.

132. Bachman KE, Argani P, Samuels Y, Silliman N, Ptak J, Szabo S, et al. The PIK3CA Gene is Mutated with High Frequency in human breast cancers. Cancer Biol. Ther. 2004;3:772–5.

133. Sarbassov DD, Guertin D a, Ali SM, Sabatini DM. Phosphorylation and regulation of Akt/PKB by the rictor-mTOR complex. Science. 2005;307:1098–101.

134. Alessi DR, James SR, Downes CP, Holmes AB, Gaffney PR, Reese CB, et al. Characterization of a 3-phosphoinositide-dependent protein kinase which phosphorylates and activates protein kinase Bα. Curr Biol. 1997;7:261–9.

135. Koboldt DC, Fulton RS, McLellan MD, Schmidt H, Kalicki-Veizer J, McMichael JF, et al. Comprehensive molecular portraits of human breast tumours. Nature. 2012;490:61–70.

136. Stemke-Hale K, Gonzalez-Angulo AM, Lluch A, Neve RM, Kuo WL, Davies M, et al. An integrative genomic and proteomic analysis of PIK3CA, PTEN, and AKT mutations in breast cancer. Cancer Res. 2008;68:6084–91.

137. Azim HA, Kassem L, Treilleux I, Wang Q, El Enein MA, Anis SE, et al. Analysis of PI3K/mTOR Pathway Biomarkers and Their Prognostic Value in Women with Hormone Receptor–Positive, HER2-Negative Early Breast Cancer. Transl. Oncol. 2016;9:114–23.

138. Dillon DA, D'Aquila T, Reynolds AB, Fearon ER, Rimm DL. The expression of p120ctn protein in breast

cancer is independent of alpha- and beta-catenin and E-cadherin. Am. J. Pathol. 1998;152:75–82.

139. Talvinen K, Tuikkala J, Nykänen M, Nieminen A, Anttinen J, Nevalainen OS, et al. Altered expression of p120catenin predicts poor outcome in invasive breast cancer. J. Cancer Res. Clin. Oncol. 2010;136:1377–87.

140. Thoreson MA, Reynolds AB. Altered expression of the catenin p120 in human cancer: implications for tumor progression. Differentiation. 2002;70:583–9.

141. Davis MA, Reynolds AB. Blocked acinar development, E-cadherin reduction, and intraepithelial neoplasia upon ablation of p120-catenin in the mouse salivary gland. Dev. Cell. 2006;10:21–31.

142. Perez-Moreno M, Davis MA, Wong E, Pasolli HA, Reynolds AB, Fuchs E. P120-Catenin Mediates Inflammatory Responses in the Skin. Cell. 2006;124:631–44.

143. Smalley-Freed WG, Efimov A, Burnett PE, Short SP, Davis MA, Gumucio DL, et al. P120-Catenin Is Essential for Maintenance of Barrier Function and Intestinal Homeostasis in Mice. J. Clin. Invest. 2010;120:1824–35.

144. Smalley-Freed WG, Efimov A, Short SP, Jia P, Zhao Z, Washington MK, et al. Adenoma formation following limited ablation of p120-catenin in the mouse intestine. PLoS One. 2011;6.

145. Stairs DB, Bayne LJ, Rhoades B, Vega ME, Waldron TJ, Kalabis J, et al. Deletion of p120-Catenin Results in a Tumor Microenvironment with Inflammation and Cancer that Establishes It as a Tumor Suppressor Gene. Cancer Cell. 2011;19:470–83.

146. Yanagisawa M, Anastasiadis PZ. P120 Catenin Is Essential for Mesenchymal Cadherin-Mediated Regulation of Cell Motility and Invasiveness. J. Cell Biol. 2006;174:1087–96.

147. Soto E, Yanagisawa M, Marlow L a., Copland J a., Perez E a., Anastasiadis PZ. p120 catenin induces opposing effects on tumor cell growth depending on E-cadherin expression. J. Cell Biol. 2008;183:737–49.

148. Soubry A, van Hengel J, Parthoens E, Colpaert C, Van Marck E, Waltregny D, et al. Expression and nuclear location of the transcriptional repressor Kaiso is regulated by the tumor microenvironment. Cancer Res. 2005;65:2224–33.

149. Albagli O, Dhordain P, Deweindt C, Lecocq G, Leprince D. The BTB/POZ domain: a new protein-protein interaction motif common to DNA- and actin-binding proteins. Cell Growth Differ. 1995;6:1193–8.

150. Kelly KF, Daniel JM. POZ for effect- POZ-ZF transcription factors in cancer and development. Trends Cell Biol. 2006;16:578–87.

151. Kim SW, Fang X, Ji H, Paulson AF, Daniel JM, Ciesiolka M, et al. Isolation and characterization of XKaiso, a transcriptional repressor that associates with the catenin Xp120ctn in Xenopus laevis. J. Biol. Chem. 2002;277:8202–8.

152. Defossez P-A, Kelly KF, Filion GJP, Pérez-Torrado R, Magdinier F, Menoni H, et al. The human enhancer blocker CTC-binding factor interacts with the transcription factor Kaiso. J. Biol. Chem. 2005;280:43017–23.

153. Koh D-I, Han D, Ryu H, Choi W-I, Jeon B-N, Kim M-K, et al. Kaiso, a critical regulator of p53-mediated transcription of CDKN1A and apoptotic genes. Proc. Natl. Acad. Sci. U. S. A. 2014;111:15078–83.

154. Yoon H-G, Chan DW, Reynolds AB, Qin J, Wong J. N-CoR mediates DNA methylation-dependent repression through a methyl CpG binding protein Kaiso. Mol. Cell. 2003;12:723–34.

155. Donaldson NS, Nordgaard CL, Pierre CC, Kelly KF, Robinson SC, Swystun L, et al. Kaiso regulates Znf131-mediated transcriptional activation. Exp. Cell Res. 2010;316:1692–705.

156. Daniel JM, Ireton RC, Reynolds AB, Al DET. Monoclonal Antibodies to Kaiso : A Novel Transcription Factor and p120-ctn-Binding Protein. Hybridoma. 2001;20:159–66.

157. Soubry A, Staes K, Parthoens E, Noppen S, Stove C, Bogaert P, et al. The transcriptional repressor Kaiso localizes at the mitotic spindle and is a constituent of the pericentriolar material. PLoS One. 2010;5:e9203.

158. Kelly KF, Otchere AA, Graham M, Daniel JM. Nuclear import of the BTB/POZ transcriptional regulator Kaiso. J. Cell Sci. 2004;117:6143–52.

159. Vermeulen JF, van de Ven R a. H, Ercan C, van der Groep P, van der Wall E, Bult P, et al. Nuclear Kaiso expression is associated with high grade and triple-negative invasive breast cancer. PLoS One. 2012;7:e37864.

160. Prokhortchouk A, Hendrich B, Jørgensen H, Ruzov A, Wilm M, Georgiev G, et al. The p120 catenin partner Kaiso is a DNA methylation-dependent transcriptional repressor. Genes Dev. 2001;15:1613–8.

161. Dai S-D, Wang Y, Zhang J-Y, Zhang D, Zhang P-X, Jiang G-Y, et al. Upregulation of δ-catenin is

associated with poor prognosis and enhances transcriptional activity through Kaiso in non-small-cell lung cancer. Cancer Sci. 2011;102:95–103.

162. Del Valle-Pérez B, Casagolda D, Lugilde E, Valls G, Codina M, Dave N, et al. Wnt controls the transcriptional activity of Kaiso through CK1ε-dependent phosphorylation of p120-catenin. J. Cell Sci. 2011;124:2298–309.

163. Kaplan J, Calame K. The ZiN/POZ domain of ZF5 is required for both transcriptional activation and repression. Nucleic Acids Res. 1997;25:1108–16.

164. Peukert K, Staller P, Schneider A, Carmichael G, Hanel F, Eilers M. An alternative pathway for gene regulation by Myc. Embo J. 1997;16:5672–86.

165. Rodova M, Kelly KF, Vansaun M, Daniel JM, Werle MJ. Regulation of the Rapsyn promoter by Kaiso and δ-catenin. Mol. Cell. Biol. 2004;24:7188–96.

166. Blattler A, Yao L, Wang Y, Ye Z, Jin VX, Farnham PJ. ZBTB33 binds unmethylated regions of the genome associated with actively expressed genes. Epigenetics Chromatin. 2013;6:13.

167. Raghav SK, Waszak SM, Krier I, Gubelmann C, Isakova A, Mikkelsen TS, et al. Integrative Genomics Identifies the Corepressor SMRT as a Gatekeeper of Adipogenesis through the Transcription Factors C/EBPβ and KAISO. Mol. Cell. 2012;1–16.

168. Lin RJ, Nagy L, Inoue S, Shao W, Miller WH, Evans RM. Role of the histone deacetylase complex in acute promyelocytic leukaemia. Nature. 1998;391:811–4.

169. Huynh KD, Bardwell VJ. The BCL-6 POZ domain and other POZ domains interact with the co-repressors N-CoR and SMRT. Oncogene. 1998;17:2473–84.

170. Wong MM, Guo C, Zhang J. Nuclear receptor corepressor complexes in cancer: mechanism, function and regulation. Am. J. Clin. Exp. Urol. 2014;2:169–87.

171. Barrett CW, Lu LC, Markham N, Stengel KR, Short SP, Zhang B, et al. Kaiso Directs the Transcriptional Corepressor MTG16 to the Kaiso Binding Site in Target Promoters. PLoS One. 2012;7:e51205.

172. Ibañez V, Sharma A, Buonamici S, Verma A, Kalakonda S, Wang J, et al. AML1-ETO decreases ETO-2 (MTG16) interactions with nuclear receptor corepressor, an effect that impairs granulocyte differentiation. Cancer Res. 2004;64:4547–54.

173. Rothbart SB, Strahl BD. Interpreting the language of histone and DNA modifications. Biochim. Biophys. Acta. 2014;1839:627–43.

174. Kouzarides T. Chromatin Modifications and Their Function. Cell. 2007;128:693–705.

175. Park J-I, Kim SW, Lyons JP, Ji H, Nguyen TT, Cho K, et al. Kaiso/p120-catenin and TCF/beta-catenin complexes coordinately regulate canonical Wnt gene targets. Dev. Cell. 2005;8:843–54.

176. Ali T, Renkawitz R, Bartkuhn M. Insulators and domains of gene expression. Curr. Opin. Genet. Dev. 2016;37:17–26.

177. Yusufzai TM, Felsenfeld G. The 5'-HS4 chicken beta-globin insulator is a CTCF-dependent nuclear matrix-associated element. Proc. Natl. Acad. Sci. U. S. A. 2004;101:8620–4.

178. Clevers H, Nusse R. Wnt/Beta-catenin signaling and disease. Cell. 2012;149:1192–205.

179. Zhao C, Deng Y, Liu L, Yu K, Zhang L, Wang H, et al. Dual regulatory switch through interactions of Tcf7l2/Tcf4 with stage-specific partners propels oligodendroglial maturation. Nat. Commun. 2016;7:10883.

180. Ruzov A, Hackett J a, Prokhortchouk A, Reddington JP, Madej MJ, Dunican DS, et al. The interaction of xKaiso with xTcf3: a revised model for integration of epigenetic and Wnt signalling pathways. Development. 2009;136:723–7.

181. Spring CM, Kelly KF, O'Kelly I, Graham M, Crawford HC, Daniel JM. The catenin p120ctn inhibits Kaiso-mediated transcriptional repression of the beta-catenin/TCF target gene matrilysin. Exp. Cell Res. 2005;305:253–65.

182. Hong JY, Park J-I, Cho K, Gu D, Ji H, Artandi SE, et al. Shared molecular mechanisms regulate multiple catenin proteins: canonical Wnt signals and components modulate p120-catenin isoform-1 and additional p120 subfamily members. J. Cell Sci. 2010;123:4351–65.

183. Park J il, Ji H, Jun S, Gu D, Hikasa H, Li L, et al. Frodo Links Dishevelled to the p120-Catenin/Kaiso Pathway: Distinct Catenin Subfamilies Promote Wnt Signals. Dev. Cell. 2006;11:683–95.

184. Sokol SY. Spatial and temporal aspects of Wnt signaling and planar cell polarity during vertebrate embryonic development. Semin. Cell Dev. Biol. 2015;42:78–85.

185. Ruzov A, Savitskaya E, Hackett J a, Reddington JP, Prokhortchouk A, Madej MJ, et al. The non-methylated DNA-binding function of Kaiso is not required in early Xenopus laevis development.

Development. 2009;136:729–38.

186. Prokhortchouk A, Sansom O, Selfridge J, Caballero IM, Salozhin S, Aithozhina D, et al. Kaiso-Deficient Mice Show Resistance to Intestinal Cancer. Mol. Cell. Biol. 2006;26:199–208.

187. Pierre CC, Longo J, Mavor M, Milosavljevic SB, Chaudhary R, Gilbreath E, et al. Kaiso overexpression promotes intestinal inflammation and potentiates intestinal tumorigenesis in ApcMin/+ mice. Biochim. Biophys. Acta. 2015;1852:1846–55.

188. Dai S-D, Wang Y, Miao Y, Zhao Y, Zhang Y, Jiang G-Y, et al. Cytoplasmic Kaiso is associated with poor prognosis in non-small cell lung cancer. BMC Cancer. 2009;9:178.

189. Jones J, Wang H, Karanam B, Theodore S, Dean-Colomb W, Welch DR, et al. Nuclear localization of Kaiso promotes the poorly differentiated phenotype and EMT in infiltrating ductal carcinomas. Clin. Exp. Metastasis. 2014;31:497–510.

190. Jones J, Wang H, Zhou J, Hardy S, Turner T, Austin D, et al. Nuclear Kaiso Indicates Aggressive Prostate Cancers and Promotes Migration and Invasiveness of Prostate Cancer Cells. Am. J. Pathol. 2012;181:49–50.

191. Wang H, Liu W, Black S, Turner O, Daniel JM, Dean-colomb W, et al. Kaiso, a transcriptional repressor, promotes cell migration and invasion of prostate cancer cells through regulation of miR-31 expression. Oncotarget. 2016;7:5677–89.

192. Donaldson NS, Pierre CC, Anstey MI, Robinson SC, Weerawardane SM, Daniel JM. Kaiso Represses the Cell Cycle Gene cyclin D1 via Sequence-Specific and Methyl-CpG-Dependent Mechanisms. PLoS One. 2012;7:e50398.

193. Wang Y, Li L, Li Q, Xie C, Wang E, Wang E. Expression of P120 catenin, Kaiso, and metastasis tumor antigen-2 in thymomas. Tumor Biol. 2012;33:1871–9.

194. Christgen M, Derksen PW. Lobular breast cancer: molecular basis, mouse and cellular models. Breast Cancer Res. 2015;17:1–9.

195. Grady WM, Willis J, Guilford PJ, Dunbier a K, Toro TT, Lynch H, et al. Methylation of the CDH1 promoter as the second genetic hit in hereditary diffuse gastric cancer. Nat. Genet. 2000;26:16–7.

196. Kalluri R, Weinberg R a. Review series The basics of epithelial-mesenchymal transition. J. Clin. Invest. 2009;119:1420–8.

197. Harris TJC, Tepass U. Adherens junctions: from molecules to morphogenesis. Nat. Rev. Mol. Cell Biol. 2010;11:502–14.

198. Turashvili G, Turashvili G, Bouchal J, Bouchal J, Burkadze G, Burkadze G, et al. Differentiation of tumours of ductal and lobular origin: II. Proteomics of invasive ductal and lobular breast carcinomas. Biomed.Pap. 2005;149:57–62.

199. Carnahan RH, Rokas A, Gaucher E a, Reynolds AB. The molecular evolution of the p120-catenin subfamily and its functional associations. PLoS One. 2010;5:e15747.

200. Cardiff RD, Kenney N. Mouse Mammary Tumor Biology: A Short History. Adv. Cancer Res. 2007;98:53–116.

201. Peppercorn J, Perou CM, Carey LA. Molecular subtypes in breast cancer evaluation and management: divide and conquer. Cancer Invest. 2008;26:1–10.

202. Nakopoulou L, Gakiopoulou-Givalou H, Karayiannakis AJ, Giannopoulou I, Keramopoulos A, Davaris P, et al. Abnormal alpha-catenin expression in invasive breast cancer correlates with poor patient survival. Histopathology. 2002;40:536–46.

203. Anastasiadis PZ, Reynolds AB. Regulation of Rho GTPases by p120-catenin. Curr. Opin. Cell Biol. 2001;13:604–10.

204. van Roy FM, McCrea PD. A role for Kaiso-p120ctn complexes in cancer? Nat. Rev. Cancer. 2005;5:956–64.

205. Schwartz S, Wongvipat J, Trigwell CB, Hancox U, Carver BS, Rodrik-Outmezguine V, et al. Feedback Suppression of PI3Kα Signaling in PTEN-Mutated Tumors Is Relieved by Selective Inhibition of PI3Kβ. Cancer Cell. 2014;109–22.

206. Debnath J, Mills KR, Collins NL, Reginato MJ, Muthuswamy SK, Brugge JS. The role of apoptosis in creating and maintaining luminal space within normal and oncogene-expressing mammary acini. Cell. 2002;111:29–40.

207. Westphal D, Dewson G, Czabotar PE, Kluck RM. Molecular biology of Bax and Bak activation and action. Biochim. Biophys. Acta. 2011;1813:521–31.

208. Strasser A, Cory S, Adams JM. Deciphering the rules of programmed cell death to improve therapy of cancer and other diseases. EMBO J. 2011;30:3667–83.

209. Hausmann M, Leucht K, Ploner C, Kiessling S, Villunger A, Becker H, et al. BCL-2 modifying factor (BMF) is a central regulator of anoikis in human intestinal epithelial cells. J. Biol. Chem. 2011;286:26533–40.

210. Puthalakath H, Villunger A, O'Reilly L a, Beaumont JG, Coultas L, Cheney RE, et al. goede Bmf: a proapoptotic BH3-only protein regulated by interaction with the myosin V actin motor complex, activated by anoikis. Science. 2001;293:1829–32.

211. Chiarugi P, Giannoni E. Anoikis: A necessary death program for anchorage-dependent cells. Biochem. Pharmacol. 2008;76:1352–64.

212. Muthuswamy SK, Li D, Lelievre S, Bissell MJ, Brugge JS. ErbB2, but not ErbB1, reinitiates proliferation and induces luminal repopulation in epithelial acini. Nat. Cell Biol. 2001;3:785–92.

213. Danes CG, Wyszomierski SL, Lu J, Neal CL, Yang W, Yu D. 14-3-3ζ Down-Regulates P53 in Mammary Epithelial Cells and Confers Luminal Filling. Cancer Res. 2008;68:1760–7.

214. Samuels Y, Whang Z, Bardelli A, Silliman N, Ptak J, Szabo S, et al. High frequency of mutations of the PIK3CA gene in human cancers. Science (80-.). 2004;304:554.

215. Datta SR, Dudek H, Xu T, Masters S, Haian F, Gotoh Y, et al. Akt phosphorylation of BAD couples survival signals to the cell- intrinsic death machinery. Cell. 1997;91:231–41.

216. Gardai SJ, Hildeman DA, Frankel SK, Whitlock BB, Frasch SC, Borregaard N, et al. Phosphorylation of Bax ser184 by Akt regulates its activity and apoptosis in neutrophils. J. Biol. Chem. 2004;279:21085–95.

217. Van Roy F, Berx G. The cell-cell adhesion molecule E-cadherin. Cell. Mol. Life Sci. 2008;65:3756–88.

218. Vaillant F, Merino D, Lee L, Breslin K, Pal B, Ritchie ME, et al. Targeting BCL-2 with the BH3 Mimetic ABT-199 in Estrogen Receptor-Positive Breast Cancer. Cancer Cell. 2013;24:120–9.

219. Muranen T, Selfors LM, Worster DT, Iwanicki MP, Song L, Morales FC, et al. Inhibition of PI3K/mTOR Leads to Adaptive Resistance in Matrix-Attached Cancer Cells. Cancer Cell. 2012;21:227–39.

220. Eijkelenboom A, Burgering BMT. FOXOs: signalling integrators for homeostasis maintenance. Nat. Rev. Mol. Cell Biol. 2013;14:83–97.

221. Brunet A, Bonni A, Zigmond MJ, Lin MZ, Juo P, Hu LS, et al. Akt Promotes Cell Survival by Phosphorylating and Inhibiting a Forkhead Transcription Factor. Cell. 1999;96:857–68.

222. Juin P, Geneste O, Gautier F, Depil S, Campone M. Decoding and unlocking the BCL-2 dependency of cancer cells. Nat. Rev. Cancer. 2013;13:455–65.

223. Eijkelenboom A, Mokry M, de Wit E, Smits LM, Polderman PE, van Triest MH, et al. Genome-wide analysis of FOXO3 mediated transcription regulation through RNA polymerase II profiling. Mol. Syst. Biol. 2013;9:638.

224. Eijkelenboom A, Mokry M, Smits LM, Nieuwenhuis EE, Burgering BMT. FOXO3 selectively amplifies enhancer activity to establish target gene regulation. Cell Rep. 2013;5:1664–78.

225. Zhang Y, Adachi M, Kawamura R, Imai K. Bmf is a possible mediator in histone deacetylase inhibitors FK228 and CBHA-induced apoptosis. Cell Death Differ. 2006;13:129–40.

226. Shao Y, Aplin AE. BH3-only protein silencing contributes to acquired resistance to PLX4720 in human melanoma. Cell Death Differ. Nature Publishing Group; 2012;19:2029–39.

227. VanBrocklin MW, Verhaegen M, Soengas MS, Holmen SL. Mitogen-activated protein kinase inhibition induces translocation of bmf to promote apoptosis in melanoma. Cancer Res. 2009;69:1985–94.

228. Shao Y, Aplin AE. ERK2 phosphorylation of serine 77 regulates Bmf pro-apoptotic activity. Cell Death Dis. 2012;3:e253.

229. Bolden JE, Shi W, Jankowski K, Kan C-Y, Cluse L, Martin BP, et al. HDAC inhibitors induce tumor-cell-selective pro-apoptotic transcriptional responses. Cell Death Dis. 2013;4:e519.

230. Chen J, Gomes AR, Monteiro LJ, Wong SY, Wu LH, Ng TT, et al. Constitutively nuclear FOXO3a localization predicts poor survival and promotes Akt phosphorylation in breast cancer. PLoS One. 2010;5:e12293.

231. Piñon JD, Labi V, Egle a, Villunger a. Bim and Bmf in tissue homeostasis and malignant disease. Oncogene. 2008;27 Suppl 1:S41–52.

232. Labi V, Erlacher M, Kiessling S, Manzl C, Frenzel A, O'Reilly L, et al. Loss of the BH3-only protein Bmf impairs B cell homeostasis and accelerates gamma irradiation-induced thymic lymphoma development. J. Exp. Med. 2008;205:641–55.

233. Ni Chonghaile T, Roderick JE, Glenfield C, Ryan J, Sallan SE, Silverman LB, et al. Maturation stage of

T-cell acute lymphoblastic leukemia determines BCL-2 versus BCL-XL dependence and sensitivity to ABT-199. Cancer Discov. 2014;4:1074–87.

234. Miller L a, Goldstein NB, Johannes WU, Walton CH, Fujita M, Norris D a, et al. BH3 mimetic ABT-737 and a proteasome inhibitor synergistically kill melanomas through Noxa-dependent apoptosis. J. Invest. Dermatol. 2009;129:964–71.

235. Choudhary GS, Al-Harbi S, Mazumder S, Hill BT, Smith MR, Bodo J, et al. MCL-1 and BCL-xL-dependent resistance to the BCL-2 inhibitor ABT-199 can be overcome by preventing PI3K/AKT/mTOR activation in lymphoid malignancies. Cell Death Dis. 2015;6:e1593.

236. Reuland SN, Goldstein NB, Partyka KA, Cooper DA, Fujita M, Norris DA, et al. The combination of BH3-mimetic ABT-737 with the alkylating agent temozolomide induces strong synergistic killing of melanoma cells independent of p53. PLoS One. 2011;6.

237. Oakes SR, Vaillant F, Lim E, Lee L, Breslin K, Feleppa F, et al. Sensitization of BCL-2-expressing breast tumors to chemotherapy by the BH3 mimetic ABT-737. Proc. Natl. Acad. Sci. U. S. A. 2012;109:2766–71.

238. Kutuk O, Letai A. Displacement of Bim by Bmf and Puma rather than increase in Bim level mediates paclitaxel-induced apoptosis in breast cancer cells. Cell Death Differ. 2010;17:1624–35.

239. Mukherjee N, Reuland SN, Lu Y, Luo Y, Lambert K, Fujita M, et al. Combining a BCL2 inhibitor with the retinoid derivative fenretinide targets melanoma cells including melanoma initiating cells. J. Invest. Dermatol. 2015;135:842–50.

240. Meerbrey KL, Hu G, Kessler JD, Roarty K, Li MZ, Fang JE, et al. The pINDUCER lentiviral toolkit for inducible RNA interference in vitro and in vivo. Proc. Natl. Acad. Sci. U. S. A. 2011;108:3665–70.

241. van de Weijer ML, Bassik MC, Luteijn RD, Voorburg CM, Lohuis MAM, Kremmer E, et al. A high-coverage shRNA screen identifies TMEM129 as an E3 ligase involved in ER-associated protein degradation. Nat. Commun. 2014;5:3832.

242. Renault VM, Thekkat PU, Hoang KL, White JL, Brady CA, Kenzelmann Broz D, et al. The pro-longevity gene FoxO3 is a direct target of the p53 tumor suppressor. Oncogene. 2011;30:3207–21.

243. Creighton CJ, Huang S. Reverse phase protein arrays in signaling pathways : a data integration perspective. Drug Des. Devel. Ther. 2015;9:3519–27.

244. Grassadonia A, Caporale M, Tinari N, Zilli M, DeTursi M, Gamucci T, et al. Effect of targeted agents on the endocrine response of breast cancer in the neoadjuvant setting: a systematic review. J. Cancer. 2015;6:575–82.

245. Korkola JE, DeVries S, Fridlyand J, Hwang ES, Estep ALH, Chen Y, et al. Differentiation of lobular versus ductal breast carcinomas by expression microarray analysis. Cancer Res. 2003;63:7167–75.

246. Gonzalez-Angulo AM, Hennessy BT, Meric-Bernstam F, Sahin A, Liu W, Ju Z, et al. Functional proteomics can define prognosis and predict pathologic complete response in patients with breast cancer. Clin. Proteomics. 2011;8:11.

247. Gonzalez-Angulo AM, Liu S, Chen H, Chavez-MacGregor M, Sahin A, Hortobagyi GN, et al. Functional proteomics characterization of residual breast cancer after neoadjuvant systemic chemotherapy. Ann. Oncol. 2013;24:909–16.

248. Sohn J, Do KA, Liu S, Chen H, Mills G, Hortobaghy G, et al. Functional proteomics characterization of residual breast cancer after neoadjuvant systemic chemotherapy. Ann. Oncol. 2013;24:909–16.

249. Christgen M, Bruchhardt H, Hadamitzky C, Rudoph C, Steinemann D, Gadzicki D, et al. Comprehensive genetic and functional characterization of IPH-926: a novel CDH1-null tumour cell line from human lobular breast cancer. J. Pathol. 2009;217:620–32.

250. Hollestelle A, Nagel JHA, Smid M, Lam S, Elstrodt F, Wasielewski M, et al. Distinct gene mutation profiles among luminal-type and basal-type breast cancer cell lines. Breast Cancer Res. Treat. 2010;121:53–64.

251. Gonzalez-Angulo AM, Krop I, Akcakanat A, Chen H, Liu S, Li Y, et al. SU2C Phase Ib Study of Paclitaxel and MK-2206 in Advanced Solid Tumors and Metastatic Breast Cancer. JNCI J. Natl. Cancer Inst. 2015;107:dju493–dju493.

252. Hudis C, Swanton C, Janjigian YY, Lee R, Sutherland S, Lehman R, et al. A phase 1 study evaluating the combination of an allosteric AKT inhibitor (MK-2206) and trastuzumab in patients with HER2-positive solid tumors. Breast Cancer Res. 2013;15:R110.

253. Sangai T, Akcakanat A, Chen H, Tarco E, Wu Y, Do KA, et al. Biomarkers of response to Akt inhibitor MK-2206 in breast cancer. Clin. Cancer Res. 2012;18:5816–28.

254. Mathieu M. The poor responsiveness of infiltrating lobular breast carcinomas to neoadjuvant chemotherapy can be explained by their biological profile. Eur. J. Cancer. 2004;40:342–51.

255. Dixon JM. Endocrine Resistance in Breast Cancer. New J. Sci. 2014;2014:1–27.

256. Paplomata E, O'Regan R. The PI3K/AKT/mTOR pathway in breast cancer: targets, trials and biomarkers. Ther. Adv. Med. Oncol. 2014;6:154–66.

257. Telford BJ, Chen A, Beetham H, Frick J, Brew TP, Gould CM, et al. Synthetic lethal screens identify vulnerabilities in GPCR signalling and cytoskeletal organization in E-cadherin-deficient cells. Mol. Cancer Ther. 2015;14:1213–23.

258. Fournier M V., Fata JE, Martin KJ, Yaswen P, Bissell MJ. Interaction of E-cadherin and PTEN Regulates Morphogenesis and Growth Arrest in Human Mammary Epithelial Cells. Cancer Res. 2009;69:4545–52.

259. Li Z, Wang L, Zhang W, Fu Y, Zhao H, Hu Y, et al. Restoring E-cadherin-mediated cell-cell adhesion increases PTEN protein level and stability in human breast carcinoma cells. Biochem. Biophys. Res. Commun. 2007;363:165–70.

260. Subauste MC, Nalbant P, Adamson ED, Hahn KM. Vinculin controls PTEN protein level by maintaining the interaction of the adherens junction protein β-catenin with the scaffolding protein MAGI-2. J. Biol. Chem. 2005;280:5676–81.

261. Hu Y, Li Z, Guo L, Wang L, Zhang L, Cai X, et al. MAGI-2 Inhibits cell migration and proliferation via PTEN in human hepatocarcinoma cells. Arch. Biochem. Biophys. 2007;467:1–9.

262. Sutherland BW, Kucab J, Wu J, Lee C, Cheang MCU, Yorida E, et al. Akt phosphorylates the Y-box binding protein 1 at Ser102 located in the cold shock domain and affects the anchorage-independent growth of breast cancer cells. Oncogene. 2005;24:4281–92.

263. To K, Zhao Y, Jiang H, Hu K, Wang M, Wu J, et al. The Phosphoinositide-Dependent Kinase-1 Inhibitor 2-Amino-N-[4-[5-(2-phenanthrenyl)-3-(trifluoromethyl)-1H-pyrazol-1-yl]phenyl]-acetamide (OSU-03012) Prevents Y-Box Binding Protein-1 from Inducing Epidermal Growth Factor Receptor. Mol. Pharmacol. 2007;72:641–52.

264. Liu X, Su L, Liu X. Loss of CDH1 up-regulates epidermal growth factor receptor via phosphorylation of YBX1 in non-small cell lung cancer cells. FEBS Lett. 2013;587:3995–4000.

265. Hirai H, Sootome H, Nakatsuru Y, Miyama K, Taguchi S, Tsujioka K, et al. MK-2206, an allosteric Akt inhibitor, enhances antitumor efficacy by standard chemotherapeutic agents or molecular targeted drugs in vitro and in vivo. Mol. Cancer Ther. 2010;9:1956–67.

266. Ma CX, Sanchez C, Gao F, Crowder R, Naughton M, Pluard T, et al. A Phase I study of the AKT inhibitor MK-2206 in combination with hormonal therapy in postmenopausal women with estrogen receptor positive metastatic breast cancer. Clin. Cancer Res. 2016;22:2650–5658.

267. Beaver JA, Gustin JP, Yi KH, Rajpurohit A, Thomas M, Gilbert SF, et al. PIK3CA and AKT1 mutations have distinct effects on sensitivity to targeted pathway inhibitors in an isogenic luminal breast cancer model system. Clin. Cancer Res. 2013;19:5413–22.

268. Vasudevan KM, Barbie DA, Davies MA, Rabinovsky R, McNear CJ, Kim JJ, et al. AKT-Independent Signaling Downstream of Oncogenic PIK3CA Mutations in Human Cancer. Cancer Cell. 2009;16:21–32.

269. Guo H, Liu W, Ju Z, Tamboli P, Jonasch E, Mills GB, et al. An efficient procedure for protein extraction from formalin-fixed, paraffin-embedded tissues for reverse phase protein arrays. Proteome Sci. 2012;10:56.

270. de Hoon MJL, Imoto S, Nolan J, Miyano S. Open source clustering software. Bioinformatics. 2004;20:1453–4.

271. Saldanha AJ. Java Treeview- Extensible visualization of microarray data. Bioinformatics. 2004;20:3246–8.

272. Vermeulen JF, van Brussel ASA, van der Groep P, Morsink FHM, Bult P, van der Wall E, et al. Immunophenotyping invasive breast cancer: paving the road for molecular imaging. BMC Cancer. 2012;12:240.

273. Vlug EJ, van de Ven R a H, Vermeulen JF, Bult P, van Diest PJ, Derksen PWB. Nuclear localization of the transcriptional coactivator YAP is associated with invasive lobular breast cancer. Cell. Oncol. (Dordr). 2013;36:375–84.

274. Mortazavi A, Williams BA, Mccue K, Schaeffer L, Wold B. Mapping and quantifying mammalian transcriptomes by RNA-Seq. Nat. Methods. 2008;5:621–8.

275. Koh DI, An H, Kim MY, Jeon BN, Choi SH, Hur SS, et al. Transcriptional activation of APAF1 by KAISO (ZBTB33) and p53 is attenuated by RelA/p65. Biochim. Biophys. Acta. 2015;1849:1170–8.

&

276. Wyrwicz LS, Gaj P, Hoffmann M, Rychlewski L. A common cis- element in promoters of protein synthesis and cell cycle genes. Acta Biochim. Pol. 2007;54:89–98.

277. Zhou VW, Goren A, Bernstein BE. Charting histone modifications and the functional organization of mammalian genomes. Nat. Rev. Genet. 2011;12:7–18.

278. Kimura H. Histone modifications for human epigenome analysis. J. Hum. Genet. 2013;58:439–45.

279. Ring A, Kim Y-M, Kahn M. Wnt/catenin signaling in adult stem cell physiology and disease. Stem Cell Rev. 2014;10:512–25.

280. de Lau W, N B, Clevers H. Wnt in normal intestine and colorectal cancer. Front. Biosci. 2007;12:471–91.

281. King TD, Suto MJ, Li Y. The Wnt/β-catenin signaling pathway: A potential therapeutic target in the treatment of triple negative breast cancer. J. Cell. Biochem. 2012;113:13–8.

282. Jacinto F V, Benner C, Hetzer MW. The nucleoporin Nup153 regulates embryonic stem cell pluripotency through gene silencing. Genes Dev. 2015;29:1–15.

283. Kaul A, Schuster E, Jennings BH. The Groucho co-repressor is primarily recruited to local target sites in active chromatin to attenuate transcription. PLoS Genet. 2014;10:e1004595.

284. Lopes EC, Valls E, Figueroa ME, Mazur A, Meng F-G, Chiosis G, et al. Kaiso contributes to DNA methylation-dependent silencing of tumor suppressor genes in colon cancer cell lines. Cancer Res. 2008;68:7258–63.

285. Dhiman VK, Attwood K, Campbell MJ, Smiraglia DJ. Hormone stimulation of androgen receptor mediates dynamic changes in DNA methylation patterns at regulatory elements. Oncotarget. 2015;6:42575–89.

286. Kangaspeska S, Stride B, Métivier R, Polycarpou-Schwarz M, Ibberson D, Carmouche RP, et al. Transient cyclical methylation of promoter DNA. Nature. 2008;452:112–5.

287. Métivier R, Gallais R, Tiffoche C, Le Péron C, Jurkowska RZ, Carmouche RP, et al. Cyclical DNA methylation of a transcriptionally active promoter. Nature. 2008;452:45–50.

288. Du Q, Luu P-L, Stirzaker C, Clark SJ. Methyl-CpG-binding domain proteins: readers of the epigenome. Epigenomics. 2015;7:1051–73.

289. Vervoort SJ, Lourenço AR, van Boxtel R, Coffer PJ. SOX4 Mediates TGF-β-Induced Expression of Mesenchymal Markers during Mammary Cell Epithelial to Mesenchymal Transition. PLoS One. 2013;8:e53238.

290. Mandoli A, Prange K, Martens JHA. Genome-wide binding of transcription factors in inv(16) acute myeloid leukemia. Genomics Data. 2014;2:170–2.

291. Zhang Y, Liu T, Meyer C a, Eeckhoute J, Johnson DS, Bernstein BE, et al. Model-based analysis of ChIP-Seq (MACS). Genome Biol. 2008;9:R137.

292. Feng J, Liu T, Qin B, Zhang Y, Liu XS. Identifying ChIP-seq enrichment using MACS. Nat. Protoc. 2012;7:1728–40.

293. Heinz S, Benner C, Spann N, Bertolino E, Lin YC, Laslo P, et al. Simple Combinations of Lineage-Determining Transcription Factors Prime cis-Regulatory Elements Required for Macrophage and B Cell Identities. Mol. Cell. 2010;38:576–89.

294. Huang DW, Sherman BT, Lempicki R a. Systematic and integrative analysis of large gene lists using DAVID bioinformatics resources. Nat. Protoc. 2009;4:44–57.

295. Mellman I, Nelson W. Coordinated protein sorting, targeting and distribution in polarized cells. Nat Rev Mol Cell Biol. 2008;9:833–45.

296. Cole BK, Curto M, Chan AW, McClatchey AI. Localization to the cortical cytoskeleton is necessary for Nf2/merlin-dependent epidermal growth factor receptor silencing. Mol Cell Biol. 2008;28:1274–84.

297. Johnston SRD. Enhancing Endocrine Therapy for Hormone Receptor–Positive Advanced Breast Cancer: Cotargeting Signaling Pathways. J. Natl. Cancer Inst. 2015;107:djv212.

298. Xu S, Li S, Guo Z, Luo J, Ellis MJ, Ma CX. Combined targeting of mTOR and AKT is an effective strategy for basal-like breast cancer in patient-derived xenograft models. Mol. Cancer Ther. 2013;12:1665–75.

299. Sommer EM, Dry H, Cross D, Guichard S, Davies BR, Alessi DR. Elevated SGK1 predicts resistance of breast cancer cells to Akt inhibitors. Biochem. J. 2013;452:499–508.

300. Kobayashi T, Cohen P. Activation of serum- and glucocorticoid-regulated protein kinase by agonists that activate phosphatidylinositide 3-kinase is mediated by 3-phosphoinositide-dependent protein kinase-1 (PDK1) and PDK2. Biochem. J. 1999;339:319–28.

301. García-Martínez JM, Alessi DR. mTOR complex 2 (mTORC2) controls hydrophobic motif phosphorylation and activation of serum- and glucocorticoid-induced protein kinase 1 (SGK1). Biochem. J. 2008;416:375–85.

302. Brunet A, Park J, Tran H, Hu LS, Hemmings BA, Greenberg ME. Protein kinase SGK mediates survival signals by phosphorylating the forkhead transcription factor FKHRL1 (FOXO3a). Mol. Cell. Biol. 2001;21:952–65.

303. Hortobagyi GN, Chen D, Piccart M, Rugo HS, Burris 3rd HA, Pritchard KI, et al. Correlative Analysis of Genetic Alterations and Everolimus Benefit in Hormone Receptor-Positive, Human Epidermal Growth Factor Receptor 2-Negative Advanced Breast Cancer: Results From BOLERO-2. J Clin Oncol. 2016;34:419–26.

304. Mayer IA, Abramson VG, Isakoff SJ, Forero A, Balko JM, Kuba MG, et al. Stand up to cancer phase Ib study of pan-phosphoinositide-3-kinase inhibitor buparlisib with letrozole in estrogen receptor-positive/human epidermal growth factor receptor 2-negative metastatic breast cancer. J. Clin. Oncol. 2014;32:1202–9.

305. Baselga J, Campone M, M P, Burris H a, Rugo HS, Sahmoud T, et al. Everolimus in Postmenopausal Hormone- Receptor–Positive Advanced Breast Cancer. N. Engl. J. Med. 2012;366:520–9.

306. Yardley DA, Noguchi S, Pritchard KI, Burris HA, Baselga J, Gnant M, et al. Everolimus plus exemestane in postmenopausal patients with HR+ breast cancer: BOLERO-2 final progression-free survival analysis. Adv. Ther. 2013;30:870–84.

307. O'Reilly KE, Rojo F, She QB, Solit D, Mills GB, Smith D, et al. mTOR inhibition induces upstream receptor tyrosine kinase signaling and activates Akt. Cancer Res. 2006;66:1500–8.

308. Chandarlapaty S, Sawai A, Scaltriti M, Rodrik-Outmezguine V, Grbovic-Huezo O, Serra V, et al. AKT inhibition relieves feedback suppression of receptor tyrosine kinase expression and activity. Cancer Cell. 2011;19:58–71.

309. Fruman DA, Rommel C. PI3K and cancer: lessons, challenges and opportunities. Nat. Rev. Drug Discov. 2014;13:140–56.

310. Mahajan K, Mahajan N. PI3K-Independent AKT activation in cancers: a treasure trove for novel therapeutics. J. cell Physiol. 2012;227:3178–84.

311. Carracedo A, Ma L, Teruya-Feldstein J, Rojo F, Salmena L, Alimonti A, et al. Inhibition of mTORC1 leads to MAPK pathway activation through a PI3K-dependent feedback loop in human cancer. J. Clin. Invest. 2008;118:3065–74.

312. Britschgi A, Andraos R, Brinkhaus H, Klebba I, Romanet V, Müller U, et al. JAK2/STAT5 inhibition circumvents resistance to PI3K/mTOR blockade: a rationale for cotargeting these pathways in metastatic breast cancer. Cancer Cell. 2012;22:796–811.

313. Oltersdorf T, Elmore SW, Shoemaker AR, Armstrong RC, Augeri DJ, Belli BA, et al. An inhibitor of Bcl-2 family proteins induces regression of solid tumours. Nature. 2005;435:677–81.

314. Roberts AW, Seymour JF, Brown JR, Wierda WG, Kipps TJ, Khaw SL, et al. Substantial susceptibility of chronic lymphocytic leukemia to BCL2 inhibition: Results of a phase I study of navitoclax in patients with relapsed or refractory disease. J. Clin. Oncol. 2012;30:488–96.

315. Wilson WH, Connor O a O, Czuczman MS, Lacasce S, Gerecitano JF, Leonard JP, et al. Safety, Pharmacokinetics, Pharcodynamics, and Activity of Navitoclax, a Targeted High Affinity Inhibitor of BCL-2, in Lymphoid Malignancies. Lancet Oncol. 2011;11:1149–59.

316. Souers AJ, Leverson JD, Boghaert ER, Ackler SL, Catron ND, Chen J, et al. ABT-199, a potent and selective BCL-2 inhibitor, achieves antitumor activity while sparing platelets. Nat. Med. 2013;19:202–8.

317. Vandenberg CJ, Cory S, Dc W, Vandenberg CJ, Cory S. aggressive Myc-driven mouse lymphomas without provoking thrombocytopenia ABT-199, a new Bcl-2–specific BH3 mimetic, has in vivo efficacy against aggressive Myc-driven mouse lymphomas without provoking thrombocytopenia. Lymphoid neoplasia. 2013;121:2285–8.

318. Cang S, Iragavarapu C, Savooji J, Song Y, Liu D. ABT-199 (venetoclax) and BCL-2 inhibitors in clinical development. J. Hematol. Oncol. 2015;8:129.

319. Zhao J, Niu X, Li X, Edwards H, Wang G, Wang Y, et al. Inhibition of CHK1 enhances cell death induced by the Bcl-2-selective inhibitor ABT-199 in acute myeloid leukemia cells. Oncotarget. 2016;7:16–8.

320. Punnoose E, Leverson JD, Peale F, Boghaert ER, Belmont L, Tan N, et al. Expression profile of BCL-2, BCL-XL and MCL-1 predicts pharmacological response to the BCL-2 selective antagonist venetoclax in multiple myeloma models. Mol. Cancer Ther. 2016;15:1132–44.

321. Miller TW, Rexer BN, Garrett JT, Arteaga CL. Mutations in the phosphatidylinositol 3-kinase pathway: role in tumor progression and therapeutic implications in breast cancer. Breast Cancer Res. 2011;13:224.

322. Crowder RJ, Phommaly C, Tao Y, Hoog J, Luo J, Perou CM, et al. PIK3CA and PIK3CB inhibition produce synthetic lethality when combined with estrogen deprivation in estrogen receptor-positive breast cancer. Cancer Res. 2009;69:3955–62.

323. Sanchez CG, Ma CX, Crowder RJ, Guintoli T, Phommaly C, Gao F, et al. Preclinical modeling of combined phosphatidylinositol-3-kinase inhibition with endocrine therapy for estrogen receptor-positive breast cancer. Breast Cancer Res. 2011;13:R21.

324. Miller TW, Hennessy BT, González-Angulo AM, Fox EM, Mills GB, Chen H, et al. Hyperactivation of phosphatidylinositol-3 kinase promotes escape from hormone dependence in estrogen receptor-positive human breast cancer. J. Clin. Invest. 2010;120:2406–13.

325. Cavazzoni A, Bonelli MA, Fumarola C, La Monica S, Airoud K, Bertoni R, et al. Overcoming acquired resistance to letrozole by targeting the PI3K/AKT/mTOR pathway in breast cancer cell clones. Cancer Lett. 2012;323:77–87.

326. Vilquin P, Villedieu M, Grisard E, Larbi S Ben, Ghayad SE, Heudel PE, et al. Molecular characterization of anastrozole resistance in breast cancer: Pivotal role of the Akt/mTOR pathway in the emergence of de novo or acquired resistance and importance of combining the allosteric Akt inhibitor MK-2206 with an aromatase inhibitor. Int. J. Cancer. 2013;133:1589–602.

327. Campbell RA, Bhat-Nakshatri P, Patel NM, Constantinidou D, Ali S, Nakshatri H. Phosphatidylinositol 3-kinase/AKT-mediated activation of estrogen receptor α: A new model for anti-estrogen resistance. J. Biol. Chem. 2001;276:9817–24.

328. Yamnik RL, Digilova A, Davis DC, Brodt ZN, Murphy CJ, Holz MK. S6 kinase 1 regulates estrogen receptor α in control of breast cancer cell proliferation. J. Biol. Chem. 2009;284:6361–9.

329. Lam L, Hu X, Aktary Z, Andrews DW, Pasdar M. Tamoxifen and ICI 182,780 increase Bcl-2 levels and inhibit growth of breast carcinoma cells by modulating PI3K/AKT, ERK and IGF-1R pathways independent of ERα. Breast Cancer Res. Treat. 2009;118:605–21.

330. Certo M, Moore VDG, Nishino M, Wei G, Korsmeyer S, Armstrong SA, et al. Mitochondria primed by death signals determine cellular addiction to antiapoptotic BCL-2 family members. Cancer Cell. 2006;9:351–65.

331. Sadok A, McCarthy A, Caldwell J, Collins I, Garrett MD, Yeo M, et al. Rho Kinase Inhibitors Block Melanoma Cell Migration and Inhibit Metastasis. Cancer Res. 2015;75:2272–84.

332. Koh D-I, Yoon J-H, Kim M-K, An H, Kim M-Y, Hur M-W. Kaiso is a key regulator of spleen germinal center formation by repressing Bcl6 expression in splenocytes. Biochem. Biophys. Res. Commun. 2013;442:177–82.

333. Liu X, Caffrey TC, Steele MM, Mohr A, Singh PK, Radhakrishnan P, et al. MUC1 regulates cyclin D1 gene expression through p120 catenin and β-catenin. Oncogenesis. 2014;3:e107.

334. Zhou L, Zhong Y, Yang F, Li Z, Zhou J, Liu X, et al. Kaiso represses the expression of glucocorticoid receptor via a methylation-dependent mechanism and attenuates anti-apoptotic activity of glucocorticoids in breast cancer cells. BMB Rep. 2016;49:167–72.

335. Ruzov A, Dunican DS, Prokhortchouk A, Pennings S, Stancheva I, Prokhortchouk E, et al. Kaiso is a genome-wide repressor of transcription that is essential for amphibian development. Development. 2004;131:6185–94.

336. Stancheva I, Median RR. Transient depletion of xDnmt1 leads to premature gene activation in Xenopus embryos. Genes Dev. 2000;14:313–27.

337. Sansom OJ, Berger J, Bishop SM, Hendrich B, Bird A, Clarke AR. Deficiency of Mbd2 suppresses intestinal tumorigenesis. Nat. Genet. 2003;34:145–7.

338. Eads C a, Nickel AE, Laird PW, Min A. Complete Genetic Suppression of Polyp Formation and Reduction of CpG-Island Hypermethylation in ApcMin/+ Dnmt1-Hypomorphic Mice Advances in Brief Complete Genetic Suppression of Polyp Formation and Reduction of CpG-Island. Reactions. 2002;1296–9.

339. Medvedeva YA, Khamis AM, Kulakovskiy I V, Ba-Alawi W, Bhuyan MSI, Kawaji H, et al. Effects of cytosine methylation on transcription factor binding sites. BMC Genomics. 2014;15:119.

340. Perissi V, Jepsen K, Glass CK, Rosenfeld MG. Deconstructing repression: evolving models of co-repressor action. Nat. Rev. Genet. 2010;11:109–23.

341. Wang Z, Zang C, Cui K, Schones DE, Barski A, Peng W, et al. Genome-wide Mapping of HATs and

HDACs Reveals Distinct Functions in Active and Inactive Genes. Cell. 2009;138:1019–31.

342. Stasevich TJ, Hayashi-Takanaka Y, Sato Y, Maehara K, Ohkawa Y, Sakata-Sogawa K, et al. Regulation of RNA polymerase II activation by histone acetylation in single living cells. Nature. 2014;516:272–5.

343. Sasai N, Nakao M, Defossez P-A. Sequence-specific recognition of methylated DNA by human zinc-finger proteins. Nucleic Acids Res. 2010;38:5015–22.

344. Rabinovich A, Jin VX, Rabinovich R, Rabinovich A, Jin VX, Rabinovich R, et al. E2F in vivo binding specificity : Comparison of consensus versus. Genome Res. 2008;18:1763–77.

345. Farnham PJ. Insights from genomic profiling of transcription factors. Nat. Rev. Genet. 2009;10:605–16.

346. Kruse JP, Gu W. Modes of p53 Regulation. Cell. 2009;137:609–22.

347. Carr SM, Poppy Roworth A, Chan C, La Thangue NB. Post-translational control of transcription factors: Methylation ranks highly. FEBS J. 2015;282:4450–65.

348. Bernard P, Harley VR. Acquisition of SOX transcription factor specificity through protein-protein interaction, modulation of Wnt signalling and post-translational modification. Int. J. Biochem. Cell Biol. 2010;42:400–10.

349. Pierre CC, Longo J, Bassey-Archibong BI, Hallett RM, Milosavljevic S, Beatty L, et al. Methylation-dependent regulation of hypoxia inducible factor-1 alpha gene expression by the transcription factor kaiso. Biochim. Biophys. Acta. 2015;1849:1432–41.

Nederlandse samenvatting

Borstkanker

In 2012 ontvingen wereldwijd bijna 1.7 miljoen vrouwen de diagnose borstkanker. Tegelijkertijd overleden er in dat jaar meer dan 500.000 vrouwen aan de gevolgen van deze ziekte. Hiermee is borstkanker de meest voorkomende vorm van kanker onder vrouwen. Het bepalen van de behandeling en het succes van deze behandeling hangt grotendeels af van het stadium en het type borstkanker. Hierbij wordt niet alleen gekeken naar de grootte van de tumor in de borst (primaire tumor) en de aanwezigheid van uitzaaingen, maar ook naar hoe de tumor er onder de microscoop uitziet (morfologie). Aan de hand van deze morfologie zijn er verschillende histologische subtypen borstkanker te onderscheiden. De meest voorkomende vorm is invasief ductaal carcinoom (IDC) dat bij ongeveer 75-80% van de vrouwen met borstkanker voorkomt. Het tweede meest voorkomende subtype is invasief lobulair carcinoom (ILC). In tegenstelling tot IDC wordt ILC gekarakteriseerd door tumorcellen die in strengen achter elkaar liggen in plaats van een harde knobbel te vormen. Door deze groeistructuur is het moeilijk om dit type kanker in een vroeg stadium waar te nemen.

Hoewel histologische subtypes bijdragen aan het diagnosticeren van het type kanker blijkt dat er tussen tumoren met dezelfde morfologische eigenschappen nog veel verschillen zijn op moleculair niveau. Een van deze verschillen is de aanwezigheid van hormoon receptor eiwitten. Eiwitten zijn in feite de uitvoerende eenheden in de cel die nodig zijn voor het functioneren van iedere cel. De aanwezigheid (oftewel: expressie) van hormoon receptor eiwitten maakt een tumor gevoelig voor hormoontherapie. Dit is een voorbeeld van zogeheten ‘targeted therapy’ waarbij de tumor wordt behandeld met targeted drugs (medicatie) die de werking tegengaan van specifieke eiwitten die essentieel zijn voor de tumor om te groeien en uit te zaaien. Zo werken we toe naar ‘personalized medicine’, waarbij er steeds specifieker per patiënt of patiëntengroep medicatie op maat kan worden ontwikkeld op basis van de signaleringsroutes die belangrijk zijn voor de progressie van de tumor.

Cel-cel adhesie

Het interessante aan ILC is dat ongeveer 90% van de gevallen wordt gekenmerkt door het verlies van een bepaald eiwit genaamd E-cadherine. Dit eiwit is al vroeg tijdens de vorming van ILC verloren en is causaal betrokken bij de ontwikkeling van ILC. Wanneer we namelijk E-cadherine verwijderen uit de borstklier van muizen voordat zich tumoren vormen, ontwikkelen deze muizen borsttumoren die qua morfologie erg lijken op humaan ILC. Deze muizen en de cellen uit de tumoren van deze muizen kunnen we dus gebruiken als model voor ILC.

E-cadherine maakt deel uit van een complex genaamd de Adherens Junctie (AJ), 1 van de complexen dat betrokken is bij het aan elkaar koppelen van individuele cellen. E-cadherine is een transmembraan eiwit wat betekent dat het door de buitenste laag (membraan) van een cel steekt. Het deel van E-cadherine dat zich aan de buitenkant van de cel bevind (extracellulair) gaat een interactie aan met het extracellulaire deel van E-cadherine van naastliggende cellen. Dit zorgt ervoor dat individuele cellen nauw met elkaar verbonden blijven om een beschermende barrière te vormen tegen de buitenwereld. Aan de binnenkant van de cel (intracelullair) bindt E-cadherine aan verschillende andere eiwitten waaronder p120-catenine (p120). P120 heeft als functie om het AJ complex te stabiliseren door ervoor te zorgen dat E-cadherine niet van de membraan wordt verwijderd en wordt afgebroken. Op het moment dat E-cadherine niet meer tot expressie komt, zoals in ILC, heeft p120 nog steeds een functie. Het draagt er namelijk aan bij dat cellen die geen E-cadherine meer tot expressie brengen (E-cadherine negatieve cellen) kunnen overleven wanneer deze niet meer aan elkaar hechten. Normaal gesproken ondergaan borstcellen namelijk een geprogrammeerde celdood (genaamd anoikis) op het moment dat ze hechting verliezen met hun omgeving. Deze geprogrammeerde celdood bestaat uit een balans tussen ‘pro-dood’ en ‘pro-leven’ signalen en p120 stimuleert de pro-leven signalen. De mogelijkheid van cellen om anoikis te vermijden (ook wel anoikis resistentie genoemd) kun je meten in petrischaaltjes door ze ‘in suspensie’ te groeien en dit kan als maat gebruikt worden voor de potentie van cellen om uit te zaaien in de mens.

Kaiso

Naast het stabiliseren van de AJ en het voorkomen van anoikis kan p120 binden aan een ander eiwit: Kaiso. Dit gebeurt echter niet op de membraan, maar in de kern van de cel. In de kern van iedere cel zit het DNA opgeslagen wat het handboek van de cel vormt met alle genetische informatie, die nodig is om iedere mogelijke functie uit te voeren. Genen zijn bepaalde regios in het DNA die elk coderen voor een ander eiwit. Elke cel heeft echter maar een beperkte hoeveelheid van de genetische informatie nodig om te functioneren: een levercel hoeft bijvoorbeeld geen melk uit te kunnen scheiden. In iedere cel wordt daarom maar een klein deel van de genen afgelezen door kopieën te maken van de genen. Die kopieën heten messenger-RNA (mRNA). mRNA wordt vervolgens afgelezen en omgezet in de eerder genoemde uitvoerders van de cel: de eiwitten. Een trancriptie factor (oftewel: een aflees factor) is in staat om op bepaalde plekken van het DNA te binden en te reguleren of het mRNA van een bepaald gen (een target gen) wél of níet wordt gemaakt en daardoor kan het dus indirect het expressieniveau van de eiwitten reguleren. Kaiso werkt als repressieve transcriptie factor en remt dus de trancriptie van zijn target-genen. Op het moment dat E-cadherine niet meer aanwezig is, zoals in ILC, kan p120 binden aan Kaiso waardoor Kaiso niet meer aan het DNA kan binden en dit resulteert dus in de expressie van Kaiso target genen.

Resultaten van dit proefschrift

We weten al dat het verlies van E-cadherine bij het merendeel van de ILC patiënten voorkomt en dat dit causaal is voor het ontstaan van deze ziekte. Daarnaast is E-cadherine essentieel voor het aan elkaar verbinden van individuele cellen en heeft p120 zowel ín het AJ complex een functie als daarbuiten. Zoals hierboven beschreven, is het bestuderen van de signaleringsroutes die belangrijk zijn voor tumoren om te groeien en uit te zaaien belangrijk voor het ontwikkelen van personalized medicine. Omdat het verlies van E-cadherine een belangrijke eigenschap is van een grote groep borstkankerpatiënten is er in dit proefschrift bekeken via welke signaleringsroutes het verlies van de AJ bijdraagt aan de progressie van borstkanker. In **hoofdstuk 1** staat een uitgebreide inleiding over de kennis van borstkanker, het verlies van de AJ en de functie van Kaiso. In **hoofdstuk 2** wordt bekeken wat de functie is van p120 tijdens de ontwikkeling van ILC. Hiervoor hebben we in het hierboven genoemde muismodel naast E-cadherine ook p120 uit de borstklier verwijderd. Deze 'triple-knockout' muizen ontwikkelen nog steeds borsttumoren, maar deze lijken niet meer op humaan ILC. In plaats daarvan vormen zich IDC-achtige tumoren. Het verlies van E-cadherine in de borst zorgt dus voor de vorming van ILC en de aanwezigheid van p120 in die tumoren draagt sterk bij aan het histologische subtype van de tumor.

Zoals hierboven beschreven zorgt p120 voor een pro-leven signaal in E-cadherine negatieve cellen op het moment dat deze niet meer verbonden zijn met elkaar en hun omgeving. In **hoofdstuk 3** hebben we bestudeerd wat er met de pro-dood signalen gebeurt in E-cadherine negatieve cellen in de afwezigheid van hechting. Hiervoor hebben we deze cellen gegroeid in suspensie en vergeleken met cellen die nog wel E-cadherine tot expressie brengen (E-cadherine positieve cellen) en dus doodgaan in suspensie. Deze E-cadherine positieve cellen verhogen de expressie van het pro-dood eiwit BMF terwijl E-cadherine negatieve cellen dit veel minder doen. Het blijkt dat dit al op mRNA niveau gereguleerd wordt: de transcriptie factor FOXO3 bindt aan het BMF gen waardoor de expressie van BMF wordt verhoogd in de E-cadherine positieve cellen. Daarnaast is bekend dat FOXO3 geremd wordt door het eiwit AKT. Actief AKT remt dus FOXO wat ervoor zorgt dat het BMF niveau niet omhoog gaat. In de E-cadherine negatieve cellen zien we daarom ook dat het toedienen van een AKT-inhibitor (een drug die in staat is om AKT te remmen) een verhoogde expressie van BMF tot gevolg heeft wat resulteert in anoikis. Bovendien kan je met een drug die qua structuur lijkt op BMF (een BMF-mimetic) anoikis induceren in de E-cadherine negatieve cellen. Dit zie je ook in de muis: artificiële verhoging van BMF expressie in ILC tumorcellen kan de groei van deze cellen in de muis remmen. De AKT-inhibitor en BMF-mimetic kunnen er dus voor zorgen E-cadherine negatieve tumorcellen niet langer anoikis resistent zijn en zouden dus gebruikt kunnen worden om het uitzaaien van E-cadherine negatieve tumorcellen te remmen.

Om andere signaleringsroutes te identificeren die E-cadherine negatieve cellen onderscheiden van E-cadherine positieve cellen hebben we in **hoofdstuk 4** een screen uitgevoerd op de expressie van meer dan 100 eiwitten in deze twee celtypen. In plaats van

het groeien van deze cellen in suspensie, groeiden we deze cellen in een ‘adherente’ setting waarbij de cellen nog steeds hechting ondervinden. Hierbij viel op dat de E-cadherine negatieve cellen een veel hogere activiteit vertoonden van de signaleringsroute die AKT bevatte. Deze signaleringsroute is in veel typen tumoren actief als gevolg van mutaties in die signaleringsroute. Wij hebben nu aangetoond dat ook het verlies van E-cadherine activatie van die signaleringsroute tot gevolg kan hebben. Het gebruik van een AKT-inhibitor induceert in de E-cadherine negatieve cellen niet alleen anoikis (zoals aangetoond in hoofdstuk 3), maar remt ook de groei van deze cellen in een adherente setting. Niet alleen het uitzaaien van de E-cadherine negatieve tumorcellen, maar dus ook de groei van de primaire tumor kan geremd worden met AKT remmers.

In **hoofdstuk 5** hebben we ons gericht op de bindingsplekken van Kaiso in het DNA. Tot voor kort was er slechts een klein aantal bindingslocaties bekend, maar wij hebben nu in het volledige genoom 6713 bindingsplekken van Kaiso geïdentificeerd. Hierdoor kan Kaiso de expressie van een groot aantal genen remmen. Opvallend is dat veel van die genen een rol spelen in processen die betrokken zijn bij de progressie van kanker. Die genen zijn namelijk betrokken bij het vermenigvuldigen van cellen of bij het repareren van DNA schade wat wordt aangebracht door bijvoorbeeld het roken van sigaretten of door UV-straling afkomstig van de zon. Het aantasten van de functie van Kaiso, zoals het geval is in ILC, kan daarom leiden tot het ongecontroleerd vermenigvuldigen van cellen en de opeenhoping van DNA schade met als gevolg de vorming van tumoren.

De uitkomsten van de studies beschreven in dit proefschrift dragen bij aan de kennis over de betrokkenheid van AJ verlies in de progressie van borstkanker. Hierbij zijn signaleringsroutes betrokken die onder andere p120, BMF, AKT en Kaiso bevatten. Bovendien biedt het gebruik van AKT-inhitibors en BMF-mimetics veelbelovende mogelijkheden om in de toekomst borstkanker beter te kunnen behandelen. In **hoofdstuk 6** worden deze conclusies samengevat en worden de resultaten van dit proefschrift bediscussieerd in de context van de reeds bekende literatuur.

Curriculum Vitae

Milou Tenhagen was born on August 26th 1988 in Deventer. She grew up in Raalte where she finished secondary school from the Carmel College Salland. In 2006 she started the Bachelor's program Biomedische Wetenschappen at Utrecht University followed by the Master's program Cancer Genomics and Developmental Biology in 2009 at Utrecht University. During her Master's she performed an internship in the lab of prof. dr. Hans Clevers studying expression profiles of intestinal stem cells and cancer stem cells. For her second internship she went to the University of California, San Francisco to work on cytokine-mediated oncogenic signaling in T-ALL in the lab of dr. Jeroen Roose under the supervision of dr. Olga Ksionda. After finishing her Master's *cum laude* in 2011 she started her PhD in the lab of Patrick Derksen and under the supervision of prof. dr. Paul van Diest at the pathology department of the UMC Utrecht. Here she studied breast cancer development and progression in the context of E-cadherin loss. During the 4.5 years in this lab she visited the lab of dr. Martin Hetzer at the Salk Institute in San Diego to get acquainted with DamID-sequencing. In October 2016 she has started working at Zilveren Kruis as a business analyst in the strategy and innovation team at the health care procurement department.

List of publications

Tenhagen M, Klarenbeek S, Braumuller TM, Hofmann I, van der Groep P, ter Hoeve N, van der Wall E, Jonkers J and Derksen PWB. p120-Catenin Is Critical for the Development of Invasive Lobular Carcinoma in Mice. Journal of Mammary Gland Biology and Neoplasia. 2016, *in press*

Hornsveld M*, **Tenhagen M***, van de Ven RA, Smits AMM, van Triest MH, van Amersfoort M, Kloet DEA, Dansen TB, Burgering BM and Derksen PWB. Restraining FOXO3-dependent transcriptional BMF activation underpins tumour growth and metastasis of E-cadherin-negative breast cancer. Cell Death and Differentiation. 2016;23:1483–92.

Ksionda O, Melton A, Bache J, **Tenhagen M**, Bakker J, Harvey R, Winter SS, Rubio I and Roose JP. RasGRP1 overexpression in T-ALL increases basal nucleotide exchange on Ras rendering the Ras/PI3K/Akt pathway responsive to protumorigenic cytokines. Oncogene. 2016;35:3658–68.

van de Ven RAH, **Tenhagen M**, Meuleman W, van Riel JJG, Schackmann RCJ and Derksen PWB. Nuclear p120-catenin regulates the anoikis resistance of mouse lobular breast cancer cells through Kaiso-dependent Wnt11 expression. Disease Models and Mechanisms. 2015;8:373–84.

Schackmann RCJ, **Tenhagen M**, van de Ven RAH, Derksen PWB. P120-Catenin in Cancer - Mechanisms, Models and Opportunities for Intervention. Journal of Cell Science. 2013;126:3515–25.

Schackmann RCJ, Klarenbeek S, Vlug EJ, Stelloo S, van Amersfoort M, **Tenhagen M**, Braumuller TM, Vermeulen JF, van der Groep P, Peeters T, van der Wall E, van Diest PJ, Jonkers J and Derksen PWB. Loss of p120-catenin induces metastatic progression of breast cancer by inducing anoikis resistance and augmenting growth factor receptor signaling. Cancer Research. 2013;73:4937–49.

Tenhagen M, Van Diest PJ, Ivanova IA, Van Der Wall E, Van Der Groep P. Fibroblast growth factor receptors in breast cancer: Expression, downstream effects, and possible drug targets. Endocrine Related Cancer. 2012;19:R115–29.

&

Dankwoord

Wat een avontuur de afgelopen 5 jaar! Ook al is het einddoel vanaf het begin af aan duidelijk: dat boekje in handen hebben en verdedigen; de weg ernaartoe is een grote verrassing. De ups en downs van die reis heb ik natuurlijk niet in mijn eentje meegemaakt en ik wil dan ook een aantal mensen bedanken die vooral de ups tot een groot plezier hebben gemaakt.

Allereerst mijn co-promotor **dr. D**. Patrick, bedankt dat ik mijn PhD in jouw lab heb mogen uitvoeren. Mijn open sollicitatie kwam op het perfecte moment, je had net een KWF beurs binnengesleept en dat zou mijn hoofdproject worden. Zoals wel vaker zijn het juist de zij-projecten die meer vooruitgang boeken dan het hoofdproject, maar ik ben je erg dankbaar dat je altijd bent blijven geloven in mijn 'opus magnus' zoals je het altijd noemde. Daarbij hebben je ongezouten mening en feedback mij uiteindelijk tot een betere wetenschapper gemaakt. Je hebt een enorm doorzettingsvermogen om van het lab een succes te maken en ik wens je dan ook heel veel succes en plezier in de rest van je carrière.

Ook mijn promotor, **Prof. dr. Paul van Diest**, hartelijk dank voor je bijdrage aan mijn promotietraject waaronder je kritische blik tijdens de breast cancer research meetings en het scoren van de TMAs. Ik vind het erg knap dat je altijd een klinische twist kunt geven aan welk onderzoek dan ook. Ondanks dat ik nu niet meer in het academisch onderzoekswereldje zit wil ik je erg bedanken voor je vertrouwen in mij als wetenschapper.

Prof. dr. Burgering, Prof. dr. de Bruyn, Prof. dr. van der Wall, Prof. dr. Maurice en Prof. dr. Vermeulen bedankt dat jullie plaats hebben willen nemen in mijn beoordelingscommissie en tijdens 13 december als opponenten mijn promotie bijwonen. Boudewijn, extra bedankt voor je input op hoofdstuk 4. Elsken, bedankt voor je input en begeleiding tijdens de breast cancer research meetings. Ongeloofelijk knap hoe iemand met zoveel verschillende werkzaamheden altijd scherp blijft.

Lieve **Dominique**, als er íemand een positieve bijdrage heeft geleverd zonder ook maar 1 seconde inhoudelijk met mijn onderzoek bezig te zijn geweest ben jij het wel. Ik ben je ongelooflijk dankbaar dat je me op 13 december bij wilt staan zoals je dat eigenlijk al meer dan 10 jaar doet. Ik hoop dat onze stap-, bak-, vakantie- en sport-avonturen nog minstens 10 jaar door blijven gaan. Je bent een schat en ik wens jou en Bouke heel veel geluk toe!

Mijn andere paranimf, **Miranda**, ook jij hebt me keihard gesteund de afgelopen jaren. Eigenlijk ben je dé stabiele factor in ons lab en zorg je voor het 'united' in mouse slayers united. Het is heerlijk om iemand te hebben om klaagzangen en triomfen mee te kunnen delen. Ik wens je een geweldige toekomst binnen en buiten het lab. **Robert**, je kennis en input op met name het Kaiso project hebben me erg geholpen. Bedankt voor de Brabantse gezelligheid, ik wens jou en **Audrey** veel succes en plezier in Boston maar dat moet zeker

weten lukken! **Amar**, bedankt voor je gezelligheid en veel succes in je volgende avontuur. **Jolien**, je bent echt een doorzetter en gezellige kamergenoot. Je weg buiten de gebaande paden begint steeds meer vorm te krijgen, ik wens je veel succes en plezier daarmee. **Eva**, wat ben je toch een schat en een echte bikkel. Ik heb enorm veel bewondering voor hoe je altijd zo goed weet wat je wilt en daar ook voor gaat, ongeacht wat andere mensen daarvan denken. Bedankt voor de gezelligheid en je steun! **Ron**, de encyclopedie van het Derksen lab en iemand die echt gemaakt is voor je wetenschap. Ookal zat je de laatste tijd van mijn PhD in Boston, door de zoektochten door jouw soms onmogelijk te lezen aantekeningen was je er toch nog vaak bij. Ik hoop dat je binnenkort weer je plekje weet te vinden in Nederland. **Ilse**, dan wel geen Derksen labmember, maar zeker weten een vrolijke aanvulling op ons kantoor! Ook jij veel succes met de voortzetting buiten de wetenschap. En dan de laatste kamergenoot: **Elvira**. Ook al was onze overlap minimaal, volgens mij kom jij er wel, laat je niet gek maken!

Ook mijn **vwo, bachelor en master studenten** hebben een grote bijdrage geleverd aan mijn tijd in het Derksen lab. Ook al verliepen niet alle projecten even smooth, jullie hebben zeker weten allemaal een hele hoop gezelligheid en blunders meegebracht! **Max**, je bent geboren voor de wetenschap en ik wens je veel succes en plezier op weg naar een mooie carrière.

De **Lens-groep**: ook jullie heel erg bedankt voor jullie hulp en gezelligheid tijdens menig borrel. **Martijn**, een onmisbaar persoon in het lab én als er biertjes gedronken moeten worden. **Sanne, Ingrid en Amanda**, thanks voor de gezellige cocktailavondjes en succes met het afronden van jullie PhD, ook **Sippe** veel succes met je PhD en al die dames! **Michael**, bedankt voor je hulp bij het virus-werk en als bron van ongelooflijk veel informatie. **Arne**, FACS-buddy, veel succes en plezier bij je nieuwe baan. **Rutger**, bedankt voor je nieuwsgierigheid op lab-gebied en naar hoe (wild?) m'n weekend was geweest, je wordt vast een top klinisch chemicus! **Livio**, manusje van alles die altijd met 100 dingen tegelijkertijd bezig is, maar als je 'm belt is hij altijd beschikbaar, hartstikke bedankt!

Een paar kantoortjes verder: de mensen van de **Kranenburg**-groep en de **Neuro-onco** meiden. Ook al was de labruimte af en toe spookstad, bedankt voor de gezelligheid en succes met jullie werkzaamheden en vervolgopleidingen! Ook de (oud)-leden van de **Kops**-groep horen in het rijtje van de tweede verdieping thuis. Ook jullie bedankt voor de gezellige borrels, etentjes en dansjes. **Bana**, je bent een topper en je gaat er echt wel komen, zowel op het gebied van je promotie als in je zoektocht naar je daaropvolgende carrière ambities. **Anna, Timo, Richard, Spiros, Bas, Wilma, Manja en Eelco**, veel succes met het afronden van jullie promotie. **Ajit**, thanks voor je altijd vrolijke noot, veel succes en plezier met het vinden van je volgende woon- en werkplek!

&

Ook de rest van de tweede en derde verdieping mag niet vergeten worden. Leden van de **van Mil**, **de Rooij**, **Snippert, Dansen, Timmers, Holstege en Bos-labs**, hartelijk dank voor jullie inhoudelijke een feestelijke input. **Sacha and Maria**, thanks for organizing my very first first-author-paperborrel with me! **Lydia,** bedankt voor je hulp bij het BMF project. **Marten**, Bad MotherFocker, zonder jou hadden we nooit in Cell (death and differentiation) gepubliceerd. Bedankt voor de fijne samenwerking en je enthousiasme op het lab en daarbuiten, daarmee ga je het ver schoppen! Ook aan **Stephin** heb ik een groot deel van hoofdstuk 5 te danken, volgens mij ligt er voor jou een glorieuze toekomst als wetenschapper in het verschiet. **Inkie en Robert**, bedankt voor jullie hulp bij het indesignen! Ook de leden van de MMM en AMP meeting, waaronder de **van Rheenen** groep, hartelijk dank voor jullie input en discussies tijdens de werkbesprekingen.

Ten slotte de mensen die achter de schermen zorgen dat de afdeling blijft draaien. **IT-guys**, zonder jullie zouden we allemaal verloren zijn. Bedankt voor het razendsnel bijhouden en oplossen van onze server en allerhande computer-problemen. **Huub**, ook jij bent vrijwel onzichtbaar bezig met het veilig en ordelijk laten verlopen van onze dagelijkse werkzaamheden, bedankt voor je relaxte houding ten opzichte van onze ietwat rommelige werkhouding. **Claudia, Sandy en Christina,** dank voor jullie secretariële werkzaamheden. **Omar**, bedankt voor laten glimmen van onze werkplek. Ik wens je veel succes met je studie en natuurlijk het winnen van de loterij.

Een paar trappen en een brug verderop zijn er een aantal mensen van de **pathologie-afdeling** die ook zeker in dit dankwoord thuishoren. **Petra**, bedankt voor het eerste contact bij de pathologie (al tijdens mijn master-scriptie!) en later als vraagbaak, vooral op het gebied van coupes kleuren. **Natalie**, bedankt voor het daadwerkelijk snijden, testen en kleuren van tig coupes. Je bent echt een analist-plus die niet te beroerd is om goed mee te denken, succes met je opleiding! **Cathy, Willemijne, Jeroen, Jan, Roel** en de overige (oud) leden van de **breast cancer research club,** jullie bedankt voor de input en hulp bij zowel de klinische kant als het meer hardcore bisulfite-sequencing. Willemijne, zó knap dat je gewoon naast je nieuwe baan je boekje hebt geschreven! Veel succes en plezier de 14^{e}! Ten slotte **Willy**, je staat altijd voor iedereen klaar ookal is het vrijdag 7 uur 's avonds of moet er nog érgens een half uurtje gevonden worden om coupes te scoren, heel erg bedankt!

Naast de labs in Utrecht hebben wetenschappers van over de hele wereld bijgedragen aan het slagen van mijn onderzoek. **Olga Ksionda and Jeroen Roose**, the amazing time with you at UCSF has without a doubt encouraged me to do a PhD. Jeroen, I hope to see you around some time in the Netherlands or the US and Olga lots of luck in New Zealand with the twins. **Sjoerd Klarenbeek en Jos Jonkers**, ook al waren de muizen van hoofdstuk 2 al ver voor het begin van mijn PhD geboren, bedankt voor jullie bijdrage. **Joost Martens and Amit Mandoli**, thanks for processing and producing tons of sequencing data for several of my projects. **Katy Teo and Valerie Brunton**, without you chapter 3 would not have even existed. Thanks for your enthusiasm during our skype sessions and mail contact. Finally, the

members of the **Hetzer** lab, in particular **Toby Franks** and **Chris Benner**: thanks for letting me visit your lab for two weeks, teaching me the ins and outs of DamID and sequencing analysis.

Gelukkig heb ik in de afgelopen jaren niet non-stop op het lab gestaan en hebben vele mensen bijgedragen aan het plezier buiten mijn werk. **Jarka, Karlijn en Joyce**, alledrie dezelfde bachelor maar uiteindelijk tóch op totaal verschillende plekken terecht gekomen. Jarka, bedankt voor het heerlijke dansen, daten en de kletsavondjes. Karlijn en Joyce, ondanks dat jullie ver weg wonen ben ik heel blij dat we altijd contact zijn blijven houden. Veel succes en geluk met jullie baan en daarbuiten! Dan de **meiden uit Raalte** en omgeving: van de 5 (en meer) butterflies en hoelahoeps tot de meiden van het 'vwo' en eigenlijk het hele bijeengeraapte zooitje wat daarbij hoort. Bedankt voor jullie steun en interesse, de heerlijke weekendjes weg, de gegarandeerd leuke avondjes uit en jullie verregaande pogingen om een man voor mij te vinden. Ondanks dat we elkaar misschien niet even vaak zien ben ik erg blij dat we nog altijd heerlijk veel ouderwets lol kunnen maken. **Sandra**, uiteraard een speciale vermelding voor jou. We kennen elkaar al bijna ons hele leven en ik ben heel erg blij dat ik je een van mijn beste vriendinnen mag noemen! Bedankt voor je betrokkenheid, vroijkheid, onze wekelijkse telefoongesprekken en heerlijke party-spirit. Ten slotte de mensen waarmee ik goede afleiding vond in de vorm van dansen op de raarste plekken van de wereld. **Jessie en Mariska**, heerlijk om goede buddies mee te hebben op reis waar ik ook daarbuiten mee kan lachen, zeuren en eindeloze grappige whatsapp-gesprekken mee kan hebben.

Mijn nieuwe collega's van **Zilveren Kruis**, het is een flinke sprong in het diepe van het academisch onderzoek naar zorgverzekeraar-land, maar jullie gezelligheid en hulp maken dat ik niet verdrink, bedankt!

De gehele familie **Tenhagen en Lieferink en Jan en Doortje**, bedankt voor de gezelligheid tijdens kerstdiners en familiedagen en voor jullie interesse in de wondere wereld van het wetenschapelijk onderzoek. **Lizzie**, je bent en blijft m'n kleine zusje en ik heb het geweldig gevonden om mijn promotie-tijd samen met jou af te ronden in New York! Je bent een topverpleegkundige, veel plezier met het zoeken van je droomafdeling! **Woody**, ik vond het heerlijk om je een paar maanden bij mij in huis te hebben. Met jouw ambitie kom je er zeker wel, veel succes met het afronden van je studie en je mag best nog eens komen koken nu dat in je nieuwe huis niet meer zo uitgebreid kan. **Anouk**, dit boekje is ook een beetje van en voor jou. En ten slotte **Pap** en **Mam**, het klinkt cliché, maar zonder jullie was dit toch écht allemaal niet gelukt. Jullie steun, hulp en vertrouwen in mij geven mij het gevoel dat ik alles aan kan, heel erg bedankt!

Liefs, Milou

&